CONJUGATE NATURAL CONVECTION HEAT TRANSFER IN A CAVITY WITH FINITE WALL THICKNESS

A Thesis Submitted to
the Graduate School of Engineering and Sciences of
İzmir Institute of Technology
in Partial Fulfillment of the Requirements for the Degree of

MASTER OF SCIENCE

in Mechanical Engineering

by
Erinç HAKYEMEZ

May 2009
İZMİR

We approve the thesis of **Erinç HAKYEMEZ**

_____

Assoc. Prof. Dr. Moghtada MOBEDİ
Supervisor

_____

Assist. Prof. Dr. Hakan F. ÖZTOP
Co-Supervisor

_____

Assist. Prof. Dr. Ünver ÖZKOL
Committee Member

_____

Assoc. Prof. Dr. Serhan KÜÇÜKA
Committee Member

26 MAY 2009

_____

Assoc. Prof. Dr. Metin TANOĞLU
Head of the Mechanical Engineering Department

_____

Prof. Dr. Hasan BÖKE
Dean of the Graduate School of Engineering and Sciences

ACKNOWLEDGMENTS

The author would like to express his sincere gratitude to his supervisor Assoc. Prof. Dr. Moghtada Mobedi for his valuable advises and continual support through the thesis.

The author also wishes to express his thanks to his family and his friends for their help and support during his studies.

ABSTRACT

CONJUGATE NATURAL CONVECTION HEAT TRANSFER IN A CAVITY WITH FINITE WALL THICKNESS

The effects of a heat barrier, located in the thick ceiling wall of a square enclosure, on conjugate conduction and natural convection heat transfer are investigated numerically. The analysis is performed by numerical solution of the continuity, unsteady momentum conservation and energy equations with finite difference solution method based on the streamfunction-vorticity formulation. The vertical walls of the enclosure are differentially heated and horizontal walls are adiabatic. A thin heat barrier, having infinite thermal resistance, is located in the ceiling wall at different locations. The calculations are made for different Rayleigh numbers ($10^3 \leq Ra \leq 10^6$), thermal conductivity ratios ($1 \leq K \leq 100$), dimensionless locations of heat barrier ($0<X_h<1$) and two dimensionless ceiling wall thicknesses ($D = 0.05$ and $D = 0.20$). By using the results of the computer program, streamlines and isotherms are plotted. Heatline visualization technique is used to simulate heat transport and the effect of heat barrier is presented by comparing and plotting heatlines for the cavity and for the solid region with and without heat barrier. The study is performed for air with Prandtl number 0.71. It is found that the effect of heat barrier is more significant in the cavity with high thermal conductivity ratio but low Rayleigh number. There are certain reductions in the average Nusselt number at the vertical walls of the cavity and dimensionless heat transfer rate of the solid region walls for high conductivity ratios, but the reduction in dimensionless heat transfer rate is greater.

ÖZET

DUVAR KALINLIĞI SINIRLI OLAN BİR HACİMDE DOĞAL TAŞINIM YOLU İLE BİRLEŞTİRİLMİŞ ISI TRANSFERİ

Bu çalışma duvar kalınlığı sınırlı olan kare şeklindeki bir hacimde doğal taşınım yolu ile birleştirilmiş ısı transferinin sayısal metodlar ile çözümlenmesidir. Çalışma kapsamında kare bir boşluk ele alınmış olup boşluk içinde Prandtl değeri 0.71 olan hava bulunduğu kabul edilmiştir. Boşluğun dikey duvarlarından sol duvar sıcak ve sağ duvar soğuk tutulmuştur, yatay duvarları ise yalıtılmıştır. Boşluğun tavan kısmında belirli bir kalınlığı olan yatay bir duvar bulunmaktadır. Bu çalışmada yatay duvarın, boşlukta gerçekleşen ısı transferine etkisinin yanında, duvar içine yerleştirilen ısı bariyerinin duvar ve boşluk kısımda oluşan ısı transferine etkileri araştırılmıştır. Çalışmanın sayısal analizi zamana bağlı momentum denkleminin vortisite-akım fonksiyonu yaklaşımından yola çıkarak, süreklilik ve enerji denklemlerinin sonlu farklar metodu ile çözümlenmesiyle elde edilmiştir. Çalışmada kullanılan ısı bariyerinin belirli bir kalınlığı vardır ve ısı geçişine imkan vermemektedir. Hesaplamalar farklı aralıklarda Rayleigh değerleri ($10^3 \leq Ra \leq 10^6$), ısı iletim katsayısı oranları ($1 \leq K \leq 100$), ısı bariyerinin tavan içindeki boyutsuz konumları ($0 < X_h < 1$) ve iki farklı boyutsuz tavan duvar kalınlıkları için yapılmıştır ($D = 0.05$ and $D = 0.20$). Bilgisayar programından elde edilen sonuçlar kullanılarak akış çizgileri ve izotermler boşluk için çizilmiştir. Ayrıca, ısı akışının görülebilmesini sağlayan "ısı akış çizgisi gösterme tekniği" kullanılmış ve boşluktaki ısı transfer yolları ısı akış çizgileri ile gösterilmiştir. Bu sayede boşluk içindeki kısımda ve tavanda gerçekleşen ısı akış yolları görsel olarak sunulmuş ve ısı bariyerinin etkileri araştırılmıştır. Sonuç olarak ısı bariyerinin ısı transferine olan etkisinin yüksek ısı iletim katsayısı oranları ve düşük Rayleigh değerleri için çok daha belirgin olduğu saptanmıştır. Isı bariyeri kullanımı, toplam ısı transferini yüksek ısı iletim katsayısı oranları için önemli ölçüde azaltmıştır.

TABLE OF CONTENTS

LIST OF FIGURES

Figure **Page**

LIST OF TABLES

Table **Page**

NOMENCLATURE

A	a constant in the nodal equation
A(i,j)	multiplier of a dependent variable
B	a constant in the nodal equation
B(i,j)	multiplier of a dependent variable
C	a generic variable
C(i,j)	multiplier of a dependent variable
d	ceiling wall thickness, (m)
D	dimensionless ceiling wall thickness, (d/L)
D(i,j)	a variable
E	a constant in the nodal equation
F	a constant in the nodal equation
f	a generic variable
g	acceleration of gravity, (m/s^2)
G	a constant in the nodal equation
Gr	Grashof number
h	number of nodes in y-direction
H	dimensionless heatfunction
I	fluid enthalpy
(i,j)	a node in Cartesian computational domain
k	thermal conductivity, (W/mK)
K	thermal conductivity ratio
L	length and height of cavity, (m)
m	number of nodes in x-direction
Nu	local Nusselt number
$\overline{Nu}$	average Nusselt number
p	pressure, (Pa)
P	dimensionless pressure
r	number of nodes in y-direction up to interface
R	a generic symbol
Pr	Prandtl number
q	heat flux, (W/m^2)

q^*	dimensionless heat flux
Q^*	dimensionless heat transfer rate
Ra	Rayleigh number based on cavity length
T	temperature, (K)
t	physical time, (s)
u, v	velocity components in x and y directions, (m/s)
U, V	dimensionless velocity components in X and Y directions
U	internal energy (kJ/kg)
$\vec{V}$	velocity vector $(u\vec{i} + v\vec{j})$
x, y	dimensional Cartesian coordinate, (m)
X,Y	dimensionless Cartesian coordinate
x_h	heat barrier location, (m)
X_h	dimensionless heat barrier location

Greek Symbols

α	thermal diffusivity, (m^2/s)
α^*	thermal diffusivity ratio
β	thermal expansion coefficient, (K^{-1})
δ	interval
δ^2	diffusion-convection term
ℓ	heat barrier thickness, (m)
ℓ^*	dimensionless heat barrier thickness
ν	kinematic viscosity, (m^2/s)
ξ	vorticity
Ω	dimensionless vorticity
θ	dimensionless temperature
τ	dimensionless time
ψ	streamfunction
Ψ	dimensionless streamfunction

Operators

$\vec{\nabla}$	gradient vector $(\frac{\partial}{\partial X}\vec{i}+\frac{\partial}{\partial Y}\vec{j})$
∇	divergence $(\frac{\partial}{\partial X}+\frac{\partial}{\partial Y})$
$\frac{D(\ )}{dt}$	total derivative,
$\frac{\partial(\ )}{\partial t}$	partial derivative

Subscripts

∞	ambient
Δ	local
c	cold
f	fluid
h	hot
(i,j)	node (i,j)
L	cavity length
s	solid
t	total
x,y,z	refer to x, y and z directions of cartesian coordinate

Superscripts

n	refer to n^{th} time step
n+1/2	refer to $(n+1/2)^{th}$ time step
n+1	refer to $(n+1)^{th}$ time step

CHAPTER 1

INTRODUCTION

Discussions of convection heat transfer have considered generally the calculation of forced convection systems where the fluid is forced through the heat transfer surface. For example, the fluid motion induced by a fan or a pump. However, there are many situations for which there is no forced velocity, yet convection currents exist within the fluid. Such situations are referred to as free or natural convection and they originate when a body force acts on a fluid in which there are density gradients. A hot radiator used for heating a room is one example of a practical device which transfers heat by free convection. The movement of fluid in the free convection, whether it is a gas or a liquid, results from the buoyancy forces imposed on the fluid when its density in the proximity of the heat transfer surface is decreased as a result of the heating process. The buoyancy forces would not be present if the fluid were not acted upon by some external force field such as gravity, although gravity is not the only type of force field which can produce the free-convection currents; a fluid enclosed in a rotating machine is acted upon by a centrifugal force field, and thus could experience free convection currents if one or more of the surface in contact with the fluid were heated. The buoyancy forces which can give rise to the free convection currents are called body forces (Holman 1990). In the most common case, the density gradient is due to a temperature gradient, and the body force is due to the gravitational field. Since free convection flow velocities are generally much smaller than those associated with forced convection, the corresponding convection transfer rates are also smaller. It is perhaps tempting to therefore attach less significance to free convection processes. This temptation should be resisted. In many systems involving multimode heat transfer effects, free convection provides the largest resistance to heat transfer and therefore plays an important role in the design or performance of the system. Moreover, when it is desirable to minimize heat transfer rates or to minimize operating cost, free convection is often preferred to forced convection. There are, of course, many applications. Free convection strongly influences heat transfer from pipes and transmission lines, as well as from various electronic devices. It is important in transferring heat from electrical

baseboard heaters or steam radiators to room air and in dissipating heat from the coil of a refrigeration system to the surrounding air. It is also relevant to the environmental sciences, where it is responsible for oceanic and atmospheric motions, as well as related heat transfer processes (Incropera and Dewitt 2002).

The effect of wall heat conduction on natural convection heat transfer in cavities has gained attention of many researchers in recent years due to its wide application areas in engineering such as building heating and cooling, thick walled enclosures, cooling of electronic equipments, internal combustion engines and solar collectors. Moreover, researchers have performed several numerical and experimental studies on natural convection to investigate the effect of wall heat conduction on heat transfer.

The problem of thermal bridge is widely faced in industrial applications since it increases heat transfer between two walls and creates local temperature gradients on the walls which may cause condensation problems, particularly in building envelopes and window frames. Heat barrier, also called thermal breaker in the industry, is used in many applications where heat flow resistance is needed. It is located in thermal bridge region to reduce heat leakage between two surfaces. For example, by using thermal breaker in windows and doors, heat loss can be reduced by half or more (Global Trade 2008). Figure 1.1 shows a thermal breaker used in aluminum profile.

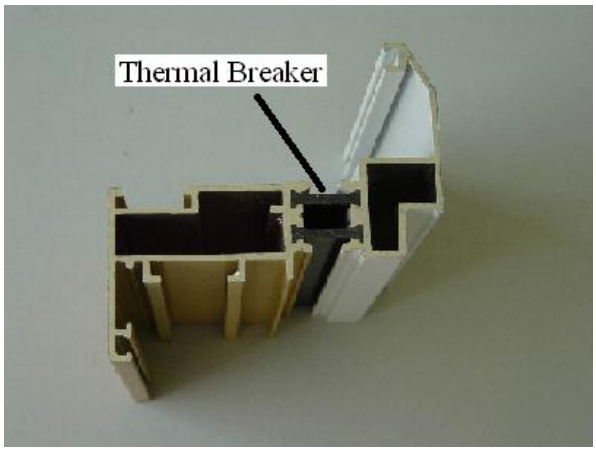

Figure 1.1. Thermal break aluminum profiles.
(Source: Global Trade 2008)

The window design must minimize the potential for condensation; therefore, thermal breaker is used. Another reason to use thermal breakers at aluminum window product lines is to enhance thermal performance of the windows by reducing thermal

bridge. Thermal strip system, shown in Figure 1.2, is an option available on all thermally broken windows as an alternative to debridge thermal breaks (Sapa Group 2009). In this figure, the black strip in the middle of the window frame is a thermal breaker which is located in thermal bridge region to reduce heat leakage between two surfaces. Advantages include superior thermal performance and the option to have two different finishes on the interior and the exterior.

Figure 1.2. Thermal strip system.
(Source: Sapa Group 2008)

In another application, extruded polystyrene thermal block is preferred for the pre-engineered metal building industry to reduce thermal bridge. The product is designed to create a thermal break between the roof purlin and the metal roof panels (Fabricated Foam Company 2008). Figure 1.3 is showing the extruded polystyene thermal block for the pre-engineered metal building industry.

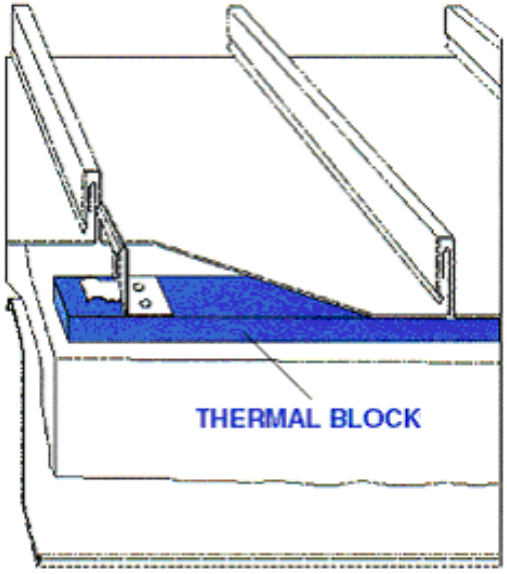

Figure 1.3. Extruded polystyene thermal block.
(Source: Fabricated Foam Company 2008)

Figure 1.4 is a fleet of Liqufield Natural Gas (LNG) tanker that uses the spherical design. The natural gas is condensed into a liquid at close to atmospheric pressure by cooling it to approximately −163 °C. LNG inside the tank must be kept cold to remain a liquid, independent of pressure (Wikipedia 2009). Since the LNG is stored cold in the tank, there will inevitably be some heat leakage into the LNG through the tank walls, resulting in vaporization of it. Tank wall material is actually thin sheets of nickel steel Invar or 304 L stainless steel which has high thermal conductivity. Therefore, the insulation of the storage tank wall is very crucial to prevent heat leakages. Thermal breakers are used in tank walls to reduce heat loss because of thermal bridges occurred in the walls.

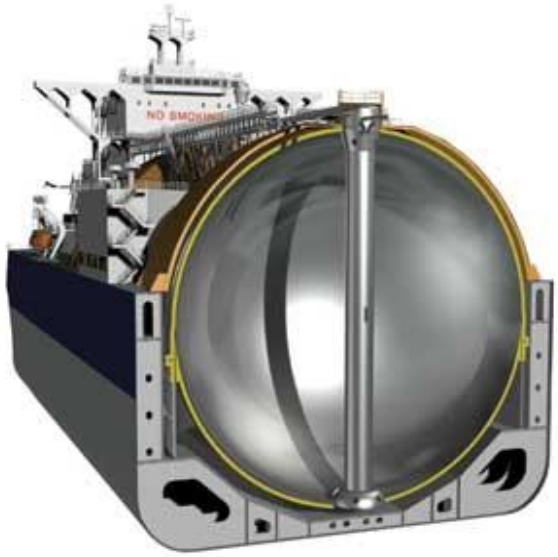

Figure 1.4. Spherical tank of LNG tanker.
(Source: Wikipedia 2008)

Figure 1.5 demonstrates the adiabats in a square solid metal plate which has a constant thermal conductivity with adiabatic bottom and right sides. Left side of the plate is kept constant hot temperature and top side of it is kept cold. Heat is transferred from hot to cold sides in the way shown at Figure 1.5. However, it is not easy to realize the direction of heat flow since heat flux is not perpendicular to isotherm in convective flows. Thus, isotherms are used to show temperature distribution in domains in many experimental and theoretical studies. Heatline is a useful tool for visualization and analysis of not only direction but also intensity of heat flux in a domain. They provide corridors where heat is transferred from the hot to cold regions by convection and/or conduction. Heatline visualization method is also a powerful method to show the heat interaction between solid-fluid interfaces. The definition of heatlines is very similar to the adiabat lines defined in many heat transfer text books.

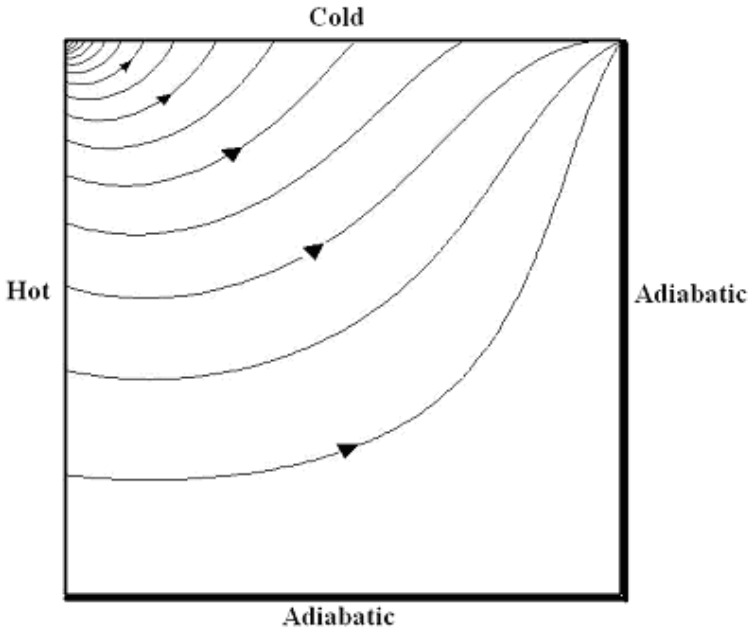

Figure 1.5. Adiabats for the solid square metal plate with constant thermal conductivity.

The main aim of this study is to investigate the effect of heat barrier or thermal breaker located in the horizontal wall of an enclosure on heat transfer through the wall and through the cavity. Heat barrier of this study has a small thickness and infinite thermal resistance. It is located in the horizontal wall to prevent conduction heat transfer through the solid in the horizontal direction. The governing equations for the problem which are continuity, momentum and energy equations are presented. The continuity and the momentum equations are transformed to the streamfunction and the vorticity equations. The boundary conditions for all dependent variables are also described. The set of governing equations are solved by finite difference method with the selected finite difference solution technique. The numerical analysis is done for an enclosure with a ceiling wall in which the dimensionless location of heat barrier is changing from $X_h = 0$ to $X_h = 1$. The streamlines, the isotherms and the heatlines inside the cavity and inside the solid region are drawn for different values of Rayleigh number ($10^3 \leq Ra \leq 10^6$) and thermal conductivity ratio ($1 \leq K \leq 100$). The study is performed for two horizontal wall thicknesses; L/5 and L/20. The temperature distribution on the solid-fluid interface is also plotted to analyze the heat transfer between the horizontal wall and the fluid. Dimensionless heat transfer rate of the horizontal wall and the average Nusselt numbers of hot and cold vertical walls of the cavity are numerically calculated and plotted for different locations of heat barrier and thermal conductivity ratios.

In the second chapter of this thesis, a review on conjugate conduction-convection natural convection problems and heatfunction studies are given. The definition of the problem is given in the third chapter, whereas the governing equations and the boundary conditions are defined in the fourth chapter. In addition to the definition of boundary conditions and governing equations, also the transformation of continuity and momentum equations into streamfunction and vorticity equations is performed in the fourth chapter. The fifth chapter of this study is about the discussion of approaches and methods for the solutions of governing equations. In this study, ADI method is selected to solve the parabolic differential equations of the problem, whereas for elliptic differential equations point by point solution approach is chosen. In the sixth chapter, the finite difference forms of diffusion and convection terms are given. In addition to that, the finite difference forms of the boundary conditions at the specified boundaries are defined. The numerical analysis and the solution procedure for the considered problem are discussed in the seventh chapter. The results are presented and explained in the eighth chapter of the study. And in the last chapter, the important findings are presented and a general evaluation of the study is performed.

CHAPTER 2

LITERATURE SURVEY

Computational method has been used by De Vahl Davis (1983) to obtain accurate numerical solutions of the equations describing 2-D natural convection heat transfer in a square cavity shown in Figure 2.1. The study is performed for air with Prandtl number 0.71 and for Rayleigh number changing from 10^3 to 10^6. The governing equations of motion and heat transfer are solved on several mesh sizes by finite difference method. The extrapolated solutions were performed to generate solutions for zero grid size. It was found that the coarse mesh for high Rayleigh number solutions are useless and in the absence of some other technique such as extrapolation, finer meshes are required to obtain accurate results.

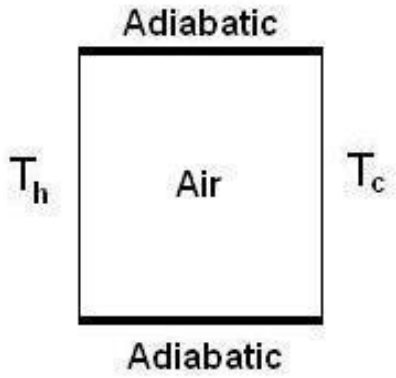

Figure 2.1. The square cavity analyzed.
(Source: De Vahl Davis 1983)

Effect of wall conductance on natural convection in differently oriented square cavities was studied by Kim and Viskanta (1984). The considered cavities are shown in Figure 2.2. In the study, experimental and numerical results on the effects of wall conductance on natural convection heat transfer in a two-dimensional rectangular cavity were reported together. The experiments were performed in a square enclosure with solid walls made from lexan (the brand name for polycarbonate sheet in thicknesses from 0.75 mm to 12 mm) and forming a square air-filled cavity. Solutions for steady

state two-dimensional equations of energy and fluid flow governing heat conduction in the solid and natural convection heat and fluid flow in the cavity were obtained numerically. The obtained results show that as the Rayleigh and Prandtl numbers increase, the average Nusselt number on the four walls of the cavity also increases. One of the important findings of the study is that natural convection heat transfer in the cavity is reduced by heat conduction in the walls and radiation exchange among surfaces.

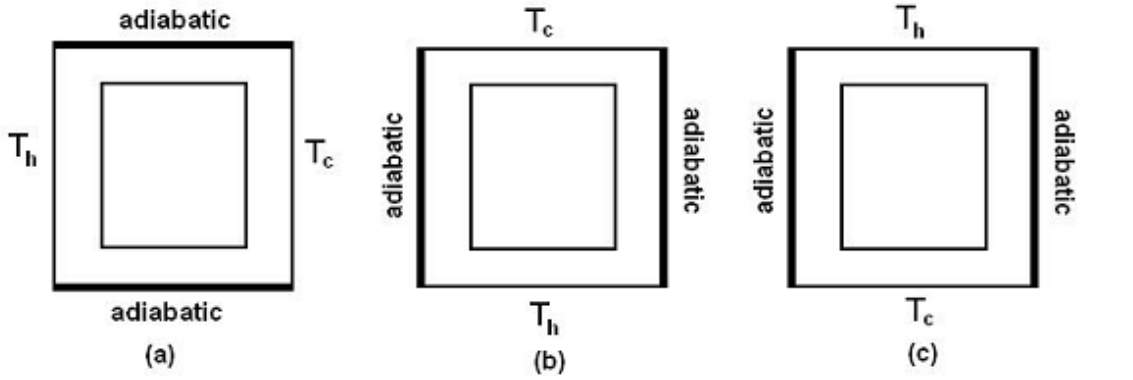

Figure 2.2. Schematics of the considered problem.
(Source: Kim and Viskanta 1984)

Kim and Viskanta (1984) performed another study on heat transfer across a rectangular cellular structure by conduction, natural convection and radiation. The effects of wall conduction and radiation heat exchange among surfaces on laminar natural convection heat transfer in a two-dimensional rectangular cavity that is shown in Figure 2.3 were investigated. The findings of the study suggest that the local or the average Nusselt number is one of many parameters that control conjugate heat transfer problems. The reported results indicate that natural convection heat transfer in the cavity is reduced by heat conduction in the walls and radiation exchange among the surfaces.

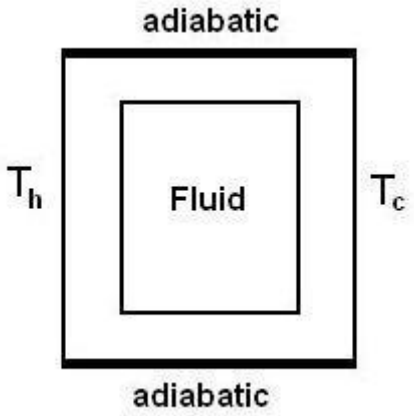

Figure 2.3. Physical model of the system analyzed.
(Source: Kim and Viskanta 1984)

Kaminski and Prakash (1986) investigated the conjugate natural convection problem in enclosure with one thick vertical wall while the other three walls are taken to be of zero thickness. The considered problem is shown in Figure 2.4. Three separate models to account for the wall conduction are investigated: (i) the complete conjugate case in which conduction in the thick vertical wall is assumed to be fully two-dimensional; (ii) a one-dimensional model in which conduction in the wall is assumed to be in the horizontal direction only; and (iii) a lumped parameter approach which assumes the solid-fluid interface temperature to be uniform. A Boussinesq fluid with Prandtl number of 0.7 (air) and Grashof numbers ranging from 10^3 to 10^7 are considered. For Grashof numbers greater than 10^5, the temperature distribution in the wall shows significant two-dimensional effects and the solid-fluid interface temperature is found to be quite non-uniform. In the parametric range investigated, all three models predict nearly the same value for the overall heat transfer.

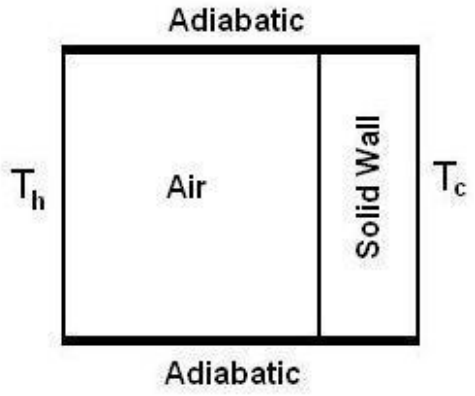

Figure 2.4. The considered problem.
(Source: Kaminski and Prakash 1986)

Finite element analysis of conjugate natural convection in a square enclosure with a conducting vertical wall shown in Figure 2.5 was performed by Misra and Sarkar (1997). The set of governing equations are reframed and put into a form that can easily fit into the Galerkin formulation. Results are presented for Rayleigh number in the range of 10^3 to 10^6. The effect of conduction in the wall is studied for three different values of the non-dimensional wall thickness (0.1, 0.2 and 0.4) with a wide range of dimensionless conductivity of the wall. Conduction in the solid zone is simulated by assigning a high value of dimensionless viscosity in this zone. It is found that the ratio of thermal conductivity to wall thickness is the determining factor for prediction of Nusselt number. The average interface temperature is found to remain the same as the Rayleigh number is increased by a factor ten and the wall conductivity to thickness ratio is increased by a factor 2.

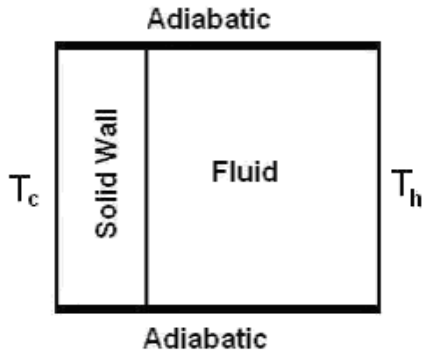

Figure 2.5. Problem geometry analyzed.
(Source: Misra and Sarkar 1997)

Baytas et al. (2001) studied steady-state conjugate natural convection in a square cavity filled with a porous medium which consists of two horizontal conductive walls of finite thickness and two vertical walls at different uniform temperatures shown in Figure 2.6. The focus is on the role of solid-fluid conductivity ratio on the flow and heat transfer characteristics and the average Nusselt number over the vertical hot and cold walls of the cavity for a limited set of particular parameters. The results show that the interface temperature along the top of the solid wall decreases with the increase of the wall conductivity.

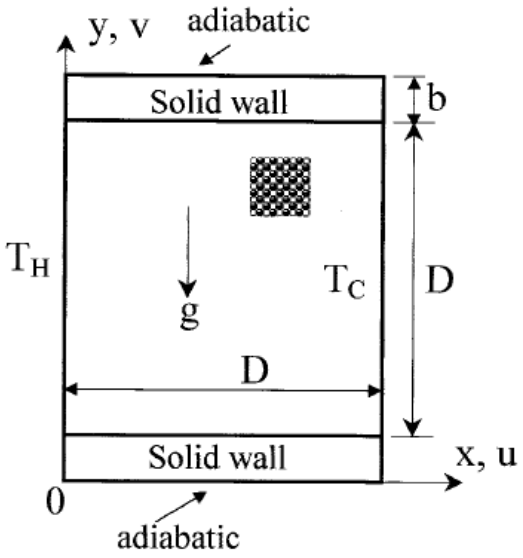

Figure 2.6. The considered problem.
(Source: Baytas et al. 2001)

Acharya and Tsang (1987) made a numerical study on natural convection in an externally heated inclined enclosure shown in Figure 2.7 with finitely conducting side walls. Results indicate that conduction along the enclosure walls has a stabilizing influence on the convective motion in the enclosure and is therefore responsible for reduced heat transfer from the enclosure.

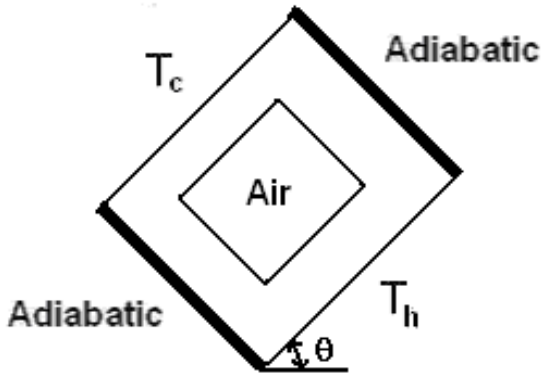

Figure 2.7. Schematic of the physical situation studied.
(Source: Acharya and Tsang 1987)

Du and Bilgen (1992) studied conjugate heat transfer in an enclosure which consists of a conducting vertical wall of finite thickness with a uniform heat input, an insulated vertical wall and two horizontal walls at a heat sink temperature. The relative heat removal contribution by conduction in the solid wall to that by natural convection in the fluid enclosure, as well as the temperature and temperature gradient on the fluid-solid interface has been obtained. The results indicate that for low Rayleigh number, high solid-fluid conductivity ratio and dimensionless solid wall thickness, the heat transfer process is dominated by the heat conduction in the solid wall. For high Rayleigh number, low solid-fluid conductivity ratio and dimensionless solid wall thickness at moderate aspect ratio, strong interaction between conduction in the solid wall and convection in the fluid influences the heat transfer.

Yedder and Bilgen (1997) analyzed laminar natural convection in an inclined enclosure shown in Figure 2.8 bounded by a solid wall with its outer boundary at constant temperature while the opposing side has a constant heat flux. The numerical calculations are done by using SIMPLER algorithm. The results are found based on parameters Rayleigh number, dimensionless conductivity of bounding wall and dimensionless wall width, aspect ratio and the inclination angle. It is observed that the heat transfer is an increasing function of the Rayleigh number, wall to fluid conductivitiy ratio, enclosure aspect ratio and a decreasing function of the wall thickness and it passes from a maximum for the angle of about 80^0.

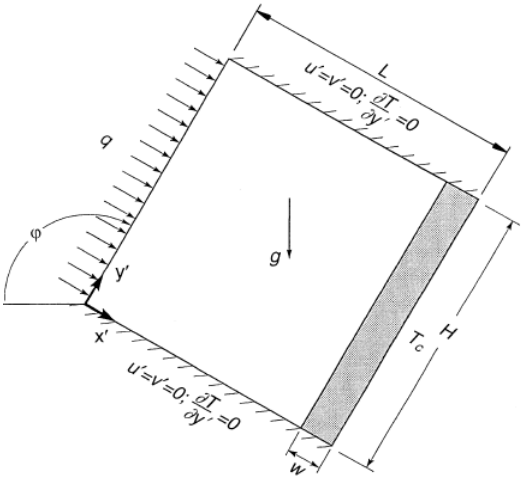

Figure 2.8. Problem considered.
(Source: Yedder and Bilgen 1997).

Steady conjugate natural-conduction heat transfer in a two-dimensional porous enclosure shown in Figure 2.9 with finite wall thickness was studied numerically by Saeid (2007). The horizontal heating is considered, where the vertical boundaries are isothermal at different temperature with adiabatic horizontal boundaries. The governing parameters considered are the Rayleigh number, the wall to porous thermal conductivity ratio and the ratio of wall thickness to its height. It is found, in most of the cases that either increasing the Rayleigh number and the thermal conductivity ratio or decreasing the thickness of the bounded wall can increase the average Nusselt number for the porous enclosure.

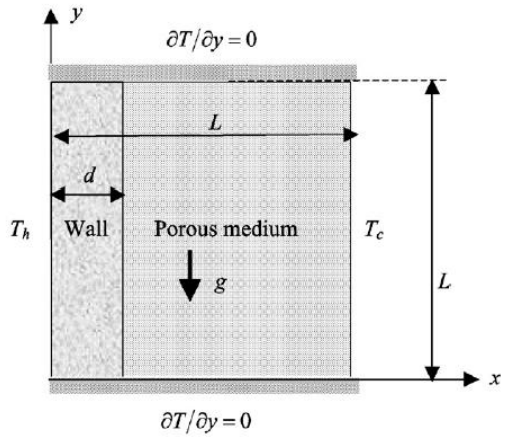

Figure 2.9. Problem geometry analyzed.
(Source: Saeid 2007)

Saeid (2007) analyzed steady conjugate natural convection in two-dimensional vertical porous layer sandwiched between two equal-thickness walls. The problem geometry is shown in Figure 2.10. The horizontal heating is considered, where the outer surfaces of the vertical walls are isothermal at different temperatures with adiabatic horizontal boundaries. Finite volume method is used to solve the dimensionless governing equations. The governing parameters considered are the ratio of the wall thickness to its height, the wall to porous thermal conductivity ratio and the Rayleigh number. It is found that as the wall thickness increases the average Nusselt numbers decreases, and the strength of the circulation of the fluid saturated the porous medium is much higher with thin walls. The numerical results indicated that for small values of Rayleigh number, where the heat is transferred mainly by conduction in both wall and porous layer, the average Nusselt number is approximately constant. As Rayleigh number increases the average Nusselt number is increasing with higher slope for the thin walls than that for thick walls.

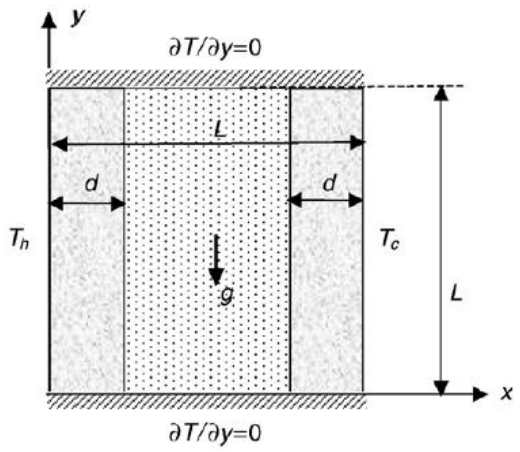

Figure 2.10. Schematics of the geometry analyzed.
(Source: Saeid 2007)

Laminar natural convection flow in a square enclosure shown in Figure 2.11 having thick conducting walls was analyzed by Liaqat and Baytas (2001). Enclosing walls are considered to have finite conductive properties and outsides of the walls are kept at constant temperature. Control volume approach is used and the square cavity is assumed to be filled with a Bousinessq fluid containing uniform volumetric sources. The obtained results with non-conjugate cases are compared and significant differences in the buoyant flow parameters are observed.

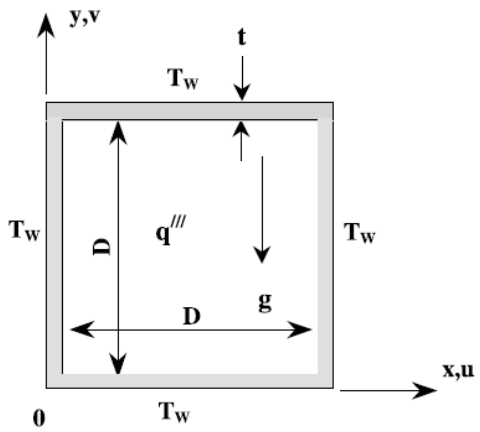

Figure 2.11. The physical situation analyzed.
(Source: Liaqat and Baytas 2001)

Heatlines were first proposed by Kimura and Bejan (1983) as adequate tools for visualization and analysis of convection heat transfer. This visualization and analysis tool is proved to be useful, and its application in the fields of convective heat transfer increases day by day. Morega and Bejan (1993) and then Dash (1996) extended heatline visualization technique at different heat transfer problems to show the heat interaction between solid and fluid interface. Costa (2003), (2006) presented a unified viewpoint in both physical and numerical aspects on treatment of the functions and lines for visualizing two-dimensional transport problem. When the heatfunction is made dimensionless in an adequate way, its value is closely related with the Nusselt number. Deng and Tang (2002) and then Zhao et al. (2007) applied heatline visualization method for conjugate heat transfer problem. Natural convection heat transfer in a porous media filled and non-isothermally heated from the bottom wall of triangular enclosure is analyzed using finite difference technique and heatline method by Varol et al. (2008). Dimensionless heatfunction is used to visualize the heat transport due to buoyancy forces. It is agreed that heatline visualization technique is a useful technique for non-isothermally heated and porous media filled triangular enclosures. Natural convection inside a two-dimensional cavity with a wavy right vertical wall has been studied by Dalal and Das (2008). The integral forms of the governing equations are solved numerically using finite volume method in non-orthogonal body-fitted coordinate system where SIMPLE algorithm with higher-order upwinding scheme is used. The method of numerical visualization of heat transport for convective heat transfer by

heatlines is carried out. In the study of Basak et al. (2009), heat flow patterns in the presence of natural convection within trapezoidal enclosures have been analyzed with heatlines concept. Natural convection within a trapezoidal enclosure for uniformly and non-uniformly heated bottom wall, insulated top wall and isothermal side walls with inclination angles 45°,30° and 0°(square) have been investigated. Heatlines are found to be continuous lines connecting the cold and hot walls, and the lines are perpendicular to the isothermal wall for the conduction dominant heat transfer. Heatline visualization technique has been used by Mobedi (2008) to show the effect of conduction of horizontal walls on natural convection heat transfer in a square cavity. Hakyemez et al. (2008) has investigated the effects of wall-located heat barrier on conjugate conduction and natural convection heat transfer and fluid flow in enclosures. Heatlines for the entire region are drawn to support discussions on the observed variations.

The transfer of heat through thermal bridge has been investigated by researchers since it increases heat transfer between two walls and creates local temperature gradients on the walls which may cause condensation problems. A method for the plotting of heat flow intensity to provide an effective visual representation of heat flows in solid matter is proposed by Fukuyo (2003). This representation of heat flow provides a stronger emphasis on the heat flows through good conductors than does the temperature distribution. The heat-flow intensities are defined as the heat gain and the heat loss per volume. Two-dimensional steady-state simulation of heat flow in a structure was carried out under two conditions and the results were represented as plots of the temperatures and the heat-flow intensities. This representation of heat flow provides a stronger emphasis on the heat flows through good conductors than does the temperature distribution; the proposed method thus enables to effectively visualize the effects of thermal bridges. Larbi (2005) developed statistical models of the thermal transmittance of two-dimensional thermal bridges. His aim is to give designers plain and practical tools for the evaluation of the most common two-dimensional thermal bridges. Ben Nakhi (2002) concerned with minimizing thermal bridging through typical window systems in buildings of hot regions. His study shows that the thermal bridging through typical window systems is significant and should be taken into account in buildings design. Accurate thermal bridging assessment is becoming more important not only to predict the peak thermal load, but also to estimate the potential for condensation. A new dynamic thermal bridging assessment module which integrates all inter-related energy subsystems occurring in buildings was presented by Ben Nakhi (2003).

Number of studies on heat barrier which is widely used for prevention of thermal bridge is very limited in literature. Tosun et al. (1998) performed an investigation on heat transfer through the casing of air handling unit. The obtained results showed that the homogenous temperature distributions on both interior and exterior surfaces can be achieved by employing heat barrier. Hoglund and Burstrand (1998) experimentally perform a study on slotted steel studs to reduce thermal bridge in insulated walls. They showed by slotting the web, the thermal bridges are significantly reduced. Hakyemez et al. (2008) numerically investigated the effects of middle located heat barrier in the thick floor wall of a square enclosure on conjugate conduction and natural convection heat transfer. The problem geometry is shown in Figure 2.12. Heatline visualization technique is used to simulate heat transport in both solid and fluid regions. The thermal effect of heat barrier is presented by comparing the achieved results for cavities with and without heat barrier. The calculations are made for wide ranges of Rayleigh number ($10^3 < Ra < 10^6$) and thermal conductivity ratio ($1 < K < 100$). It is found that for cavity with low thermal conductivity ratio, heat transfer through the cavity is not greatly affected by the existence of heat barrier. The maximum reduction in the average Nusselt number due to heat barrier is observed as 24% for $Ra=10^3$ and K=100 at the hot vertical wall.

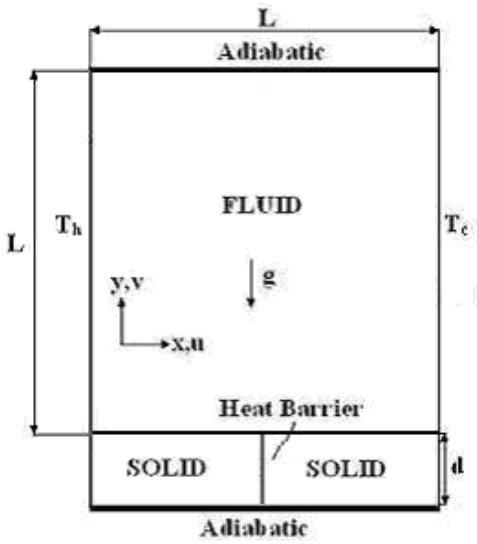

Figure 2.12. Geometry of the problem analyzed.
(Source: Hakyemez et al. 2008)

CHAPTER 3

DEFINITION OF THE PROBLEM, GOVERNING EQUATIONS AND BOUNDARY CONDITIONS

3.1. Definition of the Problem

The considered enclosure shown in Figure 3.1 consists of a square cavity with a side length of L. The ceiling wall has finite thickness d. The outer surfaces of the horizontal boundaries are insulated. The vertical walls of the enclosure are maintained at different T_h (left wall) and T_c (right wall) constant temperatures such that T_h is greater than T_c. The heat transfer in the cavity occurs by laminar natural convection and the Prandtl number is 0.71. A heat barrier having small thickness ($\ell / L = 0.001$) and infinite thermal resistance is placed at different locations in the ceiling wall. The study is performed for two different dimensionless ceiling wall thicknesses 0.2 and 0.05.

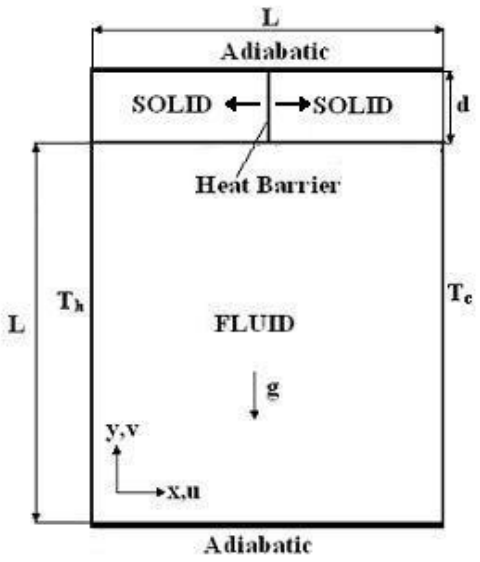

Figure 3.1. Considered problem.

3.2. Continuity, Momentum and Energy Equations

The governing equations for the problem are continuity, momentum and energy for the fluid inside the cavity, and heat conduction equation for the horizontal wall. The radiation effect is neglected and the gravity acts in the negative vertical direction. The fluid is Newtonian with constant thermal properties. Boussinesq approximation is used and the flow is 2-D and incompressible where Cartesian coordinate system is used for the analysis.

3.2.1. Continuity Equation

The continuity equation is derived based on the conservation of mass law. The general form of continuity equation is;

$$\frac{\partial \rho}{\partial t} + \vec{\nabla}.(\rho\vec{V}) = 0 \tag{3.1}$$

For an incompressible flow it can be reduced to the following form;

$$\vec{\nabla}.\vec{V} = 0 \tag{3.2}$$

Hence, the continuity equation can be written as below for rectangular coordinates for 2-D flow as;

$$\frac{\partial u}{\partial x} + \frac{\partial v}{\partial y} = 0 \tag{3.3}$$

3.2.2. Momentum Equation

Navier-Stokes equations in 2-D rectangular coordinates for any viscous, incompressible Newtonian fluid with varying viscosity are;

$$\rho\frac{Du}{Dt} = \rho f_x - \frac{\partial p}{\partial x} + \frac{\partial}{\partial x}\left[2\mu\frac{\partial u}{\partial x}\right] + \frac{\partial}{\partial y}\left[\mu\left(\frac{\partial v}{\partial x} + \frac{\partial u}{\partial y}\right)\right] \tag{3.4}$$

$$\rho \frac{D\mathrm{v}}{D\mathrm{t}} = \rho \mathrm{f_y} - \frac{\partial \mathrm{p}}{\partial \mathrm{y}} + \frac{\partial}{\partial \mathrm{y}}\left[2\mu \frac{\partial \mathrm{v}}{\partial \mathrm{y}}\right] + \frac{\partial}{\partial \mathrm{x}}\left[\mu\left(\frac{\partial \mathrm{v}}{\partial \mathrm{x}} + \frac{\partial \mathrm{u}}{\partial \mathrm{y}}\right)\right] \tag{3.5}$$

In the above equations the fluid density is constant. When there is no body force in x-direction and with a constant fluid viscosity, the Navier-Stokes equations are simplified to the following forms;

x-component of momentum;

$$\frac{\partial \mathrm{u}}{\partial \mathrm{t}} + u\frac{\partial \mathrm{u}}{\partial \mathrm{x}} + \mathrm{v}\frac{\partial \mathrm{u}}{\partial \mathrm{y}} = -\frac{1}{\rho}\frac{\partial \mathrm{p}}{\partial \mathrm{x}} + \nu\left(\frac{\partial^2 \mathrm{u}}{\partial \mathrm{x}^2} + \frac{\partial^2 \mathrm{u}}{\partial \mathrm{y}^2}\right) \tag{3.6}$$

y-component of momentum;

$$\frac{\partial \mathrm{v}}{\partial \mathrm{t}} + u\frac{\partial \mathrm{v}}{\partial \mathrm{x}} + \mathrm{v}\frac{\partial \mathrm{v}}{\partial \mathrm{y}} = \mathrm{f_y} - \frac{1}{\rho}\frac{\partial \mathrm{p}}{\partial \mathrm{y}} + \nu\left(\frac{\partial^2 \mathrm{v}}{\partial \mathrm{x}^2} + \frac{\partial^2 \mathrm{v}}{\partial \mathrm{y}^2}\right) \tag{3.7}$$

3.2.3. Energy Equation

Energy equation in terms of fluid enthalpy is defined by;

$$\rho \frac{D\mathrm{I}}{D\mathrm{t}} = \nabla(k\nabla T) + \frac{D\mathrm{p}}{D\mathrm{t}} + \Phi + \dot{q} \tag{3.8}$$

where I is the enthalpy and defined as:

$$\mathrm{I} = U + \frac{\mathrm{p}}{\rho} \tag{3.9}$$

In the energy equation 3.8, the term in the left side is the convective term. The first term in the right side is the rate of heat diffusion to the fluid particles where the second term is the rate of reversible work done on the fluid particles by compression. The third term is the rate of viscous dissipation per unit volume and the last term represents the heat generation per unit volume. For an incompressible fluid with constant thermal conductivity, no viscous heat dissipation, no compression work and without heat generation, Equation 3.8 is simplified to;

$$\frac{\partial \mathrm{T}}{\partial \mathrm{t}} + u\frac{\partial \mathrm{T}}{\partial \mathrm{x}} + \mathrm{v}\frac{\partial \mathrm{T}}{\partial \mathrm{y}} = \alpha\left(\frac{\partial^2 \mathrm{T}}{\partial \mathrm{x}^2} + \frac{\partial^2 \mathrm{T}}{\partial \mathrm{y}^2}\right) \tag{3.10}$$

3.2.4. Set of Governing Equations

Then, the set of governing equations in 2-D rectangular coordinates which are continuity, momentum in X and Y directions and energy equations are;

$$\frac{\partial u}{\partial x} + \frac{\partial v}{\partial y} = 0 \tag{3.11}$$

$$\frac{\partial u}{\partial t} + u\frac{\partial u}{\partial x} + v\frac{\partial u}{\partial y} = -\frac{1}{\rho}\frac{\partial p}{\partial x} + \nu\left(\frac{\partial^2 u}{\partial x^2} + \frac{\partial^2 u}{\partial y^2}\right) \tag{3.12}$$

$$\frac{\partial v}{\partial t} + u\frac{\partial v}{\partial x} + v\frac{\partial v}{\partial y} = f_y - \frac{1}{\rho}\frac{\partial p}{\partial y} + \nu\left(\frac{\partial^2 v}{\partial x^2} + \frac{\partial^2 v}{\partial y^2}\right) \tag{3.13}$$

$$\frac{\partial T}{\partial t} + u\frac{\partial T}{\partial x} + v\frac{\partial T}{\partial y} = \alpha\left(\frac{\partial^2 T}{\partial x^2} + \frac{\partial^2 T}{\partial y^2}\right) \tag{3.14}$$

These equations are valid for the present problem; however, density is a function of temperature. Generally, Boussinesq approximation is employed to convert the problem into steady state. In the next two sections, the Bousinesq approximation for boundary layer flows and the present problem are described.

3.3. Boussinesq Approximation for Boundary Layer Flows

As forced convection, the equations that describe momentum and energy transfer in free convection originate from the related conservation principles. The difference between the two flows is that, in free convection a major role is played by buoyancy forces. It is such forces that, in fact, sustain the flow (Incropera and Dewitt 2002).

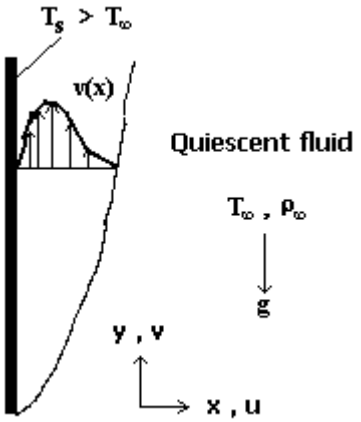

Figure 3.2. Vertical plate.

Consider a laminar boundary layer flow shown in figure above that is driven by buoyancy forces. Assume unsteady, two-dimensional, constant property conditions in which the gravity force acts in the negative y direction. Also, with one exception, assume the fluid to be incompressible. The exception involves accounting for the effect of variable density in the buoyancy force, since it is this variation that induces fluid motion. The last assumption is that boundary layer approximations are valid. With the foregoing simplifications the y-momentum equation 3.13 for the unsteady, two dimensional flow of an incompressible fluid with constant properties reduces to the boundary layer equation 3.15, except that the body force term f_y is retained. If the only contribution to this force is made by gravity, the body force per unit volume is $f_y = - g$, where g is the local acceleration due to gravity. Boussinesq approximation says that density at all terms of the momentum equation is constant except the body force term. Then, $\rho = \rho(T)$ for the body force;

$$\rho\frac{\partial \mathrm{v}}{\partial \mathrm{t}} + \rho u\frac{\partial \mathrm{v}}{\partial \mathrm{x}} + \rho \mathrm{v}\frac{\partial \mathrm{v}}{\partial \mathrm{y}} = -\frac{\partial \mathrm{p}}{\partial \mathrm{y}} + \mu\frac{\partial^2 \mathrm{v}}{\partial \mathrm{y}^2} - \rho \mathrm{g} \qquad (3.15)$$

Equation 3.15 may be couched in a more convenient form by first noting that, if there is no body force in x-direction, $(\frac{\partial \mathrm{p}}{\partial \mathrm{x}}) = 0$ from the x- momentum equation 3.12 which means the pressure does not vary in the direction normal to the surface. Hence the y-pressure gradient at any point in the boundary layer must equal to the pressure

gradient in the quiescent region outside the boundary layer. However, in this region v=0 and the Equation 3.15 reduces to;

$$\frac{\partial \mathrm{p}}{\partial \mathrm{y}} = -\rho_{\infty} g \tag{3.16}$$

By substituting Equation 3.16 into 3.15 and performing some mathematical manipulations, the following equation for the momentum in y-direction is obtained;

$$\frac{\partial \mathrm{v}}{\partial \mathrm{t}} + u\frac{\partial \mathrm{v}}{\partial \mathrm{x}} + \mathrm{v}\frac{\partial \mathrm{v}}{\partial \mathrm{y}} = g\left(\frac{\Delta\rho}{\rho}\right) + \nu\frac{\partial^2 \mathrm{v}}{\partial \mathrm{x}^2} \tag{3.17}$$

where $\Delta\rho = \rho_{\infty} - \rho$ and the expression must apply at every point in the free convection boundary layer. The first term on the right-hand side of 3.17 is the buoyancy force, and flow originates because the density ρ is a variable. If density variations are due only to temperature variations, the term may be related to a fluid property known as the volumetric thermal expansion coefficient which is;

$$\beta = -\frac{1}{\rho}\left(\frac{\partial\rho}{\partial T}\right)_p \tag{3.18}$$

This thermodynamic property of the fluid provides a measure of the amount by which the density changes in response to a change in temperature at constant pressure. If it is expressed in the following approximate form;

$$\beta \approx -\frac{1}{\rho}\left(\frac{\Delta\rho}{\Delta T}\right) = -\frac{1}{\rho}\frac{\rho_{\infty} - \rho}{T_{\infty} - T} \tag{3.19}$$

it follows that;

$$(\rho_{\infty} - \rho) \approx \rho\beta(T - T_{\infty}) \tag{3.20}$$

This simplification is known as the Boussinesq approximation and substituting into Equation 3.15, the y-momentum equation becomes;

$$\frac{\partial \mathrm{v}}{\partial \mathrm{t}} + u\frac{\partial \mathrm{v}}{\partial \mathrm{x}} + \mathrm{v}\frac{\partial \mathrm{v}}{\partial \mathrm{y}} = g\beta(T - T_{\infty}) + \nu\frac{\partial^2 \mathrm{v}}{\partial \mathrm{x}^2} \tag{3.21}$$

where it is now apparent how the bouyancy force, which drives the flow.

In fluid dynamics, the Boussinesq approximation (named for Joseph Valentin Boussinesq) is used in the field of buoyancy-driven flow that is known as natural convection. It states that density differences are sufficiently small to be neglected, except where they appear in terms multiplied by g, the acceleration due to gravity.

3.4. Boussinesq Approximation for the Considered Problem

In this study, the body force acting in the negative y-direction is the gravity force g and there is no body force in x- direction. If density variations are due only to temperature variations (p=constant), the Boussinesq approximation can be applied into the y-momentum equation 3.16 by considering the dynamic and static pressures;

$$\rho\frac{\partial \mathrm{v}}{\partial \mathrm{t}}+\rho u\frac{\partial \mathrm{v}}{\partial \mathrm{x}}+\rho \mathrm{v}\frac{\partial \mathrm{v}}{\partial \mathrm{y}}=-\frac{\partial \mathrm{p}_{\mathrm{dynamic}}}{\partial \mathrm{y}}+\mu(\frac{\partial^2 \mathrm{v}}{\partial \mathrm{x}^2}+\frac{\partial^2 \mathrm{v}}{\partial \mathrm{y}^2})-\frac{\partial \mathrm{p}_{\mathrm{static}}}{\partial \mathrm{y}}-\rho g \qquad (3.22)$$

By introducing 3.20 into 3.21;

$$\rho\frac{\partial \mathrm{v}}{\partial \mathrm{t}}+\rho u\frac{\partial \mathrm{v}}{\partial \mathrm{x}}+\rho \mathrm{v}\frac{\partial \mathrm{v}}{\partial \mathrm{y}}=-\frac{\partial \mathrm{p}_{\mathrm{dynamic}}}{\partial \mathrm{y}}+\mu(\frac{\partial^2 \mathrm{v}}{\partial \mathrm{x}^2}+\frac{\partial^2 \mathrm{v}}{\partial \mathrm{y}^2})+\rho_\infty g-\rho g \qquad (3.23)$$

Equation 3.23 can be rearranged to get $(\rho_\infty-\rho)$;

$$\rho\frac{\partial \mathrm{v}}{\partial \mathrm{t}}+\rho u\frac{\partial \mathrm{v}}{\partial \mathrm{x}}+\rho \mathrm{v}\frac{\partial \mathrm{v}}{\partial \mathrm{y}}=-\frac{\partial \mathrm{p}_{\mathrm{dynamic}}}{\partial \mathrm{y}}+\mu(\frac{\partial^2 \mathrm{v}}{\partial \mathrm{x}^2}+\frac{\partial^2 \mathrm{v}}{\partial \mathrm{y}^2})-g(\rho-\rho_\infty) \qquad (3.24)$$

And by using relation 3.20 in 3.24, following can be obtained;

$$\rho\frac{\partial \mathrm{v}}{\partial \mathrm{t}}+\rho u\frac{\partial \mathrm{v}}{\partial \mathrm{x}}+\rho \mathrm{v}\frac{\partial \mathrm{v}}{\partial \mathrm{y}}=-\frac{\partial \mathrm{p}_{\mathrm{dynamic}}}{\partial \mathrm{y}}+\mu(\frac{\partial^2 \mathrm{v}}{\partial \mathrm{x}^2}+\frac{\partial^2 \mathrm{v}}{\partial \mathrm{y}^2})+\rho g\beta(T-T_\infty) \qquad (3.25)$$

3.5. Dimensionless Continuity, Momentum and Energy Equations

The set of Equations 3.11, 3.12, 3.13 and 3.14 should be solved to obtain the unknowns u, v, p and T. By applying Boussinesq approximation and then introducing dimensionless parameters U, V, θ, τ ,P, X and Y;

$$X = \frac{x}{L},\ Y = \frac{y}{L},\ U = \frac{uL}{\alpha_f}, V = \frac{vL}{\alpha_f}, \theta_f = \frac{(T_f - T_c)}{(T_h - T_c)}, \tau = \frac{\alpha_f t}{L^2},\ P = \frac{L^2 p}{\rho \alpha_f^2} \quad (3.26)$$

Then, the set of equations in dimensionless form can be written as;

$$\frac{\partial U}{\partial X} + \frac{\partial V}{\partial Y} = 0 \quad (3.27)$$

$$\frac{\partial U}{\partial \tau} + U\frac{\partial U}{\partial X} + V\frac{\partial U}{\partial Y} = -\frac{\partial P}{\partial X} + Pr\left(\frac{\partial^2 U}{\partial X^2} + \frac{\partial^2 U}{\partial Y^2}\right) \quad (3.28)$$

$$\frac{\partial V}{\partial \tau} + U\frac{\partial V}{\partial X} + V\frac{\partial V}{\partial Y} = -\frac{\partial P}{\partial Y} + Pr\left(\frac{\partial^2 V}{\partial X^2} + \frac{\partial^2 V}{\partial Y^2}\right) + Ra.Pr.\theta_f \quad (3.29)$$

$$\frac{\partial \theta_f}{\partial \tau} + U\frac{\partial \theta_f}{\partial X} + V\frac{\partial \theta_f}{\partial Y} = \alpha\left(\frac{\partial^2 \theta_f}{\partial X^2} + \frac{\partial^2 \theta_f}{\partial Y^2}\right) \quad (3.30)$$

where Ra and Pr represents, Rayleigh and Prantdl numbers respectively; and θ_f is dimensionless temperature of fluid. The definitions of Rayleigh, Prandtl and Grashof numbers will be given in the next sections.

3.6. Definition of Dimensionless Parameters

3.6.1. Prandtl Number

The physical interpretation of the Prandtl number follows from its definition as a ratio of the momentum diffusivity ν to the thermal diffusivity α;

$$Pr = \frac{\nu}{\alpha^2} \quad (3.31)$$

The Prandtl number provides a measure of the relative effectiveness of momentum and energy transport by diffusion in the velocity and thermal boundary layers. When Prandtl number is very close to unity it means that energy and momentum transfer by diffusion are comparable. When it is smaller than one, the energy diffusion rate greatly exceeds the momentum diffusion rate. The opposite is true for Prandtl

values greater than one. From this interpretation it follows that the value of Prandtl strongly influences the relative growth of the velocity and thermal boundary layers.

3.6.2. Grashof Number

The Grashof number is a dimensionless number which is defined as follows;

$$Gr_L = \frac{g\beta(T_s - T_\infty)L^3}{\nu^2} \tag{3.32}$$

The Grashof number plays the same role in free convection that the Reynolds number plays in forced convection. Reynolds number provides a measure of the ratio of the inertial to viscous forces acting on a fluid element. In contrast, the Grashof number indicates the ratio of the buoyancy force to the viscous force acting on the fluid. Generally, the combined effects of free and forced convection must be considered when $\left(\frac{\mathrm{Gr_L}}{\mathrm{Re}_L^2}\right) \approx 1$. If the inequality $\left(\frac{\mathrm{Gr_L}}{\mathrm{Re}_L^2}\right) >> 1$ is satisfied forced convection effects may be neglected. In the strict sense, a free convection flow is one that is induced solely by buoyancy forces, in which case there is no well-defined forced convection velocity.

3.6.3. Rayleigh Number

It is important to note that free convection boundary layers are not restricted to laminar flow. Free convection flows typically originate from a thermal instability. That is warmer, lighter fluid moves vertically upward relative to cooler, heavier fluid. However, as with forced convection, hydrodynamic instabilities may also arise. That is, disturbances in the flow may be amplified, leading to transition from laminar to turbulent flow. Transition in a free convection boundary layer depends on the relative magnitude of the buoyancy and viscous forces in the fluid. It is customary to correlate its occurrence in terms of the Rayleigh number, which is simply the product of the Grashof and Prandtl numbers;

$$Ra_L = Gr_L \mathrm{Pr} = \frac{g\beta(T_s - T_\infty)L^3}{\nu\alpha} \tag{3.33}$$

For vertical plates the critical Rayleigh number is 10^9. Around this number transition to turbulence starts. Turbulence has a strong effect on heat transfer that is why special emphasis is placed on experimental results to obtain appropriate correlations for turbulence flow where Rayleigh number is greater than 10^9 (Incropera and Dewitt 2002). For square cavities, Rayleigh numbers less than 10^8 indicate a buoyancy-induced laminar flow, transition to turbulence occurs in the range of 10^8 to 10^{10} (Cai et al. 2009).

3.7. Definition of Streamfunction for Two Dimensional Flow of an Incompressible Fluid

For two-dimensional flow in the xy plane of Cartesian coordinate system, the continuity equation for an incompressible fluid is given at Equation 3.11. If a continuous function $\psi = \psi(x, y, t)$, which is known as the streamfunction, is defined such that (Aksel 2003) ;

$$\mathrm{u} = \frac{\partial \psi}{\partial \mathrm{y}} \text{ and } \mathrm{v} = -\frac{\partial \psi}{\partial \mathrm{x}} \tag{3.34}$$

Then the continuity equation 3.11 will exactly be satisfied, since;

$$\frac{\partial \mathrm{u}}{\partial \mathrm{x}} + \frac{\partial v}{\partial \mathrm{y}} = \frac{\partial}{\partial \mathrm{x}}\left(\frac{\partial \psi}{\partial \mathrm{y}}\right) + \frac{\partial}{\partial \mathrm{y}}\left(-\frac{\partial \psi}{\partial \mathrm{x}}\right) = 0 \tag{3.35}$$

By using the equation of a streamline, the following can be written;

$$udy - vdx = 0 \tag{3.36}$$

Substituting for the velocity components in terms of the streamfunction by using 3.34 yields;

$$\frac{\partial \psi}{\partial x} dx + \frac{\partial \psi}{\partial y} dy = 0 \tag{3.37}$$

Although the streamfunction is $\psi = \psi(x, y, t)$, it can be expressed as $\psi = \psi(x, y, t_0)$, at a certain instant of time, t_0. At this instant, the streamfunction can be

treated as though $\psi = \psi(x, y)$, so that the above equation becomes an exact or total differential along an instantaneous streamline.

$$\mathrm{d}\psi = \frac{\partial \psi}{\partial x} dx + \frac{\partial \psi}{\partial y} dy = 0 \tag{3.38}$$

Therefore, the streamfunction is constant along an instantaneous streamline for the two-dimensional flow of an incompressible fluid. One should note that although the streamlines can be three-dimensional, the streamfunction can only be defined for two-dimensional flow fields.

3.8. Definition of Vorticity for Two Dimensional Flow

The vorticity vector, $\vec{\xi}$, is defined as the curl of velocity vector, $\vec{V}$ (Aksel 2003);

$$\vec{\xi} = curl\,\vec{V} = \nabla x \vec{V} \tag{3.39}$$

For two-dimensional flow, Equation 3.39 can be written as;

$$\xi = \frac{\partial \mathrm{v}}{\partial \mathrm{x}} - \frac{\partial \mathrm{u}}{\partial y} \tag{3.40}$$

During rotation, the orientation of a fluid element changes but its position, shape and size remain same. When the fluid element moving in a flow field does not undergo any rotation, then the flow is known to be irrotational. For an irrotational flow;

$$\vec{\xi} = curl\,\vec{V} = \nabla x \vec{V} = 0 \tag{3.41}$$

3.9. Vorticity Transport Equation and Relation between Vorticity and Streamfunction

By taking the derivative of dimensionless x-momentum equation 3.28 with respect to Y and dimensionless y-momentum equation 3.29 with respect to X and then

arranging them together to eliminate the dimensionless pressure term P, the following equation can be obtained;

$$\frac{\partial}{\partial \tau}\left[-\frac{\partial U}{\partial Y}+\frac{\partial V}{\partial X}\right]+U\frac{\partial}{\partial \mathrm{X}}\left[-\frac{\partial U}{\partial Y}+\frac{\partial V}{\partial X}\right]+\mathrm{V}\frac{\partial}{\partial \mathrm{Y}}\left[-\frac{\partial U}{\partial Y}+\frac{\partial V}{\partial X}\right]= \\ \mathrm{Pr}\left[\frac{\partial^2}{\partial \mathrm{X}^2}\left(-\frac{\partial U}{\partial Y}+\frac{\partial V}{\partial X}\right)+\frac{\partial^2}{\partial \mathrm{Y}^2}\left(-\frac{\partial U}{\partial Y}+\frac{\partial V}{\partial X}\right)\right]+Ra\,\mathrm{Pr}\frac{\partial \theta_f}{\partial X} \tag{3.42}$$

The dimensionless vorticity can be defined as;

$$\Omega=\frac{\partial V}{\partial X}-\frac{\partial U}{\partial Y} \tag{3.43}$$

After introducing the dimensionless vorticity 3.43 into Equation 3.42;

$$\frac{\partial \Omega}{\partial \tau}+U\frac{\partial \Omega}{\partial \mathrm{X}}+\mathrm{V}\frac{\partial \Omega}{\partial \mathrm{Y}}=\mathrm{Pr}\left(\frac{\partial^2 \Omega}{\partial \mathrm{X}^2}+\frac{\partial^2 \Omega}{\partial \mathrm{Y}^2}\right)+\mathrm{Ra.Pr.}\frac{\partial \theta_{\mathrm{f}}}{\partial \mathrm{X}} \tag{3.44}$$

Equation 3.44 is the vorticity transport equation. The advantage of this equation is that the pressure term in the x-momentum and y-momentum equations is eliminated and the two equations become one single equation.

The dimensionless streamfunction can be defined as;

$$\mathrm{U}=\frac{\partial \Psi}{\partial \mathrm{Y}} \quad \text{and} \quad \mathrm{V}=-\frac{\partial \Psi}{\partial \mathrm{X}} \tag{3.45}$$

$$\frac{\partial \mathrm{U}}{\partial \mathrm{Y}}=\frac{\partial^2 \Psi}{\partial \mathrm{Y}^2} \quad \text{and} \quad \frac{\partial \mathrm{V}}{\partial \mathrm{X}}=-\frac{\partial^2 \Psi}{\partial \mathrm{X}^2} \tag{3.46}$$

From the definition of dimensionless vorticity 3.43 and by using 3.46;

$$\frac{\partial^2 \Psi}{\partial \mathrm{X}^2}+\frac{\partial^2 \Psi}{\partial \mathrm{Y}^2}=-\Omega \tag{3.47}$$

Equation 3.47 is the streamfunction equation which is showing the relation between dimensionless vorticity and dimensionless streamfunction.

3.10. Set of Equations in Vorticity-Streamfunction Form

By employing the dimensionless vorticity 3.43 and dimensionless streamfunction 3.45 parameters, the dimensionless form of the governing equations is obtained where the pressure term in the momentum equation is eliminated. With the application of vorticity-streamfunction approach, the following equations are obtained to find the unknown velocities and the temperature values;

$$\frac{\partial \Omega}{\partial \tau} + \frac{\partial U\Omega}{\partial X} + \frac{\partial V\Omega}{\partial Y} = \Pr\left(\frac{\partial^2 \Omega}{\partial X^2} + \frac{\partial^2 \Omega}{\partial Y^2}\right) + \mathrm{Ra.Pr.}\frac{\partial \theta_f}{\partial X} \tag{3.48}$$

$$\frac{\partial^2 \Psi}{\partial X^2} + \frac{\partial^2 \Psi}{\partial Y^2} = -\Omega \tag{3.49}$$

$$\frac{\partial \theta_f}{\partial \tau} + \frac{\partial U\theta_f}{\partial X} + \frac{\partial V\theta_f}{\partial Y} = \frac{\partial^2 \theta_f}{\partial X^2} + \frac{\partial^2 \theta_f}{\partial Y^2} \tag{3.50}$$

In the Equation 3.48, Rayleigh number is;

$$\mathrm{Ra} = \frac{g\beta(T_h - T_C)L^3}{\nu\alpha} \tag{3.51}$$

and the dimensionless vorticity and the dimensionless streamfunction are 3.43 and 3.45, respectively.

3.11. Dimensionless Heat Conduction Equation

Based on the defined dimensionless parameters, the dimensionless form of the heat conduction equation for the ceiling wall is;

$$\frac{\partial \theta_S}{\partial \tau} = \alpha^* \left(\frac{\partial^2 \theta_S}{\partial X^2} + \frac{\partial^2 \theta_S}{\partial Y^2}\right) \tag{3.52}$$

where $\theta_s = (T_s - T_c)/(T_h - T_c)$ and α^* are the ceiling wall dimensionless temperature and thermal diffusivity ratio (α_S / α_f), respectively.

3.12. Boundary Conditions

Boundary conditions are defined for the problem and governing equations are solved accordingly. For the study shown in Figure 3.3, the boundary conditions are defined as;

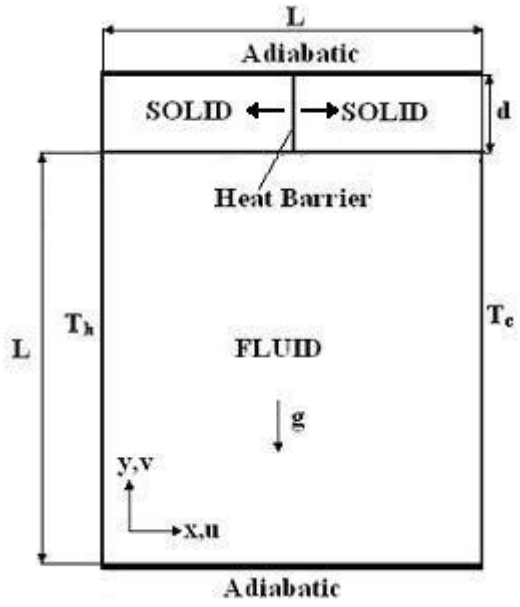

Figure 3.3. Considered enclosure.

On the bottom wall;

$$Y = 0; \qquad \Omega = -\frac{\partial U}{\partial Y}, \Psi = \frac{\partial \theta_f}{\partial Y} = 0 \tag{3.53}$$

On the top wall;

$$Y = 1 + D; \qquad \Omega = \Psi = \frac{\partial \theta_S}{\partial Y} = 0 \tag{3.54}$$

On the left and right walls;

$$X = 0,\ X = 1; \quad \Omega = \frac{\partial V}{\partial X}, \Psi = 0,\ \theta(0,Y,\tau) = 1, \theta(1,Y,\tau) = 0 \tag{3.55}$$

On the ceiling solid-fluid interface;

$$Y = 1; \qquad \Omega = -\frac{\partial \mathrm{U}}{\partial \mathrm{Y}},\ \Psi = 0,\ \theta_{\mathrm{S}} = \theta_{\mathrm{f}} \text{ and } K \left.\frac{\partial \theta_{\mathrm{S}}}{\partial \mathrm{Y}}\right|_{\mathrm{S}} = \left.\frac{\partial \theta_{\mathrm{f}}}{\partial \mathrm{Y}}\right|_{\mathrm{f}} \tag{3.56}$$

For the right and the left surfaces of heat barrier with $\ell^* = \ell / L$ thickness;

$$X = X_h + \ell^* / 2 \text{ or } \ X = X_h - \ell^* / 2, 1 < Y < 1 + D \ ; \ \frac{\partial \theta_S}{\partial X} = 0 \tag{3.57}$$

The thermal conductivity ratio and dimensionless wall thickness are shown by K and D, respectively. The following initial value for the vorticity, streamfunction and dimensionless temperature is used;

$$\Omega = \Psi = \theta_f = \theta_S = 0 \tag{3.58}$$

The dimensionless forms of the governing equations and boundary conditions reduce the number of independent dimensionless parameters to six which are Ra, Pr, K, α^*, D and $\mathrm{X_h}$. The thermal diffusivity ratio does not play role on the steady state results. The present study is performed for air with Pr = 0.71. Therefore, four dimensionless parameters which are Rayleigh number, thermal conductivity ratio, dimensionless ceiling wall thickness and dimensionless distance of heat barrier from the hot wall are taken into account.

3.13. Definition of Heatfunction for the Fluid and for the Solid Regions

Heatfunction for a dimensional convection problem is defined as;

$$J_X = \frac{\partial h}{\partial y} = \rho c_P u (T_f - T_C) - k_f \frac{\partial T_f}{\partial x} \tag{3.59}$$

$$J_Y = -\frac{\partial h}{\partial x} = \rho c_P v (T_f - T_C) - k_f \frac{\partial T_f}{\partial y} \tag{3.60}$$

where h is the dimensional heatfunction and J is the transport flux. By employing the dimensionless parameters;

$$\frac{\partial H_f}{\partial Y} = U\theta_f - \frac{\partial \theta_f}{\partial X} \quad \text{and} \quad -\frac{\partial H_f}{\partial X} = V\theta_f - \frac{\partial \theta_f}{\partial Y} \tag{3.61}$$

The symbol H_f represents dimensionless heatfunction of the fluid and it is defined based on the fluid thermal conductivity;

$$H_f = \frac{h}{(T_h - T_c)k_f} \tag{3.62}$$

Assuming H_f is continuous function to its second order derivatives yields the following dimensionless differential equation for heatfunction;

$$\frac{\partial^2 H_f}{\partial \mathrm{X}^2} + \frac{\partial^2 H_f}{\partial \mathrm{Y}^2} = \frac{\partial U\theta_f}{\partial \mathrm{Y}} - \frac{\partial V\theta_f}{\partial \mathrm{X}} \tag{3.63}$$

The dimensional definition of heatfunction for the solid region is;

$$-\frac{\partial h}{\partial x} = -k_S \frac{\partial T_S}{\partial y} \quad \text{and} \quad \frac{\partial h}{\partial y} = -k_S \frac{\partial T_S}{\partial x} \tag{3.64}$$

By employing the dimensionless parameters;

$$-\frac{\partial H_S}{\partial X} = -\frac{\partial \theta_S}{\partial Y} \quad \text{and} \quad \frac{\partial H_S}{\partial Y} = -\frac{\partial \theta_S}{\partial X} \tag{3.65}$$

The symbol H_S represents dimensionless heatfunction for the solid region and it is defined based on the solid thermal conductivity;

$$H_S = \frac{h}{(T_h - T_c)k_S} \tag{3.66}$$

The comparison between the definitions of solid and fluid dimensionless heat functions shows that the values of H_f and H_S are not the same at the solid-fluid interface and a discontinuity exits there. A point at the interface has two dimensionless heat function values due to different definitions of H_f and H_S. Modified heatfunction for solid region is defined to solve the problem;

$$H_{ms} = H_s K = \frac{h}{(T_h - T_c)k_f} \tag{3.67}$$

By using the definition of the modified heatfunction for solid region;

$$-\frac{\partial H_{ms}}{\partial X} = -K\frac{\partial \theta_s}{\partial Y} \quad \text{and} \quad \frac{\partial H_{ms}}{\partial Y} = -K\frac{\partial \theta_S}{\partial X} \tag{3.68}$$

Taking derivatives of the above equations with respect to X and Y yields the following modified heatfunction equation for solid region;

$$\frac{\partial^2 H_{ms}}{\partial \mathrm{X}^2} + \frac{\partial^2 H_{ms}}{\partial \mathrm{Y}^2} = 0 \tag{3.69}$$

3.14. Boundary Conditions for the Heatfunction Equations

Equations 3.63 and 3.69 are the dimensionless heatfunction equations governing fluid and solid regions respectively, and they can be solved numerically. The boundary conditions for equation 3.63 are obtained from the integration of Equation 3.61 along the considered boundary. In the same way, the boundary conditions for Equation 3.69 are obtained from the integration of Equation 3.68. For example, the dimensionless heat function values at X=0 and Y=1 boundaries are determined as;

At $X = 0$ and $0 < Y \leq 1$ $$H(0,Y) = H(0,0) - \int_0^Y \frac{\partial \theta_f}{\partial X} dY \tag{3.70}$$

At $X = 0$ and $1 < Y \leq 1 + D$ $$H(0,Y) = H(0,1) - \int_1^Y K\frac{\partial \theta_s}{\partial X} dY \tag{3.71}$$

At $Y = 1$ and $0 < X \leq 1$ $$H(X,1) = H(0,1) + \int_0^X \frac{\partial \theta_f}{\partial Y} dX \tag{3.72}$$

where at the boundary Y = 0, the values of heat function are taken as zero, H(X,0) = 0.

CHAPTER 4

SOLUTION APPROACHES AND METHODS

The conservation laws governing the flow and heat transfer for laminar natural convection have already been transformed to the three partial differential equations for temperature, vorticity and streamfunction. Thus, we have three equations with three unknowns (θ, Ω, Ψ) and it is mathematically possible to find a solution for these three dependent variables for any well defined problem. For the flow geometries of interest in this study, the analytical approach is not possible since the governing equations are highly nonlinear and strongly coupled. However, it is possible to solve these governing equations by using numerical techniques. In this study, finite difference technique is employed to solve the governing equations (energy, vorticity and streamfunction equations). Finite difference technique is an approximate solution technique. A differential equation is converted to a system of algebraic equations which can be solved by the finite difference solution methods.

4.1. Time Marching Approach

The steady behaviors of flow and temperature distribution are investigated in this study. The steady solution of the governing equations can be obtained from the solution of the either steady form or transient form of the governing equations (Roach 1976). The later approach is generally known as time marching approach. In fact, there is no difference between the steady results of two approaches if the solution of the governing equations is unique. The choice of the approach is important due to the stability and the convergence of the numerical procedure. For this reason, it may be useful to briefly compare these approaches.

Stability considerations are well known for time dependent partial differential equations in finite difference technique (Chapra and Candle 1988). Discretization of time and space variables can easily be performed by using the known stability criteria. However, the stability of the numerical method for the steady form of the equation

depends on the experience of the user in the numerical methods, since there is no available stability criterion.

When the governing equations are numerous and coupled, time marching approach may be more stable. In time marching approach, to find the solution of the governing equations for a time step, governing equations can be solved many times at the same time step. This repetition of solving the governing equations for a certain time step provides the simultaneous solution of the governing equations at that time step.

It is difficult to control the speed of propagation of dependent variables in the computational domain, when the steady forms of the partial differential equations are solved. For this reason, determination of the suitable relaxation factor for the solution procedure requires a computational experience. However, in time marching approach, the speed of the propagation of the dependent variables in the computational domain can be controlled by adjusting the value of the time interval. The value of time interval can be determined by considering the physical condition of the problem. If the speed of the propagation of dependent variables in the domain is very high (like a heat transfer in a highly conductive material) small time interval can be employed to prevent divergence of the solution procedure.

In time marching approach, it is possible to decrease the computational time of the solution procedure by increasing the value of time interval when the results converge to the steady state.

The main disadvantage of the time marching approach is the accumulation of truncation errors due to the discretization of time. Truncation errors of the time dependent terms can be minimized by using fine time intervals.

In the present study, time marching approach is adopted to obtain the steady results of the governing equations by solving them in the transient form, since the governing equations are numerous (3 equations) and highly coupled.

4.2. Generic Forms of the Governing Equations

Since the energy equation 3.50 and the vorticity equation 3.48 are similar to each other, they can be expressed in the form of a single generic equation (Mobedi 1994);

$$\frac{\partial \phi}{\partial \tau} + U\frac{\partial \phi}{\partial X} + V\frac{\partial \phi}{\partial Y} = C\left(\frac{\partial^2 \phi}{\partial X^2} + \frac{\partial^2 \phi}{\partial Y^2}\right) + f \qquad (4.1)$$

where ϕ is a generic dependent variable representing Ω and θ. The equivalencies of ϕ, C and f which are generic variables for Equations 3.50 and 3.48 are given in Table 4.1.

Table 4.1. Equivalencies of generic variables ϕ, C and f for Equations 3.50, 3.48.

Equation Number	ϕ	C	f
3.50	θ_f	1	----------
3.48	Ω	Pr	$Ra\,\mathrm{Pr}\frac{\partial \theta_f}{\partial X}$

Equation 4.1 contains the following four groups of terms:

i) Time term ($\frac{\partial \phi}{\partial \tau}$) which refers to the variation of dependent variable with time.

ii) Convection terms ($U\frac{\partial \phi}{\partial X}, V\frac{\partial \phi}{\partial Y}$) which refer to the convective transport.

iii) Diffusion terms ($\frac{\partial^2 \phi}{\partial X^2}, \frac{\partial^2 \phi}{\partial Y^2}$) which refer to the diffusive transport.

iv) Source term (f) which is the cause of flow of fluid in natural convection.

The streamfunction equation 3.49 and the heatfunction equation 3.63 contain diffusion terms only. Therefore, they are similar to each other and they can be written in a single generic equation;

$$\frac{\partial^2 \phi}{\partial X^2} + \frac{\partial^2 \phi}{\partial Y^2} = R \qquad (4.2)$$

The equivalencies of the generic variables ϕ and R for the Equations 3.49 and 3.63 are given in Table 4.2.

Table 4.2. Equivalencies of generic variables ϕ and R for Equations 3.49, 3.63.

Equation Number	ϕ	R
3.49	Ψ	$-\Omega$
3.63	H_f	$\frac{\partial U\theta_f}{\partial Y}-\frac{\partial V\theta_f}{\partial X}$

Energy equations (Equation 3.50 and dimensionless heat conduction equation 3.52) and the equation of vorticity 3.48 components are similar to each other; they are parabolic in time and elliptic in space. Therefore, the same finite difference solution method can be employed to solve them. However, the equation of streamfunction 3.49 and the dimensionless heatfunction equation 3.63 components are elliptic and they should be solved by another convenient finite difference method.

4.3. Finite Difference Solution Technique

Finite difference solution technique enables the determination of the values of dependent variable of a given differential equation at any discrete point in the computational domain. Figure 4.1 shows a two dimensional computational domain in Cartesian coordinate system which is subdivided into the number of small regions. There is a reference point at the center of the each subdivided region which is generally called as a node. Any node (i,j) in the two dimensional computational domain has four neighboring nodes as shown in Figure 4.2.

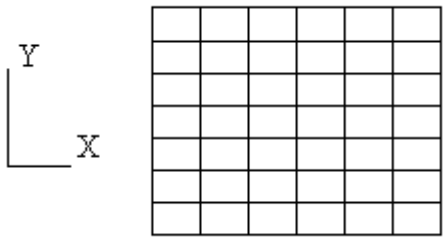

Figure 4.1. A two dimensional computational domain in Cartesian coordinate.

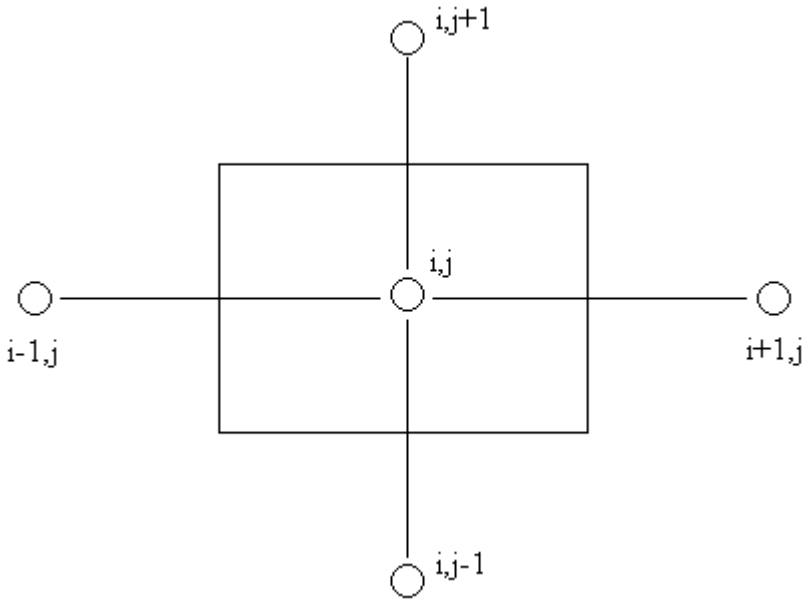

Figure 4.2. A node (i,j) with its neighboring nodes in Cartesian coordinate.

Finite difference technique enables writing the spatial derivatives of a differential equation for a node (i,j) in terms of the values of dependent variable at that node and its neighboring nodes. Hence, the differential equation for the node (i,j) can be reduced to an approximate algebraic equation and the solution of the algebraic equation yields the value of dependent variable at node (i,j).

In order to obtain the value of dependent variable of a time dependent differential equation at any node in the computational domain, addition to discretization in space, the problem must also be discretized in time. Therefore, a time interval should be defined and time derivative of the differential equation should be written in terms of values of dependent variable; for example, at the beginning and end instant of the time intervals. In this study, the superscript n is used to denote the time dependence of the dependent variable.

4.4. Finite Difference Solution Method for Parabolic Differential Equations

Equation 4.1 can be reduced to the following form;

$$\frac{\partial \phi}{\partial \tau} = \delta_X^2 \phi + \delta_Y^2 \phi + f \tag{4.3}$$

In the Equation 4.3, $\delta_X^2 \phi$ and $\delta_Y^2 \phi$ are;

$$\delta_X^2 \phi = C\frac{\partial^2 \phi}{\partial X^2} - U\frac{\partial \phi}{\partial X} \tag{4.4}$$

$$\delta_Y^2 \phi = C\frac{\partial^2 \phi}{\partial Y^2} - V\frac{\partial \phi}{\partial Y} \tag{4.5}$$

Terms δ_X^2 and δ_Y^2 refer to diffusion and convection transport in X and Y directions, respectively. For this reason, they can be called as diffusion-convection terms.

The parabolic partial differential equations can be solved by various finite difference methods. Those methods are generally classified into three types, namely, explicit, implicit and ADI (Alternating Direction Implicit) methods (Thiault 1985). In order to choose a convenient method for solving the parabolic differential equation 4.3 of this study, these finite difference solution methods are compared.

i) Explicit Methods:

Application of the explicit method on Equation 4.3 for any node (i,j) in Cartesian coordinates when a simple forward difference for the time term is used can be written as;

$$\frac{\phi_{i,j}^{n+1} - \phi_{i,j}^{n}}{\Delta \tau} = \delta_X^2 \phi_{i,j}^{n} + \delta_Y^2 \phi_{i,j}^{n} + f_{i,j}^{n} \tag{4.6}$$

where $\phi_{i,j}^{n}$ and $\phi_{i,j}^{n+1}$ refer to the value of dependent variable ϕ at node (i,j) at n^{th} and $(n+1)^{th}$ time steps, respectively. As it can be seen from Equation 4.6 the unknown value of dependent variable at a node (i,j) , $\phi_{i,j}^{n+1}$, can be determined by taking the

numerical spatial derivatives of dependent variable in the previous time step ,n^{th} . Hence, determination of the unknown $\phi_{i,j}^{n+1}$ in Equation 4.6 is simple since the values of the dependent variable at all nodes of the computational domain at n^{th} time step are known.

Practically, the explicit methods are not convenient for the computational fluid dynamic problems since strong stability requirements should be satisfied to obtain a stable solution. In explicit methods, propagation of the dependent variable is done node by node. Therefore, stability of the method requires the use of small grid sizes or small time interval which needs high computer storage and computational time (Roach 1976).

ii) Implicit Methods

Application of a fully implicit method on Equation 4.3 for any node (i,j) in Cartesian coordinates, when a simple forward difference for time term is used, can be written as;

$$\frac{\phi_{i,j}^{n+1}-\phi_{i,j}^{n}}{\Delta\tau}=\delta_{X}^{2}\phi_{i,j}^{n+1}+\delta_{Y}^{2}\phi_{i,j}^{n+1}+f_{i,j}^{n+1} \qquad (4.7)$$

In implicit method, determination of the value of dependent variable at a new time step for a node (i,j) , $\phi_{i,j}^{n+1}$, depends on the spatial derivatives of dependent variable at the same time step. Hence, in order to determine the values of dependent variable for a new time step in the computational domain with m nodes, m nodal equations have to be obtained and then solved. Therefore, the solution of the parabolic differential equations with implicit method may be more complicated than explicit method.

Fully implicit methods are more desirable for the computational fluid problems In the fully implicit methods, the speed of the propagation of dependent variable in the computational domain is infinite and therefore they become as unconditionally stable methods (Roach 1976). Results can be obtained for the larger time interval or grid size compared to the explicit methods. Although, implicit methods are theoretically

convenient for the computational fluid problems, practically large matrices must be solved to obtain results.

iii) ADI methods

ADI methods are more convenient than implicit methods for computational fluid problems. They provide simple tridiagonal matrices instead of the large matrices of the fully implicit method. The tridiagonal matrices can easily be solved without any iteration by employing Thomas Algorithm method (Roach 1976). Generally for two dimensional problems, in an ADI method, the parabolic differential equation is implicitly solved in X direction while leaving the Y direction explicit. Then, the equation is implicitly solved in a similar way in Y direction. By this way, ADI method reduces a two dimensional implicit method to a series of one dimensional implicit methods. Moreover, the most of the ADI methods are unconditionally stable methods which enable the solution of the parabolic differential equations for large grid sizes and time intervals. The problem of this study is two dimensional, and to get higher order accuracy and to get rid of large matrices of the fully implicit method, ADI method is used.

Application of the ADI method on Equation 4.3 for any node (i,j) in Cartesian coordinates when a simple forward difference for the time term is used can be written in two steps as;

$$\frac{\phi_{i,j}^{n+1/2}-\phi_{i,j}^{n}}{\Delta\tau/2}=\delta_X^2\phi_{i,j}^{n+1/2}+\delta_Y^2\phi_{i,j}^{n}+f_{i,j}^{n} \tag{4.8}$$

$$\frac{\phi_{i,j}^{n+1}-\phi_{i,j}^{n+1/2}}{\Delta\tau/2}=\delta_X^2\phi_{i,j}^{n+1/2}+\delta_Y^2\phi_{i,j}^{n+1}+f_{i,j}^{n+1/2} \tag{4.9}$$

where the Equation 4.8 is implicit for x-direction and explicit for y-direction and the Equation 4.9 is implicit for y-direction and explicit for x-direction. Determination of the value of dependent variable at a new time step $(n+1/2)^{th}$ for a node (i,j) , $\phi_{i,j}^{n+1/2}$, depends on the spatial derivatives of dependent variable at the same time step for x-direction and the numerical spatial derivatives of dependent variable in the previous time step n^{th} for y-direction. As a second step, the determination of the value of

dependent variable at a new time step (n+1)th for a node (i,j) , $\phi_{i,j}^{n+1}$, depends on the spatial derivatives of dependent variable at the same time step for y-direction and the numerical spatial derivatives of dependent variable in the previous time step (n+1/2)th for y-direction.

Equation 4.8 can be arranged as;

$$\left(1-\frac{\Delta\tau}{2}\delta_{\mathrm{X}}^{2}\right)\phi_{i,j}^{n+1/2}=\left(1+\frac{\Delta\tau}{2}\delta_{\mathrm{Y}}^{2}\right)\phi_{i,j}^{n}+\frac{\Delta\tau}{2}\mathrm{f}_{\mathrm{i,j}}^{\mathrm{n}} \tag{4.10}$$

Similarly, Equation 4.9 can be arranged as;

$$\left(1-\frac{\Delta\tau}{2}\delta_{\mathrm{Y}}^{2}\right)\phi_{i,j}^{n+1}=\left(1+\frac{\Delta\tau}{2}\delta_{\mathrm{X}}^{2}\right)\phi_{i,j}^{n}+\frac{\Delta\tau}{2}\mathrm{f}_{\mathrm{i,j}}^{\mathrm{n+1/2}} \tag{4.11}$$

Determination of δ_X and δ_Y will be explained in Chapter 5. After defining them, the value of dependent variable $\phi_{i,j}^{n+1}$ at a new time step can be found.

As it can be seen, the major advantage of ADI method with respect to a fully implicit method is that the solution of the parabolic differential equation for a time step can be obtained after two steps. However, more iteration has to be performed in order to obtain a solution for a time step if a fully implicit method is used.

4.5. Finite Difference Solution Method for Elliptic Differential Equations

Since the elliptic equations do not depend on time and they are simple diffusion equations, it is more suitable to solve these equations by iterative methods rather than using the matrix inversion. The streamfunction equation 3.49 and the heatfunction equation 3.63 written in the generic form of Equation 4.2 involve diffusion terms only. Therefore, they can be solved point by point.

CHAPTER 5

FINITE DIFFERENCE FORMULATION

As it was mentioned before, in this study, time marching approach is used to solve the set of the governing equations. In the previous section, the solution procedure, which is employed to solve the set of the governing equations, was explained. After reviewing the available finite difference solution methods for parabolic differential equations, ADI finite difference solution method was adopted to solve the energy and vorticity equations. The streamfunction and the heatfunction equations however, are solved by an iterative method rather than matrix inversion technique. In this chapter, the finite difference forms of diffusion and convection terms of Equations 4.1 and 4.2 will be given.

5.1. Finite Difference Formulation of Diffusion and Convection Terms

The finite difference forms of diffusion and convection terms are written based on three point central differencing, which has second-order accuracy. Recall that the generic equation for the energy and vorticity equations are;

$$\frac{\partial \phi}{\partial \tau} + U\frac{\partial \phi}{\partial \mathrm{X}} + \mathrm{V}\frac{\partial \phi}{\partial \mathrm{Y}} = C\left(\frac{\partial^2 \phi}{\partial \mathrm{X}^2} + \frac{\partial^2 \phi}{\partial \mathrm{Y}^2}\right) + \mathrm{f} \tag{5.1}$$

Equation 5.1 can be written as;

$$\frac{\partial \phi}{\partial \tau} = \delta_X^2 \phi + \delta_Y^2 \phi + \mathrm{f} \tag{5.2}$$

where $\delta_X^2 \phi$ and $\delta_Y^2 \phi$ were defined in the Equations 4.4 and 4.5, respectively. They are the diffusion-convection terms for X and Y directions.

The generic equation for the streamfunction and heatfunction equations are;

$$\frac{\partial^2 \phi}{\partial \mathrm{X}^2} + \frac{\partial^2 \phi}{\partial \mathrm{Y}^2} = \mathrm{R} \tag{5.3}$$

As it is seen Equation 5.3 contains diffusion terms only.

In order to write the finite difference forms of the governing equations, the finite difference forms of the diffusion terms $\left(\frac{\partial^2 \phi}{\partial X^2}, \frac{\partial^2 \phi}{\partial \mathrm{Y}^2} \right)$ and the diffusion-convection terms $\left(\mathrm{C}\frac{\partial^2 \phi}{\partial X^2} - \mathrm{U}\frac{\partial \phi}{\partial \mathrm{X}} \ , \mathrm{C}\frac{\partial^2 \phi}{\partial Y^2} - \mathrm{V} \ \frac{\partial \phi}{\partial \mathrm{Y}} \right)$ must be obtained. It may be useful to first discuss the finite difference form of the diffusion terms $\left(\frac{\partial^2 \phi}{\partial X^2}, \frac{\partial^2 \phi}{\partial \mathrm{Y}^2} \right)$, before starting discussion about the finite difference form of the diffusion-convection terms.

By considering the linear variation of the dependent variable, ϕ , in the region between two grid lines, the finite difference form of the first derivatives of the dependent variable with respect to X at lines S and N which are shown in Figure 5.1 can be written as;

$$\left. \frac{\mathrm{d}\phi}{\mathrm{dX}} \right|_{\mathrm{S}} = \frac{\phi_{\mathrm{i}+1} - \phi_{\mathrm{i}}}{\Delta \mathrm{X}_{\mathrm{i}+1}} \tag{5.4}$$

$$\left. \frac{\mathrm{d}\phi}{\mathrm{dX}} \right|_{\mathrm{N}} = \frac{\phi_{\mathrm{i}} - \phi_{\mathrm{i}-1}}{\Delta \mathrm{X}_{\mathrm{i}}} \tag{5.5}$$

where lines S and N are located in the mid-point between their neighboring grid lines.

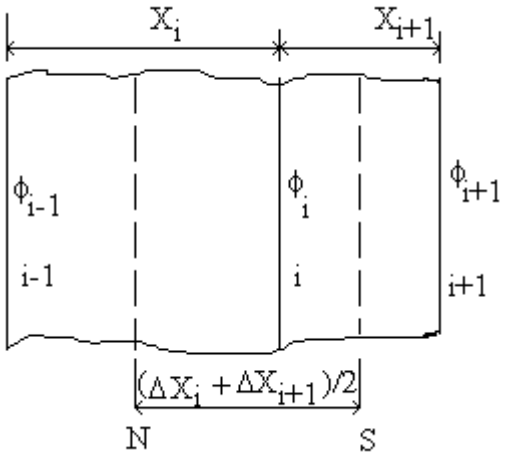

Figure 5.1. A one dimensional computational domain with non-uniform mesh grid lines.

The second derivative of the dependent variable with respect to X at grid line i can be written in terms of the first derivative of ϕ at lines S and N as;

$$\left.\frac{d^2\phi}{dX^2}\right|_i = \frac{\left.\frac{d\phi}{dX}\right|_S - \left.\frac{d\phi}{dX}\right|_N}{(\Delta X_i + \Delta X_{i+1})/2} \tag{5.6}$$

By substituting Equations 5.4 and 5.5 into Equation 5.6 yields the finite difference form of the diffusion term at grid line i for X direction;

$$\left.\frac{d^2\phi}{dX^2}\right|_i = \frac{2}{\Delta X_{i+1}(\Delta X_i + \Delta X_{i+1})}\phi_{i+1} - \frac{2}{\Delta X_i \cdot \Delta X_{i+1}}\phi_i + \frac{2}{\Delta X_i (\Delta X_i + \Delta X_{i+1})}\phi_{i-1} \tag{5.7}$$

The similar approach can be made for Y direction and the finite difference form of the diffusion term at that direction is obtained.

$$\left.\frac{d^2\phi}{dY^2}\right|_j = \frac{2}{\Delta Y_{j+1}(\Delta Y_j + \Delta Y_{j+1})}\phi_{j+1} - \frac{2}{\Delta Y_j \,.\, \Delta Y_{j+1}}\phi_j + \frac{2}{\Delta Y_j\,(\Delta Y_j + \Delta Y_{j+1})}\phi_{j-1} \tag{5.8}$$

The solution of the diffusion-convection term for the region between two neighboring grid lines i and i+1 in the one dimensional domain will be obtained. The diffusion-convection term in the region between grid lines i and i+1 for X direction is;

$$\delta_X^2 \phi = C\frac{\partial^2 \phi}{\partial X^2} - U\frac{\partial \phi}{\partial X} \tag{5.9}$$

The finite difference form of the term $C\dfrac{\partial^2 \phi}{\partial X^2}$ can be obtained by using 5.7.

In this study, the velocity value U of node i is taken as the velocity value of that node at the previous time step. The following form of finite difference is used for convection term;

$$U\frac{\partial \phi}{\partial X} = \frac{U_{i+1}\phi_{i+1} - U_{i-1}\phi_{i-1}}{\Delta X_i + \Delta X_{i+1}} \tag{5.10}$$

This kind of the finite difference is called as central difference scheme. This assumption is working so well for diffusion-convection problems where the convection effects are not strong. This is because the diffusion process affects the distribution of a transported quantity ϕ along its gradients in all directions, whereas convection spreads influence only in the flow direction. One of the major inadequacies of the central differencing for strong convective flow is that this scheme does not involve flow direction. Therefore, this study is limited for Rayleigh numbers up to 10^6 to get accurate results since above this value; the convective flow is very strong.

Then, the finite difference form of the diffusion-convection term $\left(C\frac{\partial^2 \phi}{\partial X^2} - U\frac{\partial \phi}{\partial X} \right)$ for node (i,j) is;

$$\delta_X^2 \phi = C\frac{\partial^2 \phi}{\partial X^2} - U\frac{\partial \phi}{\partial X} = C\frac{2}{\Delta X_{i+1}(\Delta X_i + \Delta X_{i+1})}\phi_{i+1,j} - C\frac{2}{\Delta X_i \cdot \Delta X_{i+1}}\phi_{i,j} + C\frac{2}{\Delta X_i (\Delta X_i + \Delta X_{i+1})}\phi_{i-1,j} - \frac{U_{i+1,j}\phi_{i+1,j} - U_{i-1,j}\phi_{i-1,j}}{\Delta X_i + \Delta X_{i+1}} \quad (5.11)$$

The same procedure can be done for determining the finite difference form of the diffusion-convection term $\left(C\frac{\partial^2 \phi}{\partial Y^2} - V\frac{\partial \phi}{\partial Y} \right)$ of Y direction for node (i,j) as;

$$\delta_Y^2 \phi = C\frac{\partial^2 \phi}{\partial Y^2} - V\frac{\partial \phi}{\partial Y} = C\frac{2}{\Delta Y_{j+1}(\Delta Y_j + \Delta Y_{j+1})}\phi_{i,j+1} - C\frac{2}{\Delta Y_j \cdot \Delta Y_{j+1}}\phi_{i,j} + C\frac{2}{\Delta Y_j (\Delta Y_j + \Delta Y_{j+1})}\phi_{i,j-1} - \frac{V_{i,j+1}\phi_{i,j+1} - V_{i,j-1}\phi_{i,j-1}}{\Delta Y_j + \Delta Y_{j+1}} \quad (5.12)$$

By using Equations 5.11 and 5.12, the Equations 4.10 and 4.11 can be solved and the value of dependent variable $\phi_{i,j}^{n+1}$ at a new time step can be found.

By considering Equation 5.11, the finite difference form of diffusion-convection term for X direction at node (i,j) can be simplified into an equation in terms of the values of dependent variable at nodes (i-1,j) , (i,j) and (i+1,j) as follows;

$$\left. C\frac{\partial^2 \phi}{\partial X^2} - U\frac{\partial \phi}{\partial X} \right|_{i,j} = A_X(i,j).\phi_{i+1,j} + B_X(i,j,).\phi_{i,j} + C_X(i,j,).\phi_{i-1,j} \quad (5.13)$$

where $A_X(i, j)$, $B_X(i, j)$ and $C_X(i, j)$ are the multipliers of the dependent variables for node (i,j) and their equivalencies are tabulated in Table 5.1.

Table 5.1. Equivalencies of multipliers $A_X(i, j)$, $B_X(i, j)$ and $C_X(i, j)$ for a node (i,j).

A_X (i,j)	B_X (i,j)	C_X (i,j)
$\dfrac{2C - \Delta X_{i+1} U_{i+1, j}}{\Delta X_{i+1}(\Delta X_i + \Delta X_{i+1})}$	$\dfrac{-2C}{\Delta X_i \cdot \Delta X_{i+1}}$	$\dfrac{2C + \Delta X_i U_{i-1, j}}{\Delta X_{i+1}(\Delta X_i + \Delta X_{i+1})}$

The same method can be employed to obtain the finite difference form of diffusion-convection terms in Y direction for node (i,j);

$$C\frac{\partial^2 \phi}{\partial Y^2} - V\frac{\partial \phi}{\partial Y}\bigg|_{i, j} = A_Y(i, j).\phi_{i, j+1} + B_Y(i, j).\phi_{i, j} + C_Y(i, j,).\phi_{i, j-1} \qquad (5.14)$$

where the equivalencies of multipliers of node (i,j) in Y direction, $A_Y(i, j)$, $B_Y(i, j)$ and $C_Y(i, j)$ are given in Table 5.2.

Table 5.2. Equivalencies of multipliers $A_Y(i, j)$, $B_Y(i, j)$ and $C_Y(i, j)$ for a node (i,j).

A_Y (i,j)	B_Y (i,j)	C_Y (i,j)
$\dfrac{2C - \Delta Y_{j+1} V_{i, j+1}}{\Delta Y_{j+1}(\Delta Y_j + \Delta Y_{j+1})}$	$\dfrac{-2C}{\Delta Y_j \cdot \Delta Y_{j+1}}$	$\dfrac{2C + \Delta Y_j V_{i, j-1}}{\Delta Y_{j+1}(\Delta Y_j + \Delta Y_{j+1})}$

In the first step of ADI method, the values of the dependent variable in n^{th} time step, ϕ^n, should be employed to determine the values of $\phi^{n+1/2}$ at the all nodes of the computational domain. In the second step, the values of ϕ^{n+1} at all nodes of the computational domain should be obtained by using the values of $\phi^{n+1/2}$. The

application of the steps of ADI method on the generic form of energy and vorticity equations is going to be explained.

i) First step of ADI method:

Application of the ADI method on Equation 5.1 for any node (i,j) in Cartesian coordinates when a simple forward difference for the time term is used can be written in the first step as;

$$\frac{\phi_{i,j}^{n+1/2}-\phi_{i,j}^{n}}{\Delta\tau/2}=\left(C\frac{\partial^2\phi^{n+1/2}}{\partial X^2}-U\frac{\partial\phi^{n+1/2}}{\partial X}\right)\Bigg|_{i,j}+\left(C\frac{\partial^2\phi^{n}}{\partial Y^2}-V\frac{\partial\phi^{n}}{\partial Y}\right)\Bigg|_{i,j}+f_{i,j}^{n} \tag{5.15}$$

where the Equation 5.15 is implicit for x-direction and explicit for y-direction. Equation 5.15 can be rearranged as;

$$\frac{2}{\Delta\tau}\phi_{i,j}^{n+1/2}-\left(C\frac{\partial^2\phi^{n+1/2}}{\partial X^2}-U\frac{\partial\phi^{n+1/2}}{\partial X}\right)\Bigg|_{i,j}=\left(C\frac{\partial^2\phi^{n}}{\partial Y^2}-V\frac{\partial\phi^{n}}{\partial Y}\right)\Bigg|_{i,j}+\frac{2}{\Delta\tau}\phi_{i,j}^{n}+f_{i,j}^{n} \tag{5.16}$$

A new variable $D_X(i,j)$ can be defined and the right side of Equation 5.16 can be assigned to $D_X(i,j)$;

$$D_X(i,j)=\left(C\frac{\partial^2\phi^{n}}{\partial Y^2}-V\frac{\partial\phi^{n}}{\partial Y}\right)\Bigg|_{i,j}+\frac{2}{\Delta\tau}\phi_{i,j}^{n}+f_{i,j}^{n} \tag{5.17}$$

As it can be seen from Equation 5.17, all computations for the right side of the equation are based on the values of the dependent variable and the source term in the

previous time step. Hence, the value of $D_X(i, j)$ can be computed for any node (i,j) in the computational domain by substituting Equation 5.14 into 5.17;

$$D_X(i, j)=A_Y(i, j)\phi^{n}_{i, j+1}+B_Y(i, j,)\phi^{n}_{i, j}+C_Y(i, j,)\phi^{n}_{i, j-1}+\frac{2}{\Delta\tau}\phi^{n}_{i, j}+f^{n}_{i, j} \qquad (5.18)$$

where the values of multipliers $A_Y(i, j)$, $B_Y(i, j)$ and $C_Y(i, j)$ of node (i,j) in Y direction can be determined by using Table 5.2.

Then, the Equation 5.16 can be written in the following form;

$$\frac{2}{\Delta\tau}\phi^{n+1/2}_{i, j}-\left(C\frac{\partial^2\phi^{n+1/2}}{\partial X^2}-U\frac{\partial\phi^{n+1/2}}{\partial X}\right)\Bigg|_{i, j}=D_X(i, j) \qquad (5.19)$$

The left side of Equation 5.19 contains $\phi^{n+1/2}$ which is unknown and its values for all nodes of the computational domain have to be computed. By substituting Equation 5.13 into 5.19;

$$A_X(i, j)\phi^{n+1/2}_{i+1, j}+\left(1-\frac{2}{\Delta\tau}\right)B_X(i, j)\phi^{n+1/2}_{i, j}+C_X(i, j,)\phi^{n+1/2}_{i-1, j}=-D_X(i, j) \qquad (5.20)$$

where $A_X(i, j)$, $B_X(i, j)$ and $C_X(i, j)$ are multipliers of node (i,j) in X direction and as it was mentioned before, they are determined by using Table 5.1.

The application of Equation 5.20 to all nodes which are on a line of the computational domain in X direction yields the system of algebraic equations as 5.21, where m is the number of the nodes along X line;

$$A_X(2,j).\phi_{3,j}^{n+1/2}+\left(1-\frac{2}{\Delta\tau}\right)B_X(2,j).\phi_{2,j}^{n+1/2}+C_X(2,j).\phi_{1,j}^{n+1/2}=-D_X(2,j)$$

$$A_X(3,j).\phi_{4,j}^{n+1/2}+\left(1-\frac{2}{\Delta\tau}\right)B_X(3,j).\phi_{3,j}^{n+1/2}+C_X(3,j).\phi_{2,j}^{n+1/2}=-D_X(3,j)$$

$$A_X(4,j).\phi_{5,j}^{n+1/2}+\left(1-\frac{2}{\Delta\tau}\right)B_X(4,j).\phi_{4,j}^{n+1/2}+C_X(4,j).\phi_{3,j}^{n+1/2}=-D_X(4,j)$$

……. (5.21)

$$A_X(m-3,j).\phi_{m-2,j}^{n+1/2}+\left(1-\frac{2}{\Delta\tau}\right)B_X(m-3,j).\phi_{m-3,j}^{n+1/2}+C_X(m-3,j).\phi_{m-4,j}^{n+1/2}=-D_X(m-3,j)$$

$$A_X(m-2,j).\phi_{m-1,j}^{n+1/2}+\left(1-\frac{2}{\Delta\tau}\right)B_X(m-2,j).\phi_{m-2,j}^{n+1/2}+C_X(m-2,j).\phi_{m-3,j}^{n+1/2}=-D_X(m-2,j)$$

$$A_X(m-1,j).\phi_{m,j}^{n+1/2}+\left(1-\frac{2}{\Delta\tau}\right)B_X(m-1,j).\phi_{m-1,j}^{n+1/2}+C_X(m-1,j).\phi_{m-2,j}^{n+1/2}=-D_X(m-1,j)$$

The solution of system of tridiagonal algebraic equations 5.21 along the line X is possible since there are m-2 equations with m-2 unknowns when the boundary conditions for boundary nodes (1,j) and (m,j) are defined.

Although the system of the tridiagonal algebraic equations can be written in matrix form and solved by using matrix inversion technique or iterative method, Thomas Algorithm enables the solution of these equations without using the matrix inversion technique or iterative methods which decreases computational time. The solution method of the tridiagonal algebraic equations using Thomas Algorithm is given in (Roach 1976).

The solution of the system of tridiagonal algebraic equations 5.21 yields the values of $\phi^{n+1/2}$ at all nodes which are on the first row of X direction. However, the values of $\phi^{n+1/2}$ have to be determined for all nodes of the computational domain. In order to obtain those values, Equation 5.20 should be applied to the all lines of the computational domain which are in X direction by the same method explained above.

It may be useful to mention the finite difference form of the source term f before the application of the second step of ADI method. The finite difference form of the source term given at Table 4.1 for a node (i,j) can be written as:

$$f_{i,j} = RaPr \frac{\theta_{i+1,j} - \theta_{i-1,j}}{\Delta X_{i+1} + \Delta X_i} \tag{5.22}$$

ii) Second step of ADI method:

After obtaining the values of $\phi^{n+1/2}$ at all nodes of the computational domain, the second step of ADI method has to be applied to all nodes of the computational domain in order to determine the values of ϕ^{n+1} . The second step of ADI method for a node (i,j) in Cartesian coordinates is written in the following form;

$$\frac{\phi_{i,j}^{n+1} - \phi_{i,j}^{n+1/2}}{\Delta\tau/2} = \left(C\frac{\partial^2 \phi^{n+1/2}}{\partial X^2} - U\frac{\partial \phi^{n+1/2}}{\partial X} \right)\Bigg|_{i,j} + \left(C\frac{\partial^2 \phi^{n+1}}{\partial Y^2} - V\frac{\partial \phi^{n+1}}{\partial Y} \right)\Bigg|_{i,j} + f_{i,j}^{n+1/2} \tag{5.23}$$

Equation 5.23 is implicit for y-direction and explicit for x-direction and it can be rearranged as;

$$\frac{2}{\Delta\tau}\phi_{i,j}^{n+1} - \left(C\frac{\partial^2 \phi^{n+1}}{\partial Y^2} - V\frac{\partial \phi^{n+1}}{\partial Y} \right)\Bigg|_{i,j} = \left(C\frac{\partial^2 \phi^{n+1/2}}{\partial X^2} - U\frac{\partial \phi^{n+1/2}}{\partial X} \right)\Bigg|_{i,j} + \frac{2}{\Delta\tau}\phi_{i,j}^{n+1/2} + f_{i,j}^{n+1/2} \tag{5.24}$$

The above Equation 5.24 is similar to the Equation 5.16. The right side of 5.24 contains the known variables $\phi^{n+1/2}$ and the left side of it contains the unknown dependent variable ϕ^{n+1} which has to be determined for all nodes of the computational domain. The same procedure which was employed to obtain the finite difference form of Equation 5.16 can be employed to obtain the finite difference form of Equation 5.24.

For a node (i,j), the variable $D_Y(i,j)$ can be defined as;

$$D_Y(i,j)=\left(C\frac{\partial^2 \phi^{n+1/2}}{\partial X^2}-U\frac{\partial \phi^{n+1/2}}{\partial X} \right)\Bigg|_{i,j} + \frac{2}{\Delta\tau}\phi_{i,j}^{n+1/2} + f_{i,j}^{n+1/2} \qquad (5.25)$$

As it is seen from Equation 5.25, all computations for the right side of the equation are based on the values of the dependent variable found in the previous time step. Hence, the value of $D_Y(i,j)$ can be computed for any node (i,j) in the computational domain by substituting Equation 5.13 into 5.25;

$$D_Y(i,j)=A_X(i,j).\phi_{i+1,j}^{n+1/2}+B_X(i,j,).\phi_{i,j}^{n+1/2}+C_X(i,j,).\phi_{i-1,j}^{n+1/2}+\frac{2}{\Delta\tau}\phi_{i,j}^{n+1/2}+f_{i,j}^{n+1/2} \qquad (5.26)$$

where the values of multipliers $A_X(i,j)$, $B_X(i,j)$ and $C_X(i,j)$ of node (i,j) in X direction can be determined by using Table 5.1.
Then, the Equation (5.24) can be written in the following form;

$$\frac{2}{\Delta\tau}\phi_{i,j}^{n+1}-\left(C\frac{\partial^2 \phi^{n+1}}{\partial Y^2}-V\frac{\partial \phi^{n+1}}{\partial Y} \right)\Bigg|_{i,j} = D_Y(i,j) \qquad (5.27)$$

The left side of 5.27 contains ϕ^{n+1} which is unknown and its values for all nodes of the computational domain have to be computed. By substituting Equation 5.14 into 5.27;

$$A_Y(i,j).\phi_{i,j+1}^{n+1}+\left(1-\frac{2}{\Delta\tau}\right)B_Y(i,j).\phi_{i,j}^{n+1}+C_Y(i,j,).\phi_{i,j-1}^{n+1}=-D_Y(i,j) \qquad (5.28)$$

where $A_Y(i,j)$, $B_Y(i,j)$ and $C_Y(i,j)$ are multipliers of node (i,j) in Y direction and as it was mentioned before, they are determined by using Table 5.2.

The application of Equation 5.28 to all nodes which are on a line of the computational domain in Y direction yields the system of algebraic equations as 5.29, where h is the number of nodes along Y line;

$$A_Y(i,2).\phi_{i,3}^{n+1}+\left(1-\frac{2}{\Delta\tau}\right)B_Y(i,2).\phi_{i,2}^{n+1}+C_Y(i,2).\phi_{i,1}^{n+1}=-D_Y(i,2)$$
$$A_Y(i,3).\phi_{i,4}^{n+1}+\left(1-\frac{2}{\Delta\tau}\right)B_Y(i,3).\phi_{i,3}^{n+1}+C_Y(i,3).\phi_{i,2}^{n+1}=-D_Y(i,3)$$
$$A_Y(i,4).\phi_{i,5}^{n+1}+\left(1-\frac{2}{\Delta\tau}\right)B_Y(i,4).\phi_{i,4}^{n+1}+C_Y(i,4).\phi_{i,3}^{n+1}=-D_Y(i,4)$$

…… (5.29)

$$A_Y(i,h-3).\phi_{i,h-2}^{n+1}+\left(1-\frac{2}{\Delta\tau}\right)B_Y(i,h-3).\phi_{i,h-3}^{n+1}+C_Y(i,h-3).\phi_{i,h-4}^{n+1}=-D_Y(i,h-3)$$
$$A_Y(i,h-2).\phi_{i,h-1}^{n+1}+\left(1-\frac{2}{\Delta\tau}\right)B_Y(i,h-2).\phi_{i,h-2}^{n+1}+C_Y(i,h-2).\phi_{i,h-3}^{n+1}=-D_Y(i,h-2)$$
$$A_Y(i,h-1).\phi_{i,h}^{n+1}+\left(1-\frac{2}{\Delta\tau}\right)B_Y(i,h-1).\phi_{i,h-1}^{n+1}+C_Y(i,h-2).\phi_{i,h-2}^{n+1}=-D_Y(i,h-1)$$

The solution of system of tridiagonal algebraic equations 5.29 along the line Y is possible since there are h-2 equations with h-2 unknowns when the boundary conditions for boundary nodes (i,1) and (i,h) are defined. When the algebraic equations 5.29 are solved, the values of ϕ^{n+1} at all nodes which are on the first column of Y direction will be obtained. However, the values of ϕ^{n+1} have to be determined for all nodes of the computational domain. In order to obtain those values, equation 5.28 should be applied to the all lines of the computational domain which are in Y direction by the same method explained above.

It is mentioned that the streamfunction and the heatfunction equations contain only diffusion terms so they are written in the single generic equation 5.3. Since there is no time term in this equation, it can be solved point by point by iteration with the finite difference formulations of the diffusion terms given at 5.7 and 5.8.

By using 5.7 and 5.8 in the generic equation 5.3 for node (i,j) with the finite difference formulation, the following nodal equation is obtained;

$$F\phi_{i,j}=A\phi_{i+1,j}+B\phi_{i-1,j}+G\phi_{i,j+1}+E\phi_{i,j-1}-R \qquad (5.30)$$

where A, B, G, E and F are constants and they can be expressed as follows;

$$F = 2\frac{\left[\left(\Delta X_i \,.\, \Delta X_{i+1} + \Delta Y_j \,.\, \Delta Y_{j+1}\right)\right]}{\left[\left(\Delta X_i \,.\, \Delta X_{i+1}\right)\left(\Delta Y_j \,.\, \Delta Y_{j+1}\right)\right]} \tag{5.31}$$

$$A = \frac{2}{\Delta X_{i+1}(\Delta X_i + \Delta X_{i+1})} \tag{5.32}$$

$$B = \frac{2}{\Delta X_i (\Delta X_i + \Delta X_{i+1})} \tag{5.33}$$

$$G = \frac{2}{\Delta Y_{j+1}(\Delta Y_j + \Delta Y_{j+1})} \tag{5.34}$$

$$E = \frac{2}{\Delta Y_j (\Delta Y_j + \Delta Y_{j+1})} \tag{5.35}$$

The nodal equation 5.30 can be solved point by point by iteration.

5.2. Finite Difference Forms of the Boundary Conditions

Governing equations of the problem are solved according to the determined boundary conditions. Thus, finite difference forms of the boundary conditions at the specified boundaries will be given. In the x-direction, there are m nodes; and in the y-direction there are h nodes. In this study, boundary conditions are defined at the bottom, right, left and top walls, and at the solid-fluid interface.

On the bottom wall where i is changing from 1 to m and j=1;

$$U(i,1) = V(i,1) = \Psi(i,1) = 0 \;,\; \theta(i,1) = \theta(i,2) \tag{5.36}$$

The formulation of Wong and Baker (2002) is used to define the vorticity at the boundaries. According to this formulation the vorticity value of the boundary node at the bottom wall shown in Figure 5.2 can be calculated as follows;

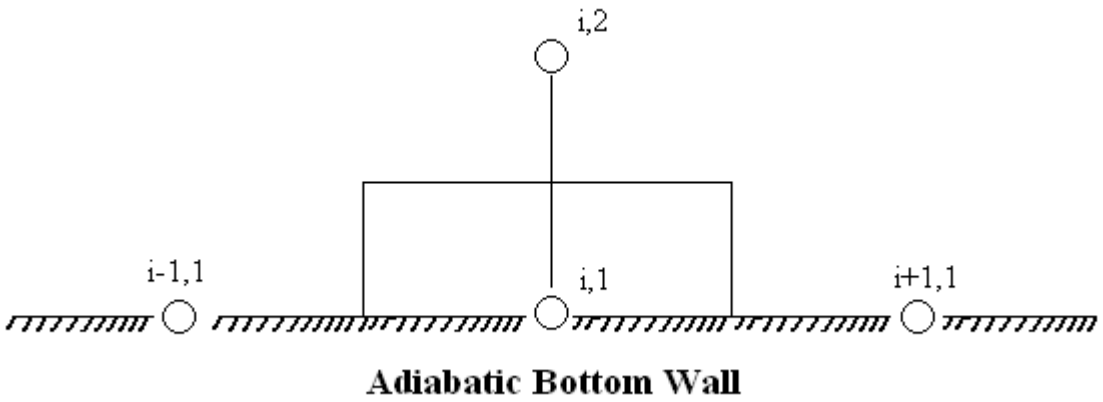

Figure 5.2. Boundary node at the bottom wall (i,1) with its neighboring nodes.

The vorticity value at the node $\Omega(i,1)$ is;

$$\Omega(i,1) = \frac{2}{\Delta Y_1}\left[U(i,2) - U(i,1)\right] - \Omega(i,2) \tag{5.37}$$

where U(i,1)=0, thus for the bottom wall 5.37 is written as;

$$\Omega(i,1) = \frac{2}{\Delta Y_1} U(i,2) - \Omega(i,2) \tag{5.38}$$

The Equation 5.38 can be applied to the other boundary nodes to determine the vorticity values at them.

On the left wall where j is changing from 1 to h and i=1;

$$U(1, j) = V(1, j) = \Psi(1, j) = 0 \ , \ \theta(1, j) = 1 \tag{5.39}$$

The vorticity value at the node $\Omega(1, j)$ can be found from;

$$\Omega(1, j) = \frac{2}{\Delta X_1} V(2, j) - \Omega(2, j) \tag{5.40}$$

On the right wall where j is changing from 1 to h and i=m;

$$U(m, j) = V(m, j) = \Psi(m, j) = 0 \ , \ \theta(m, j) = 0 \tag{5.41}$$

The vorticity value at the node $\Omega(m, j)$ can be found from;

$$\Omega(m, j) = \frac{2}{\Delta X_m} V(m-1, j) - \Omega(m-1, j) \tag{5.42}$$

On the ceiling solid-fluid interface where i is changing from 1 to m and j=r;

$$U(i, r) = V(i, r) = \Psi(i, r) = 0 \tag{5.43}$$

where r is the number of nodes in Y direction from the bottom wall to the interface. The vorticity value at the node $\Omega(i, r)$ can be found from;

$$\Omega(i, r) = \frac{2}{\Delta Y_r} U(i, r-1) - \Omega(i, r-1) \tag{5.44}$$

Figure 5.3 is showing the node (i,h) at the ceiling solid-fluid interface.

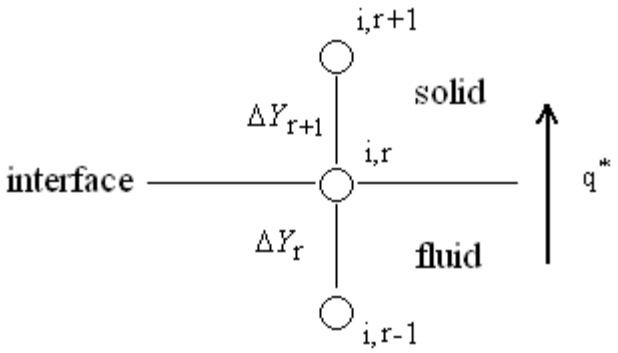

Figure 5.3. Boundary node at the ceiling solid-fluid interface (i,r) with its neighboring nodes.

For the considered node (i,r), the dimensionless temperature value $\theta(i, r)$ can be determined from;

$$q_f^* = q_s^* \tag{5.45}$$

$$K \left.\frac{\partial \theta_S}{\partial Y}\right|_S = \left.\frac{\partial \theta_f}{\partial Y}\right|_f \text{ and for the interface } \theta_f = \theta_s \tag{5.46}$$

By writing the finite difference forms of the terms in Equation 5.46 for the node (i,r);

$$K \frac{\theta(i, r) - \theta(i, r-1)}{\Delta Y_r} = \frac{\theta(i, r+1) - \theta(i, r)}{\Delta Y_{r+1}} \tag{5.47}$$

After rearranging 5.47, the following nodal equation is obtained to determine $\theta(i, r)$;

$$\theta(i, r) = \left(\frac{\Delta Y_r}{K\Delta Y_{r+1} + \Delta Y_r} \right) \theta(i, r+1) + \left(\frac{K\Delta Y_{r+1}}{K\Delta Y_{r+1} + \Delta Y_r} \right) \theta(i, r-1) \tag{5.48}$$

By using the nodal equation 5.48, the temperature values of the nodes at the ceiling solid-fluid interface can be obtained.

On the top wall where i is changing from 1 to m and j=h;

$$U(i, h) = V(i, h) = \Psi(i, h) = 0 \text{ , } \theta(i, h) = \theta(i, h-1) \tag{5.49}$$

Since there is no flow inside the solid region;

$$\Omega(i, h) = 0 \tag{5.50}$$

CHAPTER 6

NUMERICAL ANALYSIS

The finite difference forms of the governing equations have been derived in Chapter 5. The solution of these equations can be made by a computer code. To obtain accurate results from the code, discretization of the computational domain (the grid size) should be made carefully. A suitable discretization provides accurate results, whereas an unsuitable discretization may lead to the results with low accuracy. In this chapter, the discretization of the computational domain, the convergence criteria and the the solution procedure will be explained.

6.1 Solution Procedure

The governing equations 3.48, 3.49 and 3.50 are solved by starting from an initial state for the entire computational domain. The vorticity equation is solved for a time step to compute the vorticity field in the computational domain. Then, the stream function equation is solved and the velocity values are obtained from the stream function field. At the same time step and by using the new values of velocity, the energy equation is solved and temperature field is computed. The procedure is continued until the steady state is reached (Mobedi and Yuncu 2003). Figure 6.1 is showing a flow chart for the solution procedure. The energy and the vorticity equations are solved line by line by employing ADI method, whereas the streamfunction and the heatfunction equations are solved point by point. The finite difference forms of diffusion and convection terms are written based on three points central differencing which has second order accuracy.

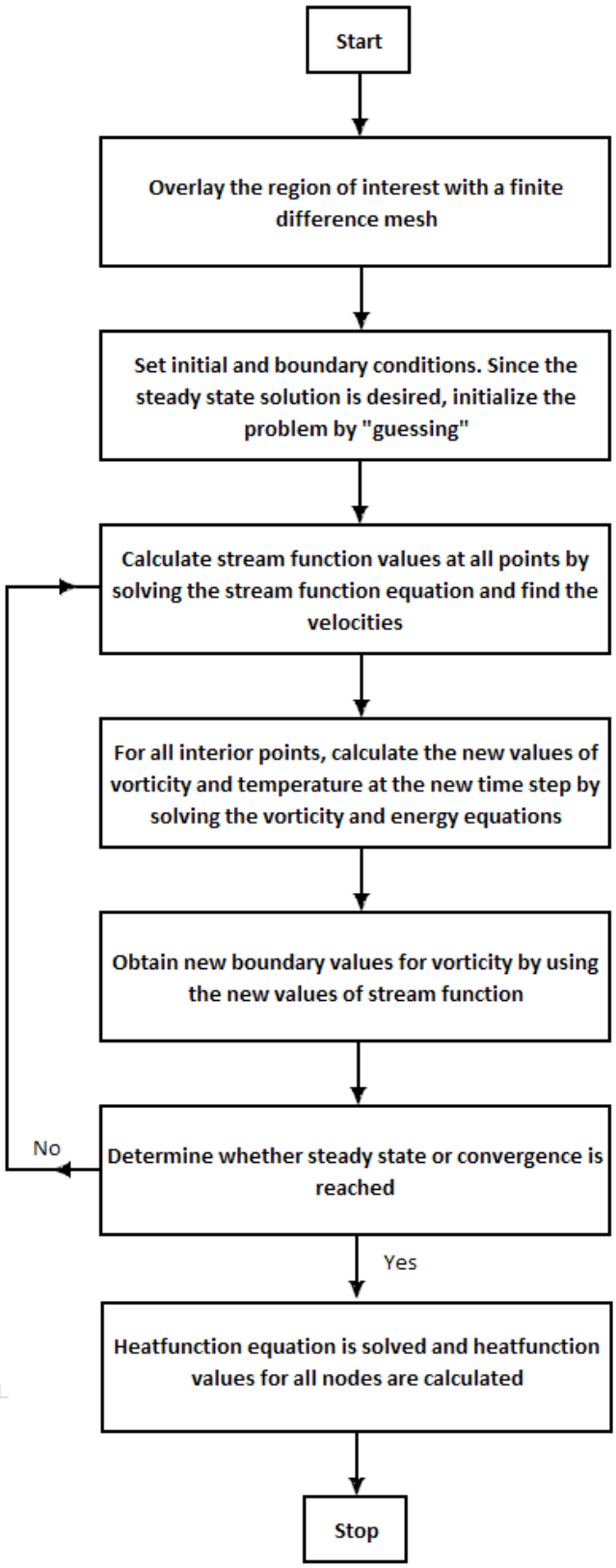

Figure 6.1. Flow chart for the solution procedure.

The value of Prandtl number for flow region is assigned as 0.71 while for the solid region it is changed to $Pr=10^{20}$. This change of Prandtl number value makes the values of vorticity, streamfunction and velocity in the horizontal wall automatically zero and consequently the convection heat transfer equation is converted to the heat conduction equation of the ceiling wall. The temperature of solid-fluid interface is obtained by employing backward and forward differences with the first order accuracy for the determination of local heat flux. The vorticity values on the solid boundaries are calculated by using the relation developed by Wong and Baker (2002). The convergence criterion for the solution procedure is defined as;

$$\frac{\sum\left|\theta^{\,n+1}-\theta^{\,n}\right|}{\Delta\tau\sum\theta^{n}} \le 5.10^{-3} \tag{6.1}$$

where θ represents the dimensionless temperature in the entire computational domain. Local and average Nusselt numbers for the vertical walls of the fluid region are calculated according to the gradient of dimensionless temperature in the normal direction of the considered wall. For instance, Nu and $\overline{Nu}$ for the hot and cold vertical walls of the cavity (X=0, X=1) are calculated by the following equations;

$$\mathrm{Nu} = \frac{q_f L}{k_f (T_h - T_c)} = -\left.\frac{\partial \theta_f}{\partial X}\right|_{wall} \tag{6.2}$$

$$\overline{Nu} = \int_0^1 Nu\,dY \tag{6.3}$$

The dimensionless heat transfer rate from a wall of the fluid region can be calculated as;

$$Q_f^* = \int_0^1 -\left.\frac{\partial \theta_f}{\partial X}\right|_{wall} dY \tag{6.4}$$

As is seen from Equations 6.3 and 6.4, the dimensionless heat transfer rate from a wall of fluid region equals to the average Nusselt number of that wall ($Q_f^* = \overline{Nu}$) since dimensionless height and width of the fluid region is unity. The dimensionless

heat flux and heat transfer rate, q_s^* and Q_s^* , from the vertical boundaries of the horizontal wall can be calculated by the following relations;

$$q_s^* = \frac{q_s L}{k_s(T_h - T_c)} = -\left.\frac{\partial \theta_S}{\partial X}\right|_{wall} \tag{6.5}$$

$$Q_s^* = \int_1^{1+D} -\left.\frac{\partial \theta_S}{\partial X}\right|_{wall} dY \tag{6.6}$$

In order to determine the dimensionless overall heat transfer rate from the vertical boundary of enclosure, the definitions of Q_f^* and Q_S^* should be the same. The heat transfer rates should be made non-dimensional according to the same variables. Hence, the dimensionless heat transfer rate of the ceiling wall is multiplied with the thermal conductivity ratio. And the dimensionless overall heat transfer rate to/from the entire area of the hot or cold vertical wall can be calculated by the following equation;

$$Q_t^* = Q_s^* K + Q_f^* \tag{6.7}$$

Non uniform mesh grid size is used both for the fluid and solid regions which is shown in Figure 6.2. The grid size is selected fine near the walls and heat barrier. They are expanded continuously towards the center of enclosure. The number of nodes in X and Y directions is 80 x 130 in which 80x50 nodes are used in the ceiling wall. The smallest grid spacing which was in the regions adjacent to the solid walls is 0.001.

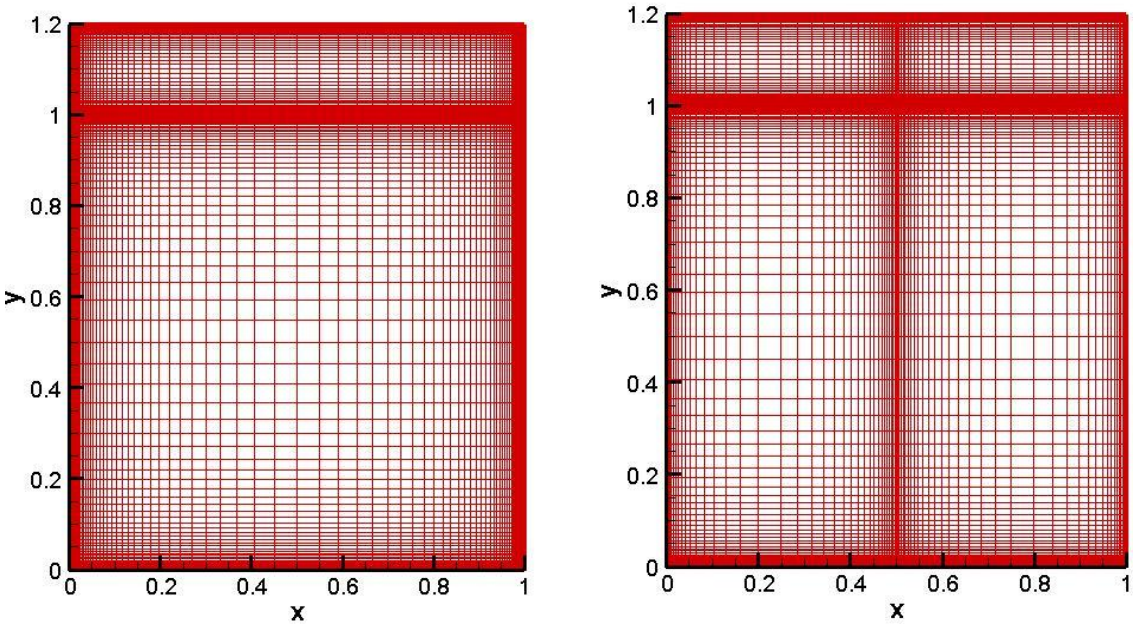

Figure 6.2. Example of non uniform mesh grid size for the enclosure with ceiling wall; a) Ceiling wall without heat barrier, b) Ceiling wall with heat barrier at X_h=0.5.

Table 6.1 shows the average Nusselt number of the hot vertical wall and dimensionless overall heat transfer rate for different number of grids for Ra = 10^6 and K=100. As is seen, 80 X 80 grids for the fluid region and 80 X 50 grids for the solid region are sufficient to achieve the accurate results for the problem.

Table 6.1. $\overline{Nu}$ and Q_t^* of hot vertical wall for different number of grids for Ra=10^6 and K=100.

Number of grids		$\overline{Nu}$	Q_t^*
In cavity	In ceiling wall		
20 X 20	20 X 6	10.83	29.93
40 X 52	40 X 12	9.55	28.44
60 X 85	60 X 25	9.45	28.34
70 X 110	70 X 40	9.46	28.36
80 X 130	80 X 50	9.46	28.36

6.2. Computer Code

A computer code written in FORTRAN is used to solve the governing equations of the problem. There are two separate codes which are the grid generator and the solver. Grid generator is generating grids for the considered case and the solver is used to solve the governing equations of the problem for the generated grids. Solver includes the following subprograms:

- Main program
- Boundary subprogram
- Temperature equation solver
- Vorticity equation solver
- Streamline equation solver
- Nusselt number calculator
- Heat function equation solver
- File printer

In the present study, the input data into main program by the user are Rayleigh number, thermal conductivity ratio and time interval. Other subprograms which are boundary subprogram, temperature equation solver, vorticity equation solver, streamline equation solver, Nusselt number calculator and heat function equation solver are called by order in the main program and the results are printed by the file printer.

6.3. Validation of the Code

In order to validate the employed method and check the written computer code, results for the benchmark solution of de Vahl Davis (1983) for non-conjugate natural convection in an air filled square cavity was obtained and compared. Table 6.2 shows the comparison between the results of two solutions.

Table 6.2. Comparison of the present numerical results with the solution (Source: De Vahl Davis 1983)

Ra	De Vahl Davis		Present study	
	$\lvert\psi\rvert_{max}$	$\overline{Nu}$	$\lvert\psi\rvert_{max}$	$\overline{Nu}$
10^3	-	1.118	1.174	1.114
10^4	-	2.243	5.109	2.240
10^5	9.612	4.519	9.693	4.510
10^6	16.750	8.800	16.916	8.803

Another validation check was performed by comparing the results with the results of Kaminski and Prakash (1986) shown in Table 6.3.

Table 6.3. Comparison between the obtained results with the solution (Source: Kaminski and Prakash (1986).

Ra		Kaminski et al.	Present study
		$\overline{Nu}$	$\overline{Nu}$
$7.1x10^2$	K=1	0.87	0.866
	K=∞	1.06	1.062
$7.1x10^4$	K=1	2.08	2.074
	K=∞	4.08	4.034
$7.1x10^5$	K=1	2.87	2.850
	K=∞	7.99	7.911

These tables show that there is good agreement between the results of the present code written for conjugate conduction-convection heat transfer and reported studies in literature. It should be mentioned that for all obtained results, the values of

dimensionless overall heat transfer from the hot and cold boundaries were equal which proves the conservation of energy for the entire domain.

CHAPTER 7

RESULTS AND DISCUSSION

In this thesis, streamlines and isotherms inside the cavity and inside the solid region are drawn for different values of Rayleigh number and thermal conductivity ratio. Moreover, the heatline visualization method is used to show the heat interaction between solid-fluid interface. By using this technique, heatlines are drawn and the path of heat flow is observed. Temperature distribution on the solid-fluid interface is plotted to demonstrate the character of heat transfer between the horizontal wall and the fluid. The dimensionless heat transfer rate from the horizontal wall boundaries, mean Nusselt numbers of the fluid region walls and dimensionless overall heat transfer rate of the enclosure for the cases with and without heat barrier are numerically calculated. The effects of heat barrier location, thermal conductivity ratio and Rayleigh number on $\overline{Nu}$, Q_s^* and Q_t^* are investigated. Height and width of the fluid region are unity; therefore, $\overline{\mathrm{Nu}}$ represents dimensionless heat transfer rate (Q_f^*) to/from the fluid region at the same time.

7.1. Effect of Ceiling Wall on Heat Transfer

The effect of ceiling wall on the average Nusselt numbers of the cavity vertical walls X=0 and X=1 is being presented in Table 7.1 for different Rayleigh numbers. The results with the ceiling wall case is calculated for thermal conductivity ratio K=100 and for dimensionless ceiling wall thickness value D=0.2. For a cavity without a ceiling wall, the average Nusselt number of the vertical cavity wall X=0, $\overline{\mathrm{Nu}}\big|_{X=0}$, is equal to the average Nusselt number of the vertical cavity wall X=1, $\overline{\mathrm{Nu}}\big|_{X=1}$. This is because the top and the bottom surfaces of the cavity are adiabatic. Thus, the heat transferred from the hot side to the cold side of the cavity via fluid only. It is seen from the table that the existence of ceiling wall has an increasing effect on $\overline{\mathrm{Nu}}\big|_{X=0}$ and a decreasing effect on

$\overline{\mathrm{Nu}}\big|_{X=1}$. The average Nusselt number of the cavity wall X=1 decreases because some part of the heat is transferred from the fluid to the ceiling wall and conducted to the cold side of the cavity by ceiling wall.

Table 7.1. The average Nusselt numbers of the cavity walls for different Rayleigh numbers and for the cavities with and without ceiling wall.

	Without ceiling wall	With ceiling wall (D=0.2)	
Rayleigh number	$\overline{\mathrm{Nu}}\big\|_{X=0}$	$\overline{\mathrm{Nu}}\big\|_{X=0}$	$\overline{\mathrm{Nu}}\big\|_{X=1}$
10^3	1.11	1.22	0.94
10^4	2.24	2.52	1.53
10^5	4.51	4.93	3.03
10^6	8.80	9.46	6.11

7.2. Effect of Heat Barrier

Heat barrier was placed at different locations of ceiling in this study. However, to see the effects of it on heat transfer and heat flow; firstly, results of an enclosure without heat barrier will be compared with the results of a middle located heat barrier enclosure where the ceiling wall thickness is constant and it is D=0.2.

Figure 7.1 is given to show the effects of heat barrier on flow fields, temperature distributions and heat transport by using the isotherms (on the left), streamlines (on the middle) and heatlines (on the right) of two enclosures without heat barrier (Fig. 7.1 (a)) and with heat barrier (Fig. 7.1 (b)) for Ra = 10^3 and K = 1. The value written on the top of heatline figures represents the dimensionless overall heat transfer rate. Single circulation cell is formed in clockwise rotation in the fluid region as shown from the streamlines. The isotherms and streamlines in the fluid region of both enclosures (with barrier and without barrier) are similar to each other. The existence of thermal barrier does not considerably affect heat transfer rate through the fluid region of the enclosure. However, the direction of heat flow is changed around the heat barrier in the ceiling. Heat can not be directly transferred from the hot to cold vertical walls due to heat barrier. It is transferred from the hot region of ceiling to the fluid and then it passes to the cold region of the ceiling. Hence, a reduction in the heat transfer through the ceiling should be expected.

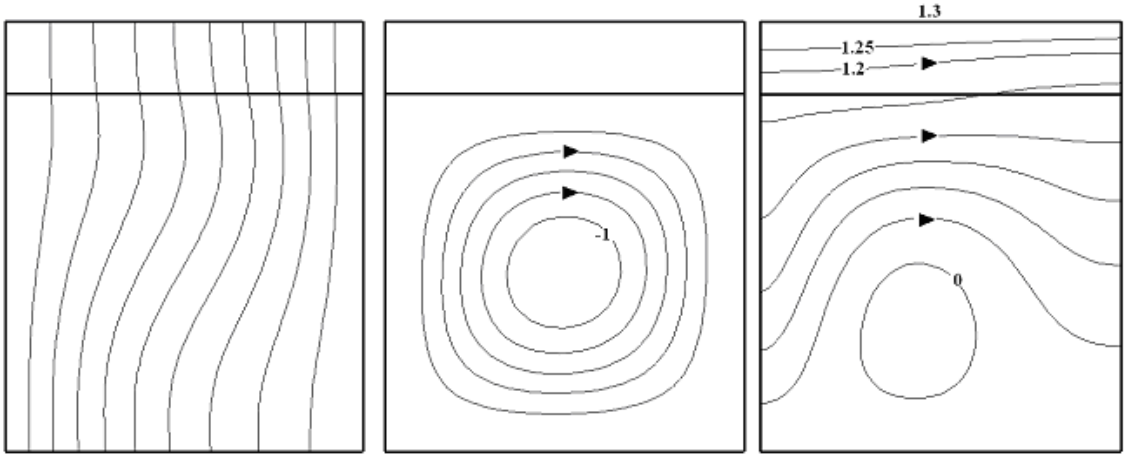

a)

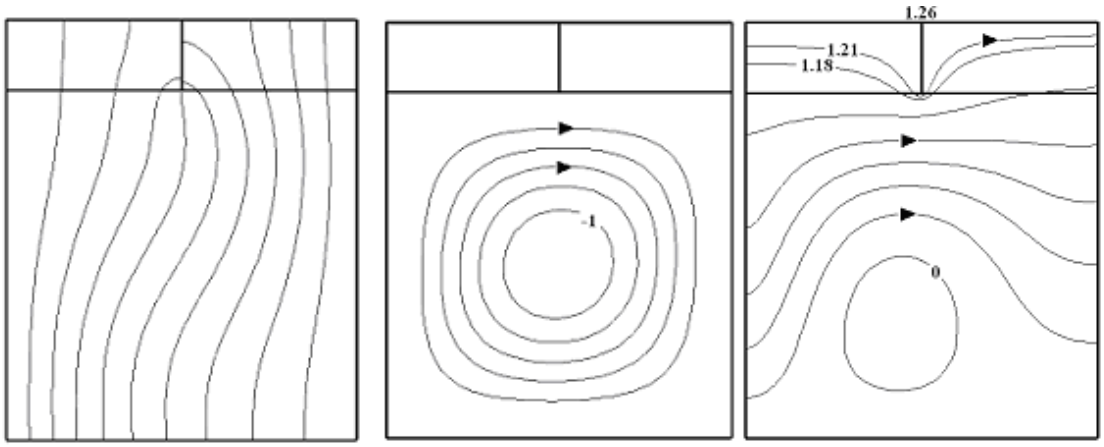

b)

Figure 7.1. Isotherms (on the left), streamlines (on the middle) and heatlines (on the right) for Ra=10^3 and K=1, a) without heat barrier where $\delta\Psi = -0.2$, $\delta\theta = 0.1, \delta H = 0.22$ (heatlines 1.2 and 1.25 were added). b) with middle located heat barrier where $\delta\theta = 0.1, \delta\Psi = -0.2$, $\delta H = 0.21$ (heatlines 1.18 and 1.21 were added)

Results are presented in Figure 7.2 for Ra = 10^3 and K = 100 to see the effects of high conductivity ratio on flow and temperature fields of the enclosures with and without heat barrier. Similar to the case of Figure 7.1, isotherms in the ceiling without heat barrier are parallel due to high conductivity ratio and they are nearly parallel in the fluid region. The great amount of heat is directly transferred from the hot to cold vertical wall via conduction mode of heat transfer in the ceiling.

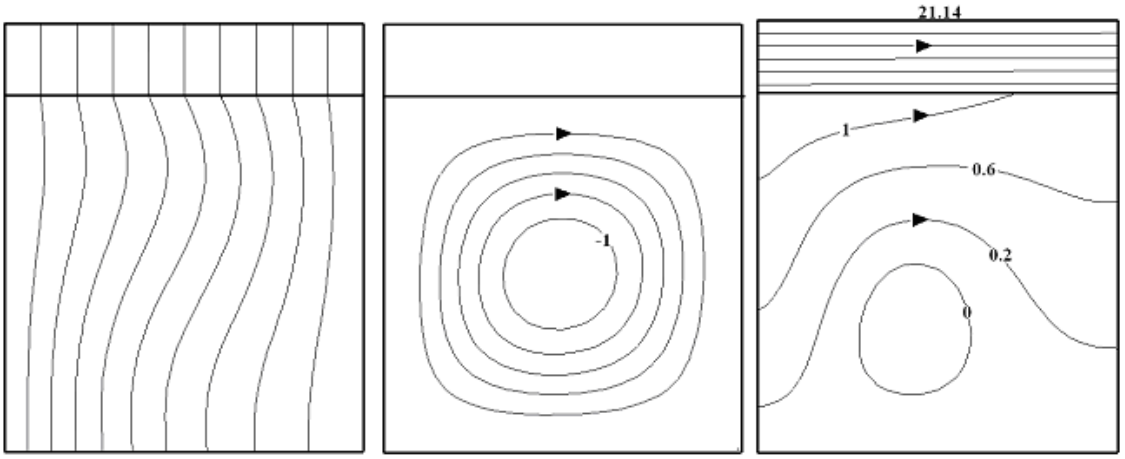

a)

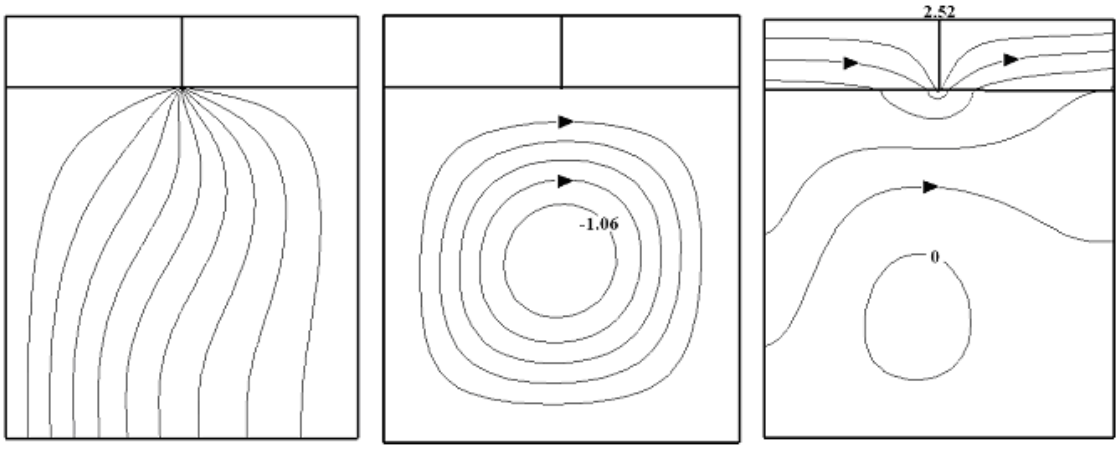

b)

Figure 7.2. Isotherms (on the left), streamlines (on the middle) and heatlines (on the right) for Ra=10^3 and K=100, a) without heat barrier where $\delta\theta = 0.1$, $\delta\Psi = -0.2$, $\delta H = 3.52$ (heatlines 0.2, 0.6 and 1 were added), b)with middle located heat barrier where $\delta\theta = 0.1$, $\delta\Psi = -0.21$, $\delta H = 0.42$.

The heat barrier prevents transfer of heat from hot to cold vertical wall of the ceiling. Two separate hot and cold regions with almost uniform temperature distributions form at the right and left sides of heat barrier due to high thermal conductivity ratio. Hence, isotherms in the upper side of fluid region are distributed from the edge of heat barrier. The formation of separate hot and cold regions in the ceiling wall with heat barrier for high values of K (i.e. K=100) can also be observed from Figure 7.3 in which ceiling interface temperature distribution for Ra = 10^3 and different K values are shown. A small gap at the heat barrier location can be seen in the interface temperature of K = 1 since heat transport and fluid flow in the most region of enclosure is not greatly influenced by heat barrier. The gap between the temperatures of the left and right sides of heat barrier increases with increasing K and a sharp drop is

observed at the interface temperature for X_h=0.5 and K=100. Hence, a significant reduction in the dimensionless heat transfer rate of the ceiling wall with K=100 is expected.

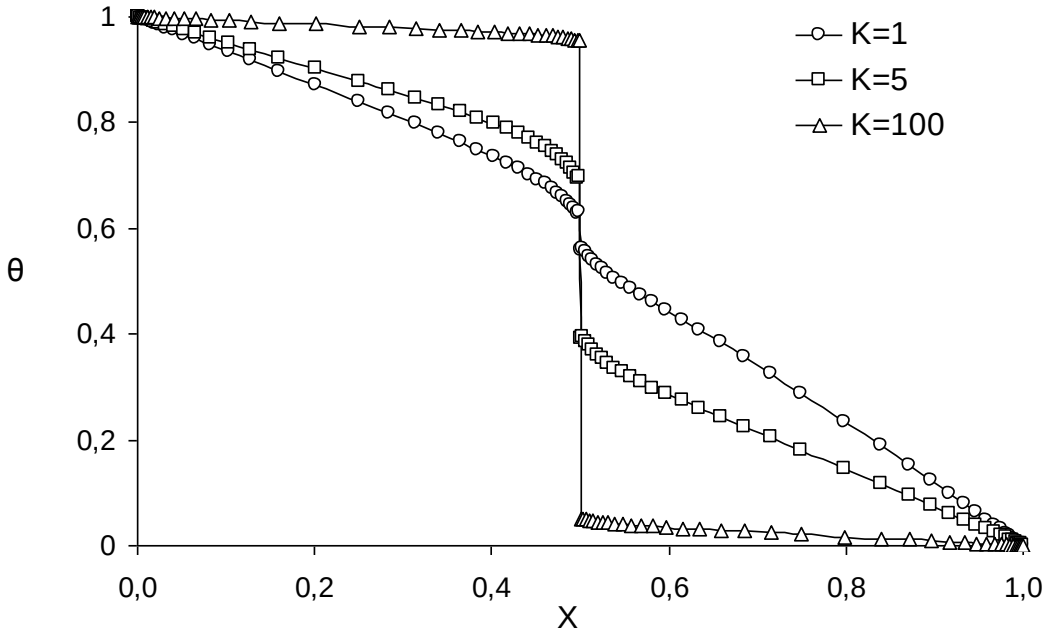

Figure 7.3. The variation of temperature at the ceiling interface for different conductivity ratio where Ra=10^3.

Figure 7.4 shows isotherms (on the left), streamlines (on the middle) and heatlines (on the right) for the enclosure with Ra = 10^6 and K = 1 without (Fig. 7.4 (a)) and with (Fig. 7.4 (b)) heat barrier. For both cases, the convection effect is dominant and most of the heat in the fluid region is transferred via convection. Since the conduction in the ceiling is weak, the existence of heat barrier does not considerably change isotherms and streamlines in the most of fluid region. However, heat transfer through the ceiling is affected by heat barrier since the direction of heat flow is changed.

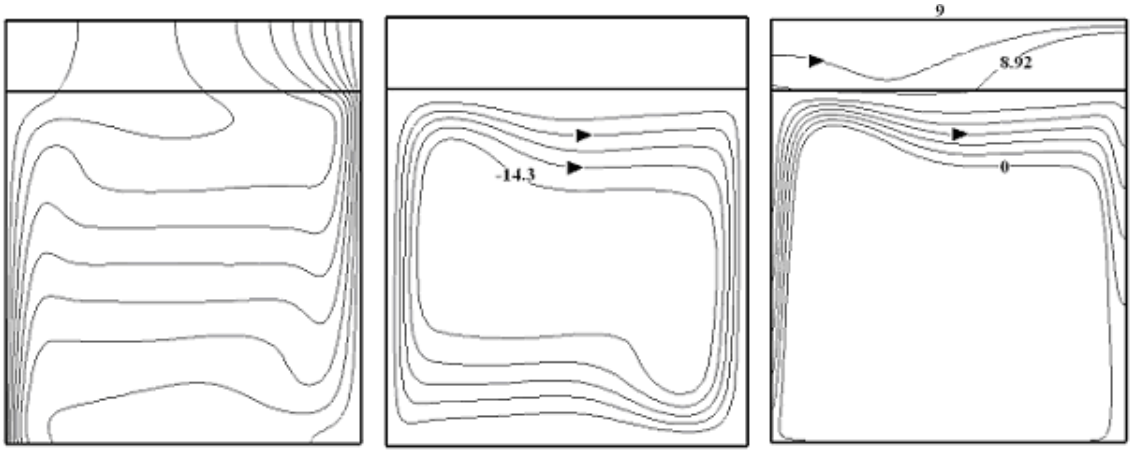

a)

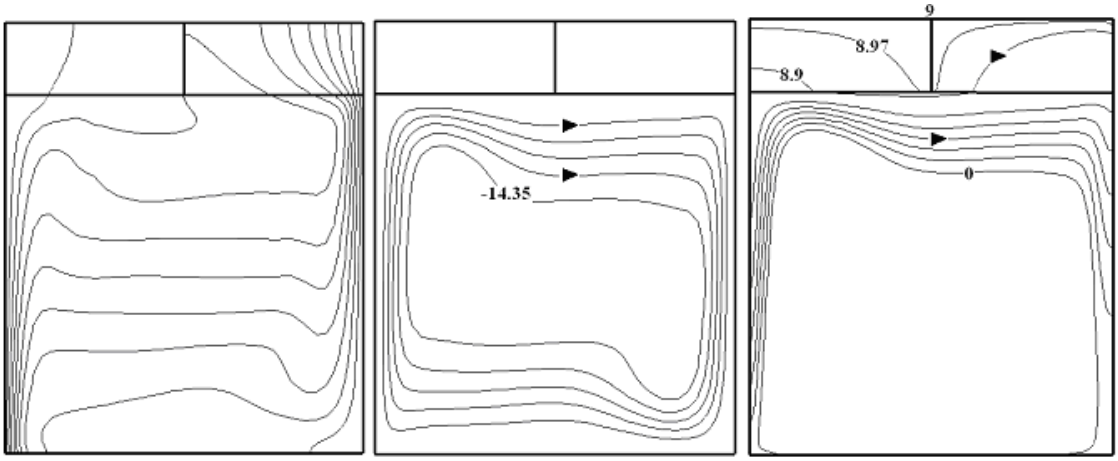

b)

Figure 7.4. Isotherms (on the left), streamlines (on the middle) and heatlines (on the right) for Ra=10^6 and K=1, a) without heat barrier where $\delta\theta = 0.1$, $\delta\Psi = -2.86$, $\delta H = 1.5$ (8.92 and 8.98 were added), b) with middle located heat barrier where $\delta\theta = 0.1$, $\delta\Psi = -2.87$, $\delta H = 1.5$ (heatlines 8.9 and 8.97 were added).

Effects of the highest conductivity ratio on isotherms, streamlines and heatlines are given in Figure 7.5 (a) (without barrier) and Figure 7.5 (b) (with barrier) for Ra = 10^6. The conduction in the ceiling is strong and similar to the case of Figure 7.2; the isotherms are joined at the edge of heat barrier due to the formation of hot and cold regions. Heat barrier significantly affects on heat transfer through the ceiling wall as seen from heatlines and isotherms.

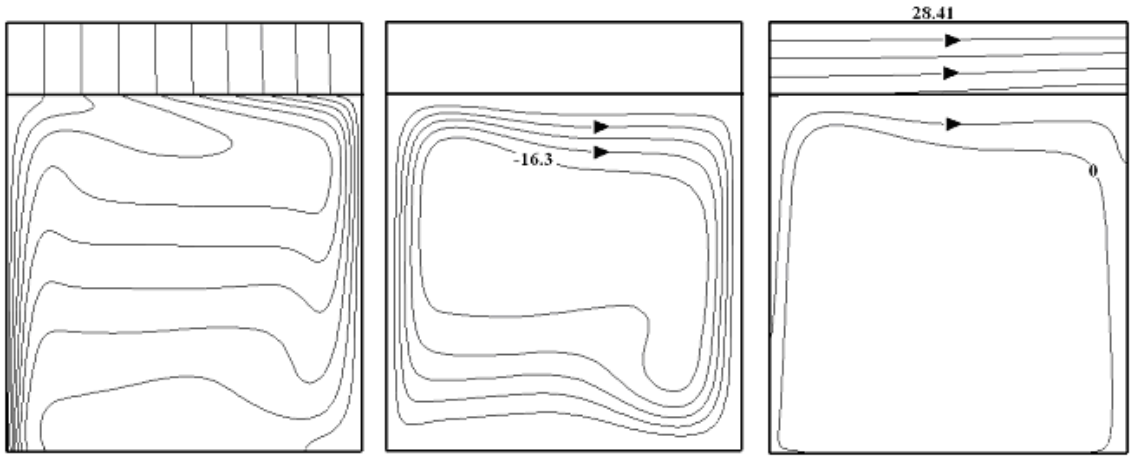

a)

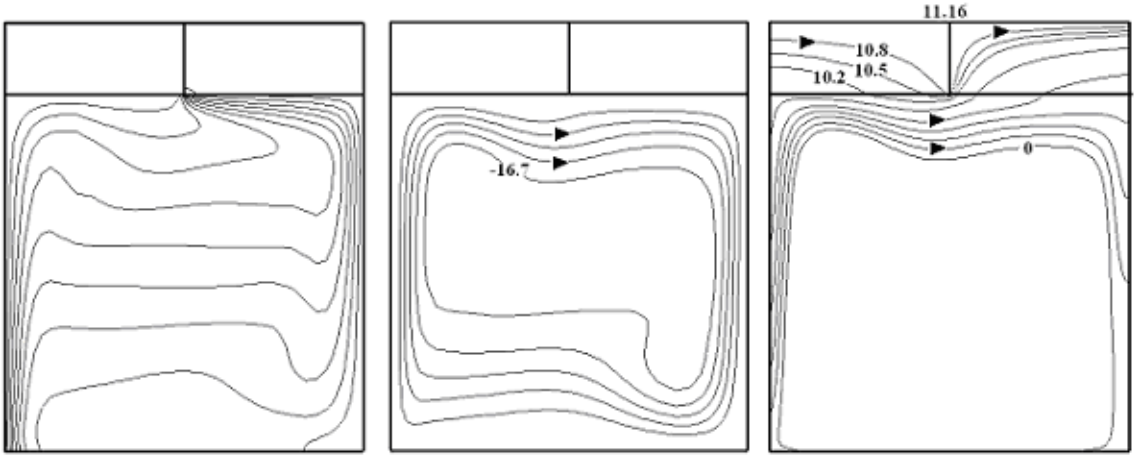

b)

Figure 7.5. Isotherms (on the left), streamlines (on the middle) and heatlines (on the right) for Ra=10^6 and K=100, a) Without heat barrier where $\delta\Theta = 0.1$, $\delta\Psi = -3.26$, $\delta H = 4.73$ b) With middle located heat barrier where $\delta\Theta = 0.1$, $\delta\Psi = -3.34$, $\delta H = 1.86$ (heatlines 10.2, 10.5 and 10.8 were added).

The variations of average Nusselt number at the hot and cold vertical walls and the interface with thermal conductivity ratio are seen in Figure 7.6 (a) and Figure 7.6 (b) for Ra = 10^3 and Ra = 10^6, respectively. For the cavity with Ra = 10^3, the heat barrier reduces the values of average Nusselt number at the hot and cold vertical walls of the fluid region. However, it enhances the heat transfer on the interface since heat is transferred around the heat barrier via fluid. The measure of heat barrier effect on $\overline{Nu}$ depends on thermal conductivity ratio.

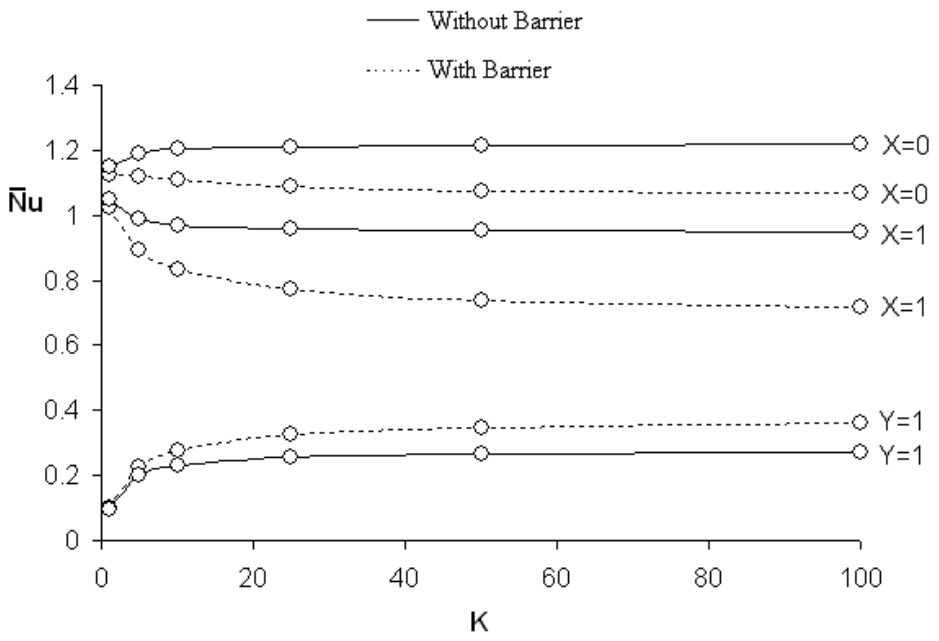

a)

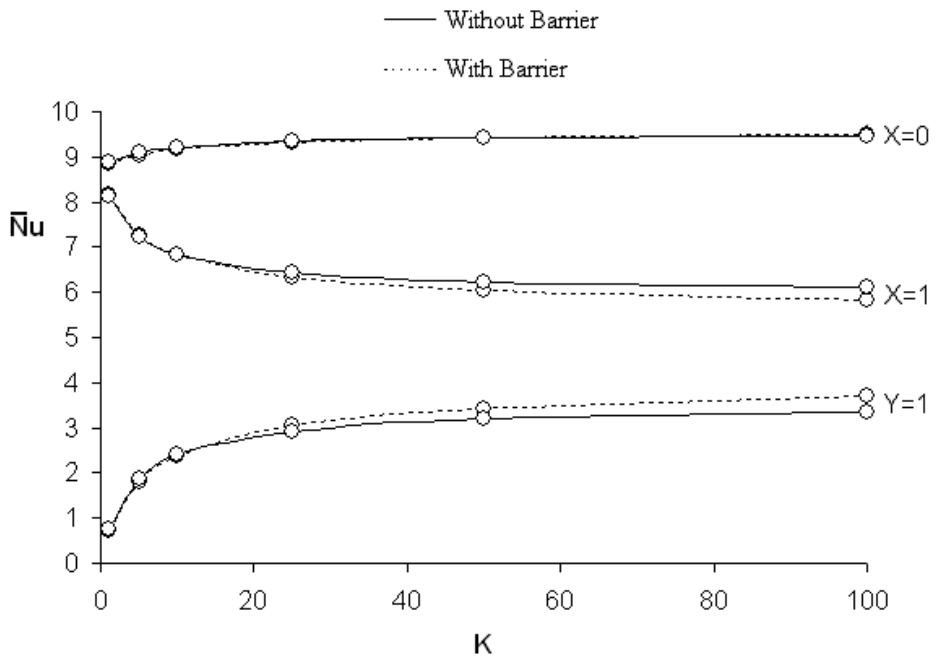

b)

Figure 7.6. Variation of average Nusselt number with thermal conductivity ratio at hot and cold vertical walls and ceiling interface for enclosures without heat barrier and middle located heat barrier, a) Ra=10^3, b) Ra=10^6.

For small values of K, heat barrier does not considerably influence heat transfer and fluid flow in the fluid region; however, the increase of K causes obvious reduction of $\overline{Nu}$ at hot and cold vertical walls. For the enclosure with Ra = 10^3 and K = 1, the decrease of Nusselt number at X = 1 due to heat barrier is 2.5%; however, this value for

K = 100 is 24.3%. The effect of heat barrier on average Nusselt number decreases with increasing Ra as shown in Figure 7.6 (b) since the convection heat transfer becomes dominant. Heat barrier reduces $\overline{Nu}$ at X = 1 only by 4.7% for Ra = 10^6 and K = 100.

Figure 7.7 (a) and (b) show the variation of dimensionless conduction heat transfer rate at the right and left vertical boundaries of ceiling wall for Ra = 10^3 and Ra = 10^6, respectively. For the ceiling wall without heat barrier, the dimensionless heat transfer rates at X = 0 and X = 1 approach to $Q_S^* = 0.2$, which is the dimensionless heat transfer rate of one dimensional heat conduction case, as conductivity ratio becomes larger. For Ra = 10^3, heat barrier significantly reduces heat transfer rate at X = 0 and X = 1 ceiling boundaries. The effect of heat barrier on Q_S* increases with increasing thermal conductivity ratio. For K = 1 and Ra = 10^3, the reduction in the dimensionless heat transfer rate at X = 1 boundary is 11.5% and this value is 91.5% for K = 100. The variation of ceiling wall dimensionless heat transfer rate with thermal conductivity ratio for Ra = 10^6 is shown in Figure 7.7 (b). For small values of conductivity ratio (i.e. K = 1), Q_S^* is not influenced by heat barrier since the strong convection in the fluid region transfers heat from hot to cold region of the ceiling. The increase of thermal conductivity ratio enhances conduction heat transfer through the ceiling. However, the reduction of heat transfer in the ceiling due to heat barrier can not be compensated by strong convection. For Ra = 10^6, the percentage of dimensionless conduction heat transfer reduction due to heat barrier at X = 1 for K = 1 and K = 100 are 3% and 76.6% respectively. Heat transfer through the ceiling wall for Ra = 10^3 is much affected by heat barrier when it is compared to Ra = 10^6.

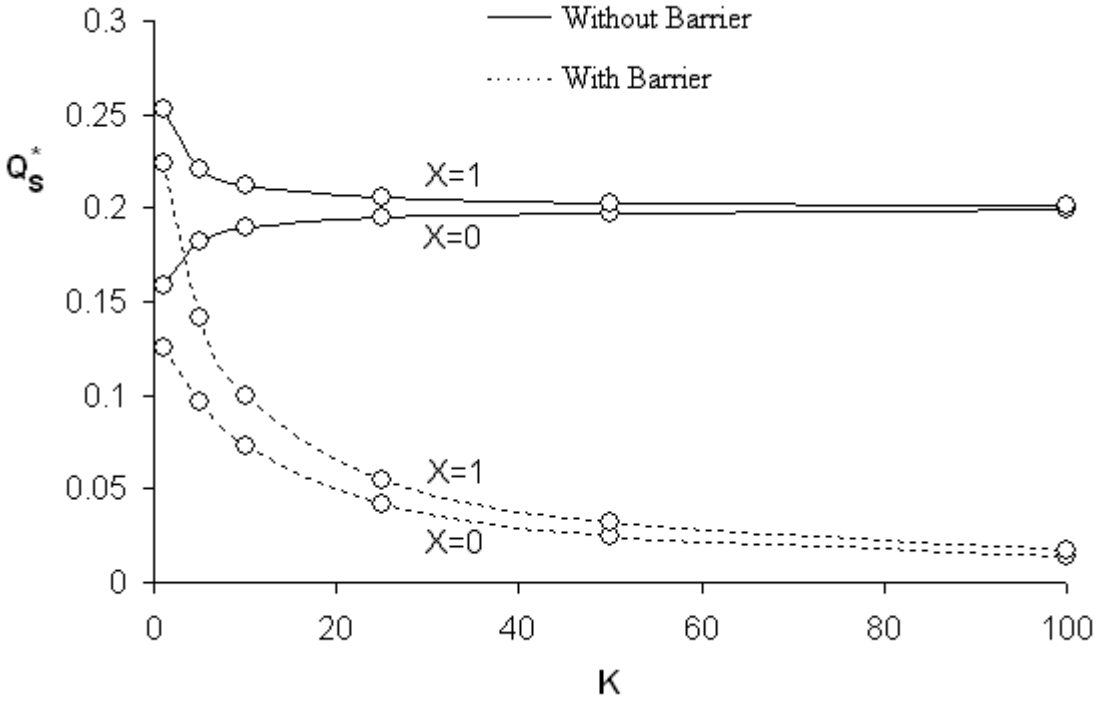

a)

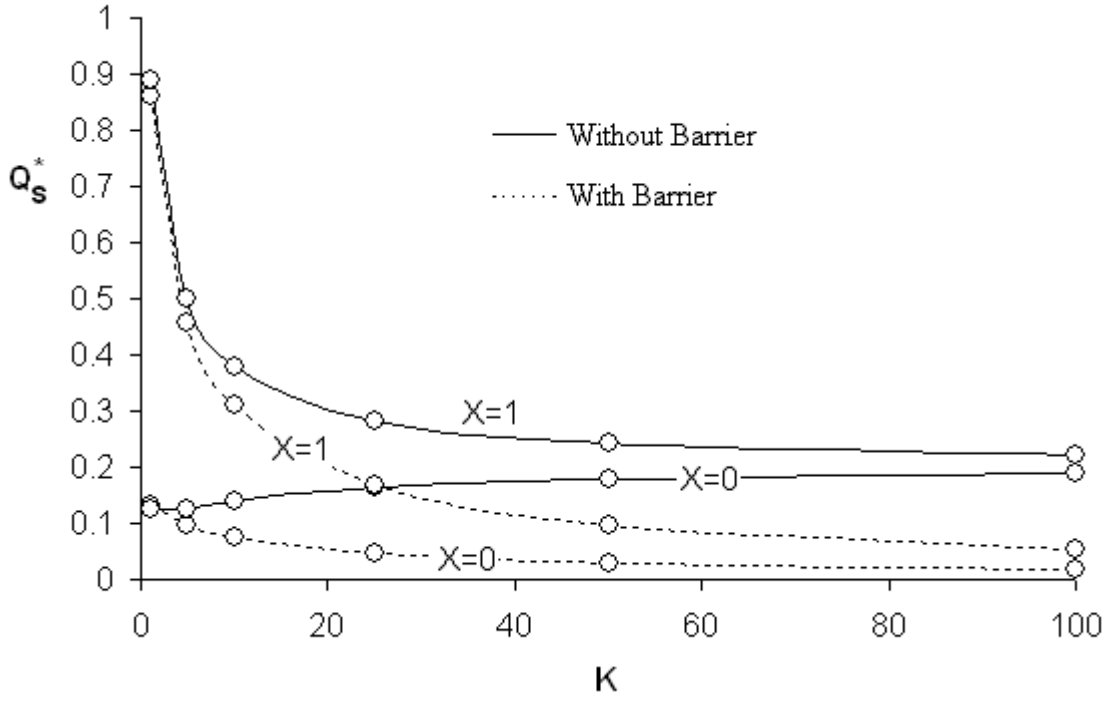

b)

Figure 7.7. Variation of Q_S^* with thermal conductivity ratio at X=0 and X=1 ceiling walls for enclosures without heat barrier and middle located heat barrier, a) $Ra=10^3$, b) $Ra=10^6$.

The variation of dimensionless overall heat transfer rate through the enclosure with thermal conductivity ratio for two different Rayleigh numbers, Ra = 10^3 and Ra = 10^6, are shown in Figure 7.8. For the enclosure without heat barrier, the domination of conduction heat transfer rate in the ceiling wall can be observed since Q_t^* proportionally increases with thermal conductivity ratio due to the proportional increase of one dimensional conduction heat transfer. For the enclosures with heat barrier, the overall dimensionless heat transfer rate does not vary for the wide range of thermal conductivity ratio. Reductions in dimensionless overall heat transfer rate due to heat barrier for Ra = 10^3 and Ra = 10^6 when K = 100 are 88% and 60% respectively.

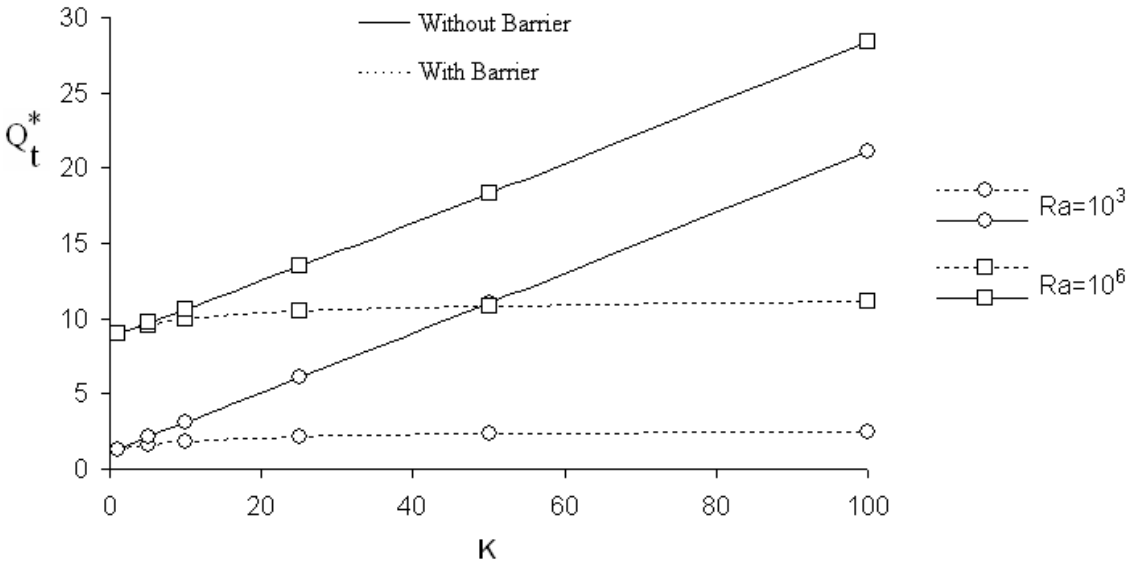

Figure 7.8. The change of dimensionless overall heat transfer rate with conductivity ratio for enclosures without heat barrier and middle located heat barrier, Ra=$10^3$and Ra=10^6.

7.3. Effect of Heat Barrier Location

For different locations of heat barrier in the ceiling wall with D = 0.20, the numerical results were achieved. Figure 7.9 (a) and (b) show the isotherms, streamlines and heatlines for enclosures with Ra = 10^3 and Ra = 10^6, respectively. In these figures, heat barrier is located at X_h = 0.25 and the conductivity ratio is the highest value of the present study (K = 100). Similar streamline, isotherm and heatline contours are observed like the enclosure with middle located heat barrier (X_h = 0.5). Two separate

hot and cold regions occur in the ceiling and isotherms are distributed from the edge of the heat barrier. Heat is transferred from the hot to cold region of the ceiling via fluid. Since the heat barrier is close to the hot vertical boundary, 75% of the ceiling wall area is at cold temperature.

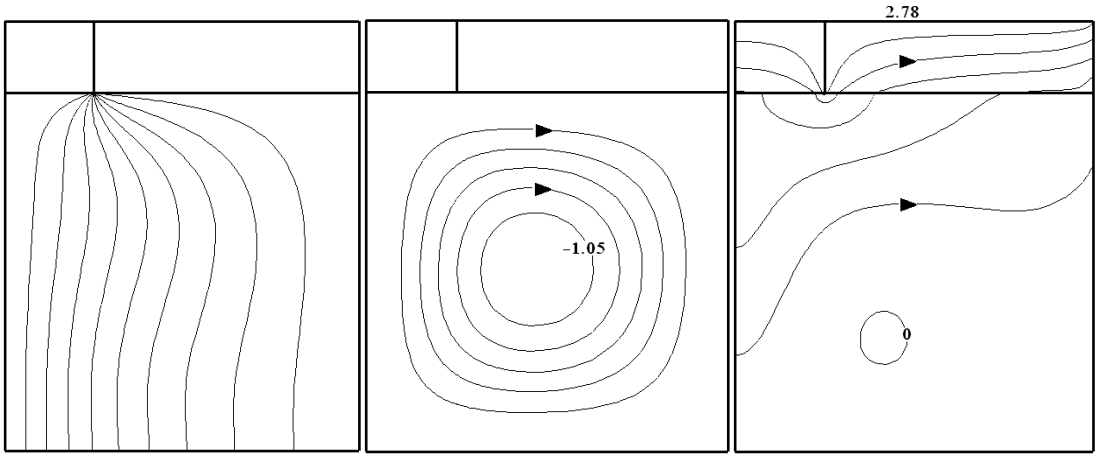

a)

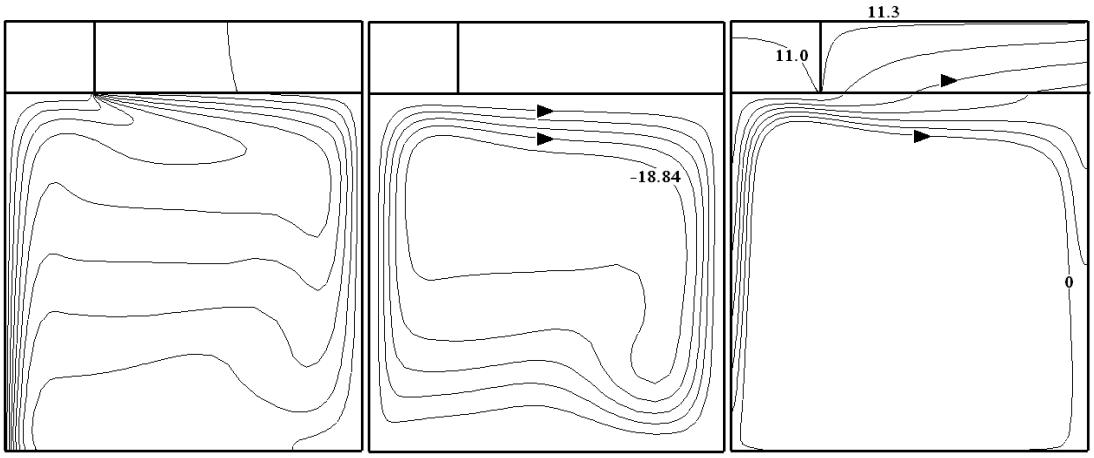

b)

Figure 7.9. Isotherms (on the left), streamlines (on the middle) and heatlines (on the right) for X_h=0.25 and K=100, a) Ra=$10^3$where $\delta\Theta = 0.1, \delta\Psi = -0.21, \delta H = 0.46$ b) Ra=10^6 where $\delta\Theta = 0.1,\ \delta\Psi = -3.76,\ \delta H = 1.88$ (heatline 11.0 was added).

Figure 7.10 is showing isotherms, streamlines and heatlines for X_h=0.75 where K=100 and Rayleigh is 10^3 for part (a) and 10^6 for part (b).Similar observations can be made of Figure 7.9. The only difference here is that since the heat barrier is close to the cold vertical boundary, 75% of the ceiling wall area is at high temperature.

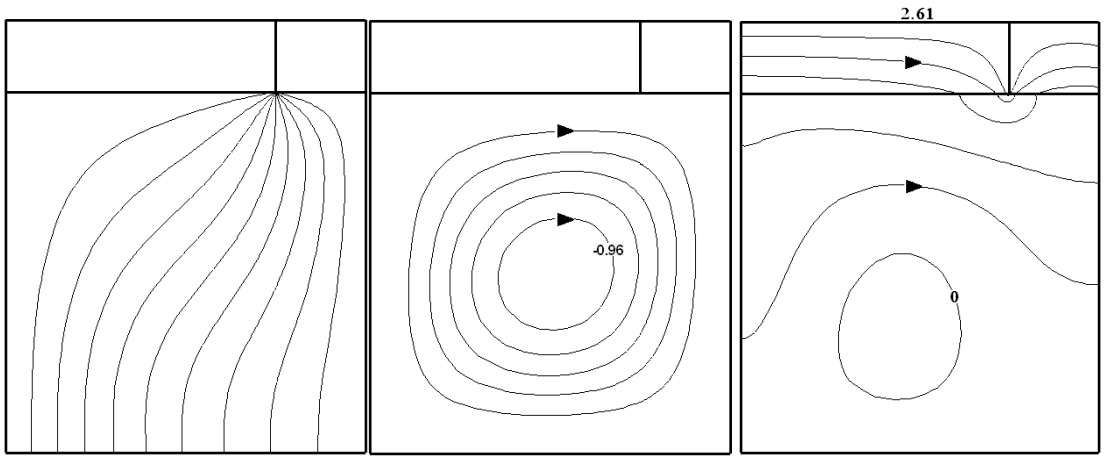

a)

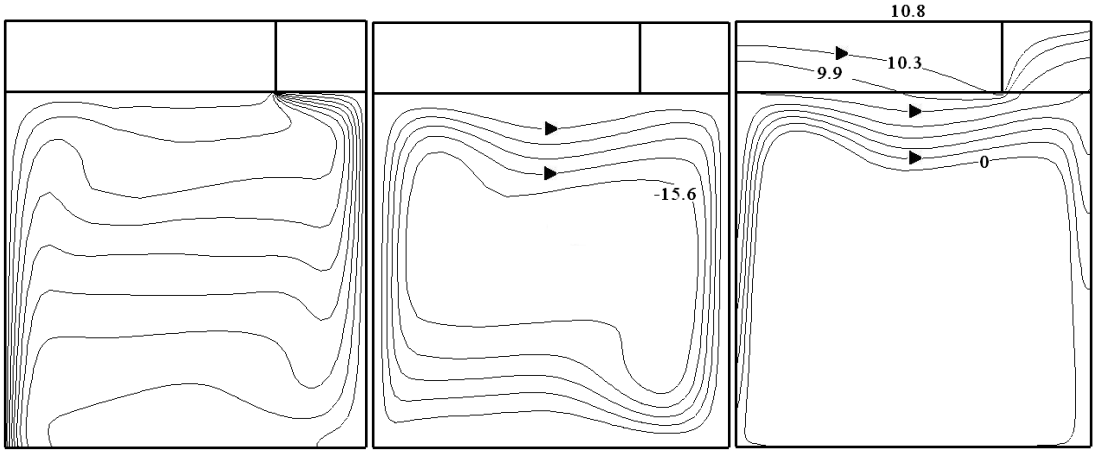

b)

Figure 7.10. Isotherms (on the left), streamlines (on the middle) and heatlines (on the right) for X_h=0.75 and K=100, a) Ra=10^3 where $\delta\Theta = 0.1$, $\delta\Psi = -0.19$, $\delta H = 0.43$, b) Ra=10^6 where $\delta\Theta = 0.1$, $\delta\Psi = -3.1$, $\delta H = 1.8$ (heatline 9.9 and 10.3 were added).

The variations of average Nusselt number of the hot and cold vertical walls and ceiling interface versus heat barrier location are shown in Figure 7.11 (a) for enclosures with K = 1 and K = 100 when Ra = 10^3. The variation of $\overline{Nu}$ with heat barrier location for enclosure with low thermal conductivity ratio (i.e. K = 1) is considerably less than the enclosure with high thermal conductivity ratio (K = 100). Numerical results show that the change of heat barrier location from hot to cold wall of ceiling reduces $\overline{Nu}\big|_{X=0}$; however, it increases $\overline{Nu}\big|_{X=1}$. For K = 1 and Ra = 10^3, the change of heat barrier location from the left to right vertical boundary of the ceiling results 12% decrease and 24% increase in the average Nusselt numbers of the hot and cold vertical walls

respectively. For K = 100 and Ra = 10^3, the movement of heat barrier in the ceiling from left to right vertical wall causes 80% decrease and 748% increase in the average Nusselt numbers of boundaries at X = 0 and X = 1, respectively. As it was mentioned before, two separate cold and hot regions form in the right and left sides of the heat barrier of the ceiling wall as thermal conductivity ratio increases. The change of heat barrier location from left to right increases hot region area and consequently the cold region area is reduced. It causes the decrease of $\overline{Nu}\big|_{X=0}$ and rise of $\overline{Nu}\big|_{X=1}$ curves. The value of average Nusselt number at the interface, $\overline{Nu}\big|_{Y=1}$, is positive and maximum at X_h = 0. The change of heat barrier location from left to right results reduction in the average Nusselt number of the interface. It becomes zero for heat barrier location around X_h = 0.80 and X_h = 0.65 for the ceiling walls with K = 1 and K = 100, respectively and then $\overline{Nu}\big|_{Y=1}$ takes negative values. The negative sign of average Nusselt number shows that the rate of heat transfer from solid to fluid is greater than that from fluid to solid at the interface. The variation of average Nusselt number with heat barrier location for the cavity with Ra = 10^6 is shown in Figure 7.11 (b). Similar to the enclosure with Ra = 10^3 (Figure 7.11 (a)), the change of heat barrier location reduces the value of $\overline{Nu}\big|_{X=0}$ while it increases $\overline{Nu}\big|_{X=1}$. For K = 1, the shift of heat barrier from left to right boundary of the ceiling results 2% decrease and 11% increase of the average Nusselt numbers at X = 0 and X = 1. For K = 100, the average Nusselt number at X = 0 and X = 1 vertical walls decreases 30% and increases 178% respectively with the change of heat barrier location. The value of $\overline{Nu}\big|_{Y=1}$ is maximum for X_h = 0 and it decreases when the heat barrier moves to X_h = 1. The interface average Nusselt number becomes zero around X_h = 0.96 for K = 1 and X_h = 0.90 for K = 100 when Ra = 10^6.

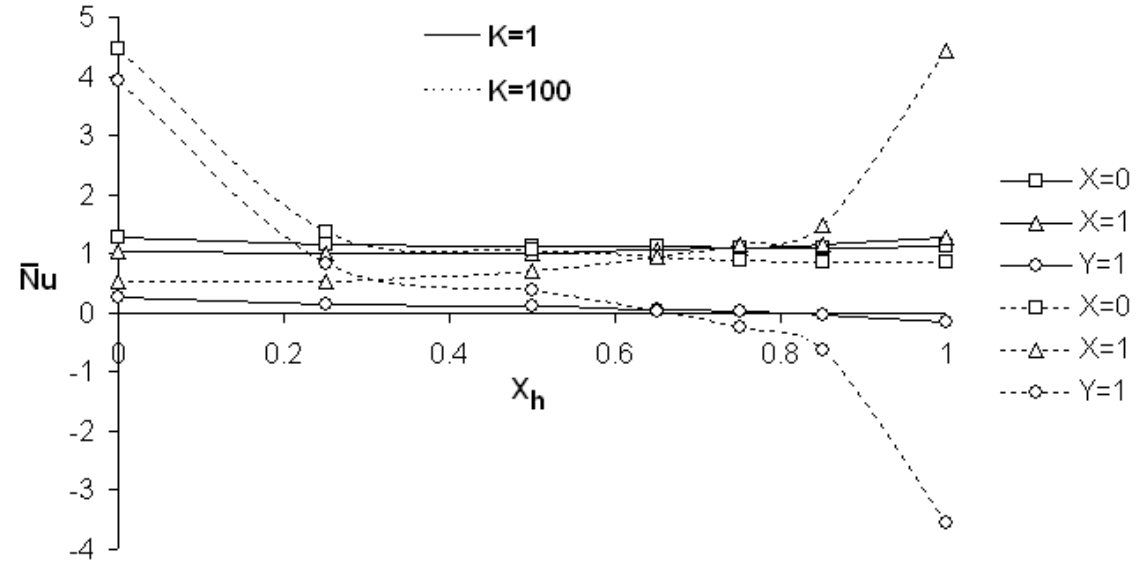

a)

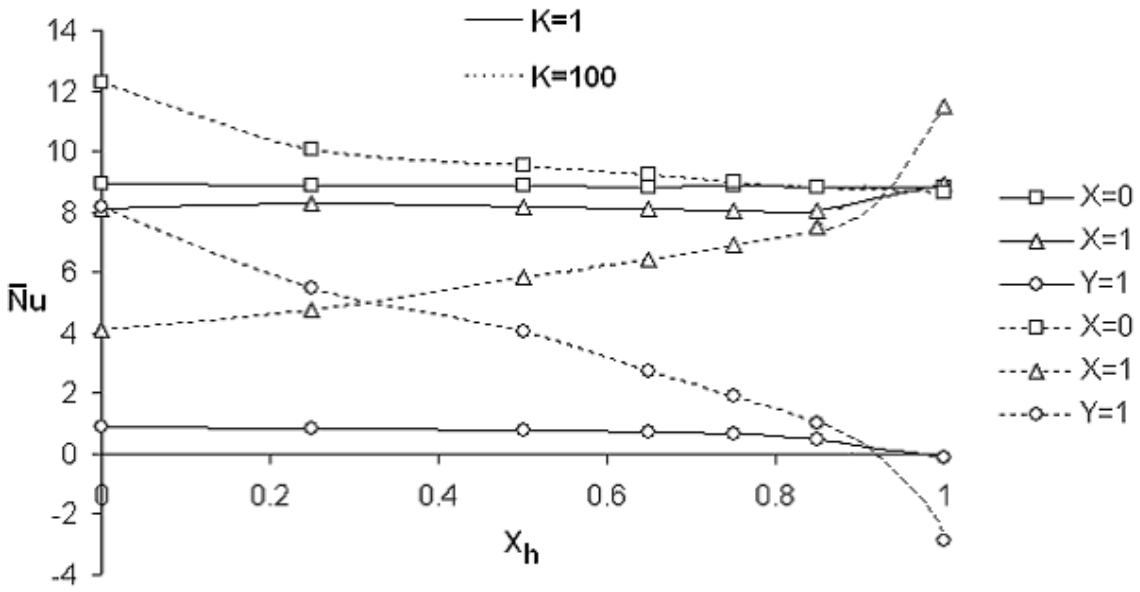

b)

Figure 7.11. The change of average Nusselt number of hot and cold walls, and ceiling interface with heat barrier location, a) Ra=10^3, b) Ra=10^6.

The variation of overall dimensionless heat transfer rate Q_t^*, with heat barrier location is illustrated in Figure 7.12 for K = 1 and K = 100 and for two different Rayleigh numbers Ra = 10^3 and Ra = 10^6. The change of heat barrier location does not considerably affect dimensionless overall heat transfer rate through the enclosure for K = 1, though, an effect of heat barrier location is seen for K = 100 and Ra = 10^3.

Particularly, for enclosure with Ra = 10^3 a minimum point for dimensionless overall heat transfer rate is observed. The movement of heat barrier from $X_h = 0$ to $X_h = 0.5$ results a decrease of 53% in the dimensionless overall heat transfer rate for K=100 and then an increase behind $X_h = 0.5$. However; for K = 100 and Ra = 10^6, Q_t^* decreases, it is almost constant behind X_h=0.5 and then slightly increases in the region close to cold wall. The movement of heat barrier from $X_h = 0$ to X_h=0.5 results a decrease of 11% in the overall dimensionless heat transfer rate which is smaller than the results of the enclosure with Ra = 10^3 due to strong convection heat transfer in the fluid region.

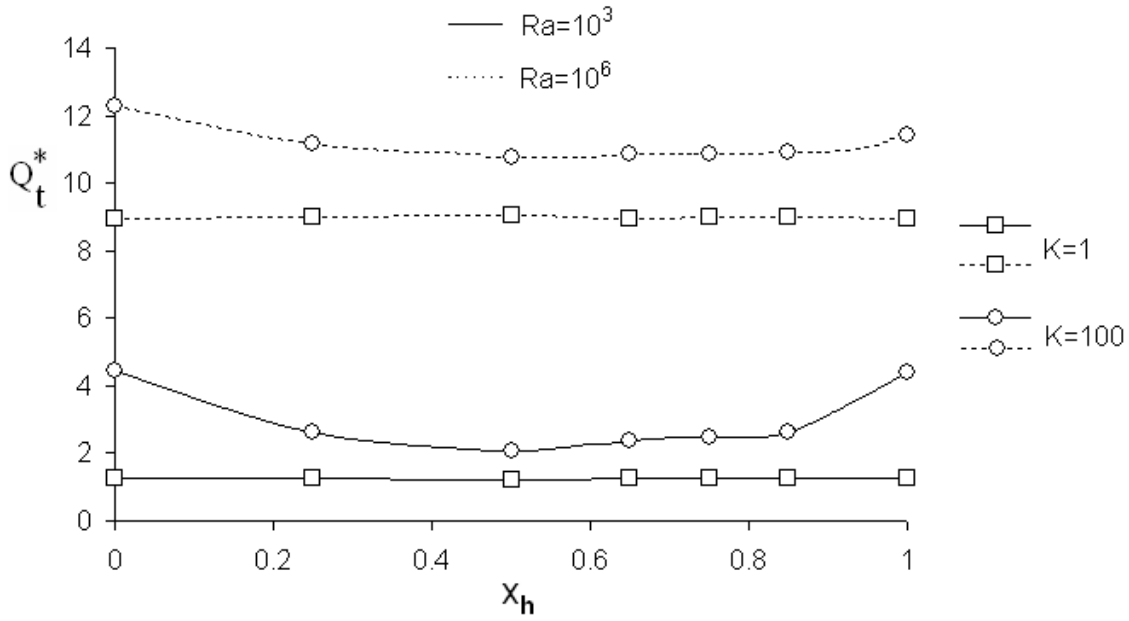

Figure 7.12. The change of dimensionless overall heat transfer rate with heat barrier barrier location for Ra=10^3 and Ra=10^6, and for two conductivity ratio values K=1 and K=100.

7.4. Effect of Rayleigh Number

The variations of average Nusselt number and dimensionless overall heat transfer rate with Rayleigh number are shown in Figure 7.13 (a) and (b), for enclosures with and without heat barrier for thermal conductivity ratio K=100. The heat barrier is located at the middle of ceiling. The average Nusselt numbers at the hot walls of both enclosures are almost same for all values of Rayleigh number. The temperature of air which flows horizontally on the upper region of fluid region is influenced by heat

barrier and consequently $\overline{Nu}\big|_{X=1}$ slightly decreases. Figure 7.13 (b) shows the variation of dimensionless overall heat transfer rate with Rayleigh number for the same enclosure of Figure 7.13 (a). As is seen, the increase of Rayleigh number causes the increase of overall dimensionless heat transfer rate for the enclosures with and without heat barrier. Heat barrier considerably reduces dimensionless overall heat transfer rate through the enclosure since heat is greatly transferred between the vertical walls of the enclosure by conduction in the ceiling.

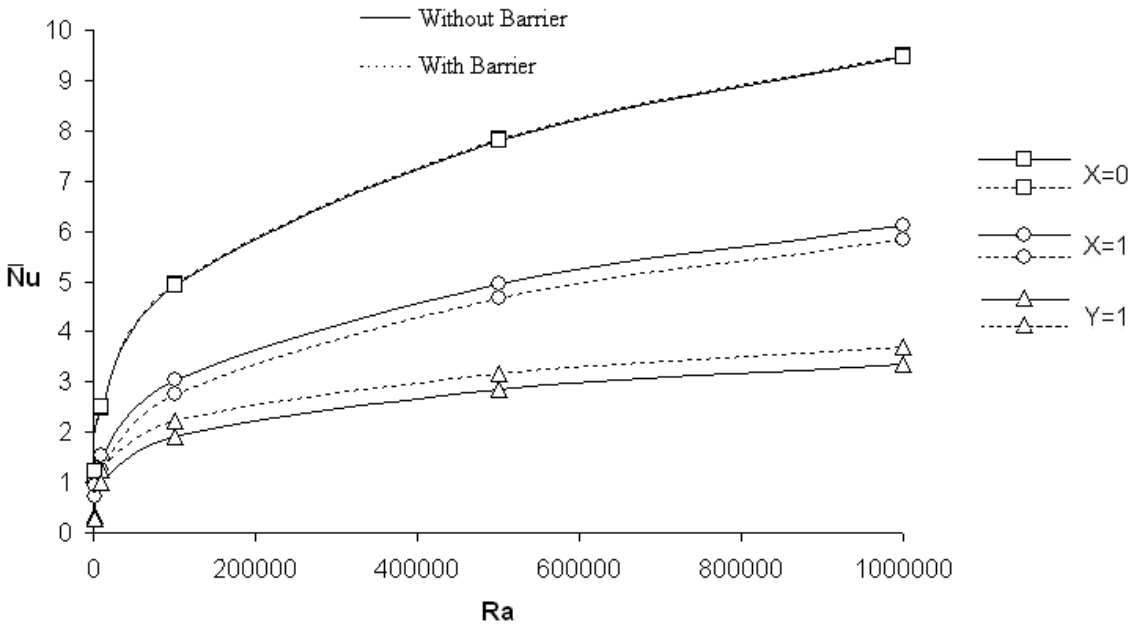

Figure 7.13(a)

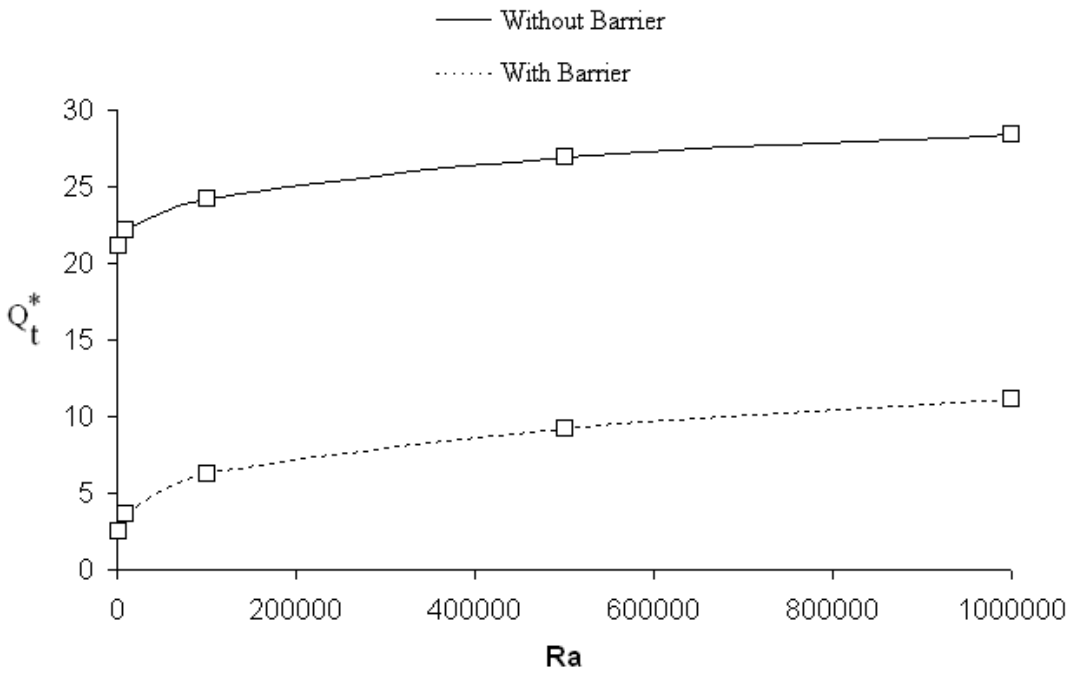

b)

Figure 7.13. The change of average Nusselt number (at X=0, X=1 and Y=1) and dimensionless overall heat transfer rate with Rayleigh number for enclosures with heat barrier located at X_h=0.5 and without heat barrier where K=100, a) average Nusselt number, b) dimensionless overall heat transfer rate.

7.5. Effect of Ceiling Wall Thickness

Two different ceiling wall thicknesses are examined to see the effects of this parameter on the dimensionless heat transfer through the enclosure with X_h=0.5. Figure 7.14 shows the variation of average Nusselt number at hot and cold walls, and interface with thermal conductivity ratio for two different dimensionless ceiling wall thicknesses (D = 0.05 and D = 0.2) and for two Rayleigh numbers 10^3 and 10^6. For Ra = 10^3, the increase of ceiling thickness slightly increases $\overline{Nu}$ at the interface and it decreases $\overline{Nu}$ of cold vertical wall. However, the wall thickness does not have significant influence on the average Nusselt number of hot wall. For Ra = 10^6, the increase of ceiling wall thickness has the same effect as Ra=10^3 case; however, it slightly increases $\overline{Nu}\big|_{X=0}$.The change of wall thickness from 0.05 to 0.2 results 2% and 14% increase in $\overline{Nu}\big|_{X=0}$ and $\overline{Nu}\big|_{Y=1}$ respectively, and 6% decrease in $\overline{Nu}\big|_{X=1}$ for Ra = 10^6 and K=100.

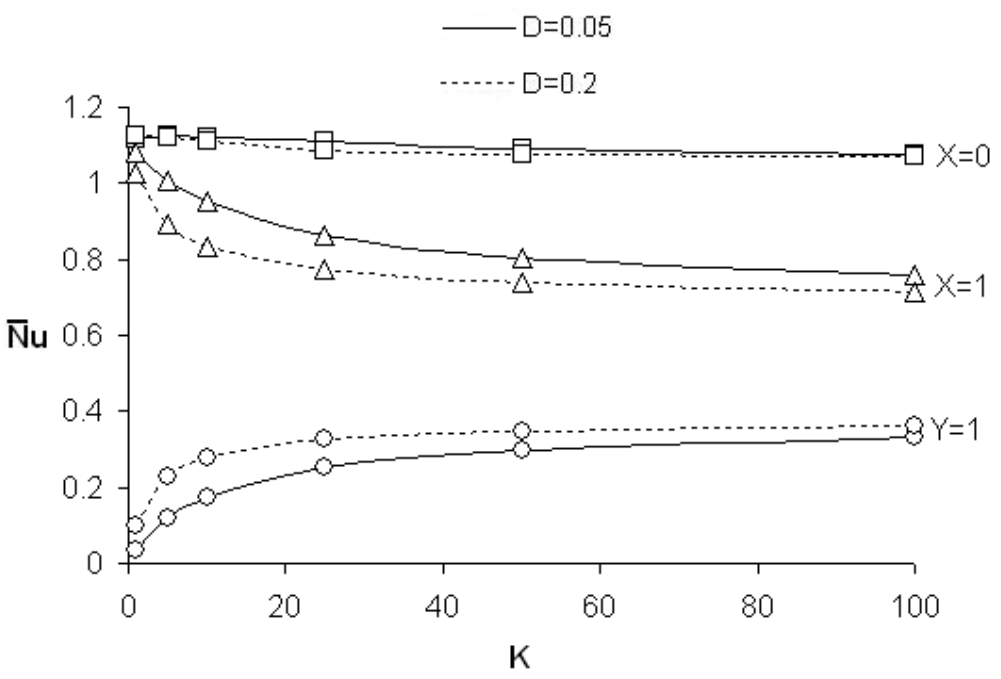

a)

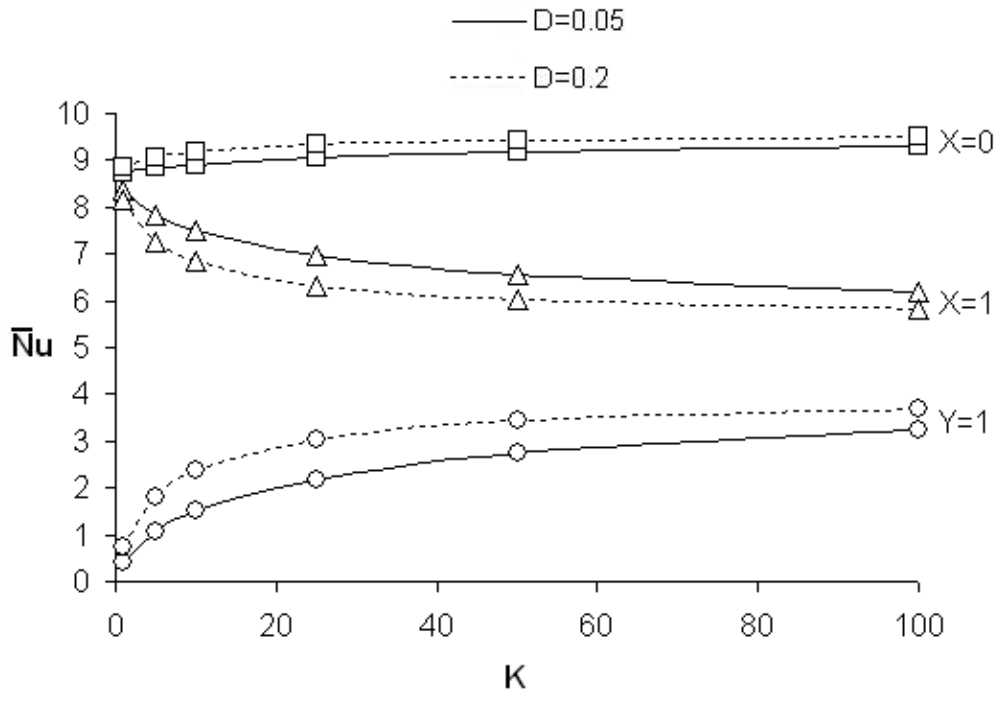

b)

Figure 7.14. The variation of average Nusselt number (at X=0, X=1 and Y=1) with dimensionless ceiling wall thicknesses D=0.05 and D=0.2 a) $Ra=10^3$, b) $Ra=10^6$.

The variation of dimensionless overall heat transfer rate through the enclosure with conductivity ratio for two Rayleigh number values as Ra = 10^3 and Ra = 10^6, and for two different middle located heat barrier with ceiling wall thicknesses (D = 0.05 and D = 0.20) is shown in Figure 7.15. For low conductivity ratios (i.e. K = 1), the increase of wall thickness has a smaller effect on the dimensionless overall heat transfer rate compared with the high conductivity ratios (i.e. K = 100). Heat barrier considerably prevents heat transfer in the ceiling wall and Q_t^* is not highly affected with the increase of ceiling wall thickness. For K=1, the increase of ceiling thickness causes 9% and 2% increase in Q_t^* for Ra=10^3 and Ra=10^6, respectively. For K=100, the increase of ceiling thickness from 0.05 to 0.2 causes the increase of total dimensionless heat transfer rate by 25% and 6.5% for Ra=10^3 and Ra=10^6, respectively.

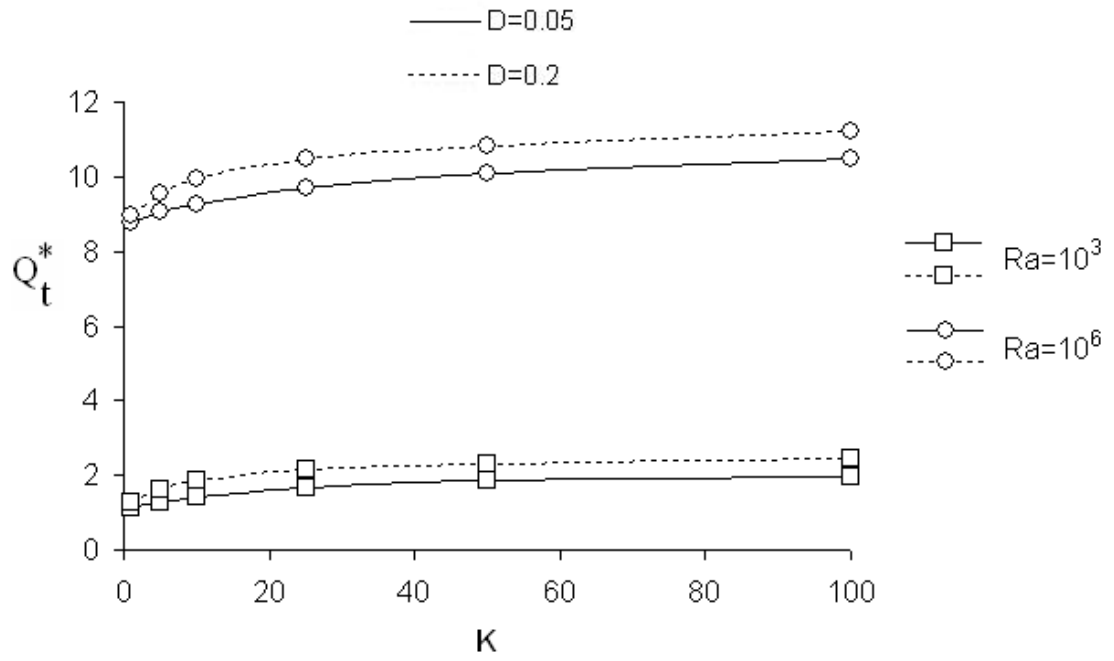

Figure 7.15. The variation of dimensionless overall heat transfer rate with thermal conductivity ratio for Ra=$10^3$and Ra=10^6, with two dimensionless wall thicknesses D=0.05 and D=0.2 where X_h=0.5.

CHAPTER 8

CONCLUSIONS

The effects of a heat barrier and its location in the ceiling wall of an enclosure have been investigated for Rayleigh number changing from 10^3 to 10^6 and in the thermal conductivity ratio range of 1 to 100 for two dimensionless ceiling wall thicknesses. Heatlines are employed to observe the mechanism of heat transfer between the ceiling wall and the fluid. It is observed that heatlines are efficient tools since they indicate the path of heat flow from solid to fluid and vice versa.

The governing equations for the problem are continuity, momentum and energy for the fluid inside the cavity, and heat conduction equation for the horizontal wall. The analytical approach is not possible since the governing equations are highly nonlinear and strongly coupled. However, it is possible to solve these governing equations by using numerical techniques. In order to solve them numerically, the Boussinesq approximation is used and then, the dimensionless parameters are introduced to make the governing equations non-dimensional. Making the governing equations non-dimensional enables to find the results for different types of flows and fluids.

The advantage of the Boussinesq approximation is that it makes the mathematics and physics simpler. It states that density differences are sufficiently small to be neglected, except where they appear in terms multiplied by g, the acceleration due to gravity.

There is a point which needs to be taken into consideration for the numerical solution. Solution of the Navier-Stokes equations is complicated because of the lack of an independent equation for the pressure, whose gradient contributes to each of the momentum equations. By using the vorticity-streamfunction approach, the pressure term in the momentum equation is eliminated and the number of unknowns reduces to three.

The steady behaviors of flow and temperature distribution are investigated in this study. Time marching approach is adopted to obtain the steady results of the governing equations by solving them in the transient form, since the governing equations are numerous (three equations) and highly coupled. In time marching

approach, it is possible to decrease the computational time of the solution procedure by increasing the value of time interval when the results converge to the steady state. The main disadvantage of the time marching approach is the accumulation of truncation errors due to the discretization of time. However, truncation errors of the time dependent terms can be minimized by using fine time intervals.

It is possible to write the vorticity and the energy equations in a single generic form since they have similar terms. A time term, convection terms and diffusion terms are included in the equations. Same approach can be made for the streamfuction and heatfunction equations since they only have diffusion terms. Grouping them in a single generic equation makes the finite difference formulation and numerical solution easier.

In this study, finite difference solution technique is used. By using this technique, the determination of the values of dependent variable of a given differential equation at any discrete point in the computational domain is possible. After reviewing the available finite difference solution methods for parabolic differential equations, ADI finite difference solution method is adopted to solve the energy and vorticity equations. The streamfunction and the heatfunction equations however, are solved by an iterative method rather than matrix inversion technique.

Finite difference formulations of diffusion and convection terms are written based on three-point central differencing. One of the major inadequacies of the central differencing for strong convective flow is that this scheme does not involve flow direction. Therefore, this study is limited for Rayleigh numbers up to 10^6 to get accurate results since above this value; the convection flow is very strong. Finite difference forms of the boundary conditions at the specified boundaries are defined to solve the equations by finite difference solution technique. The formulation of Wong and Baker (Wong and Baker 2002) is used to define the vorticity at the boundaries.

In many systems involving multimode heat transfer effects, free convection provides the largest resistance to heat transfer and therefore plays an important role in the design or performance of the system. Moreover, when it is desirable to minimize heat transfer rates or to minimize operating cost, free convection is often preferred to forced convection. The effect of wall heat conduction on natural convection heat transfer in cavities is very important since the occurance of thermal bridge increases heat transfer rates considerably. The obtained results of the present study are useful for manufacturers who work on the design of thermal breakers to reduce heat leakage. By considering the obtained results following conclusions are drawn:

1- For low thermal conductivity ratio, mean Nusselt number is not greatly affected by a heat barrier. The heat barrier changes the direction of heat flow in the ceiling and, as a result, heat has to be transferred from the hot to the cold side of the ceiling via fluid. For higher thermal conductivity ratio, the heat barrier causes the formation of two separate cold and hot regions in the ceiling. The dimensionless overall heat transfer through the enclosure is considerably influenced by the heat barrier.

2- The average Nusselt numbers of the hot and cold walls are reduced by the heat barrier. The decreasing effect is greater for high thermal conductivity ratio and low Rayleigh number values.

3- A heat barrier location is observed where the average Nusselt numbers of the hot and cold vertical walls are equal.

4- The heat barrier causes significant changes in the dimensionless heat transfer rate at the vertical boundaries of the ceiling. It considerably reduces dimensionless heat transfer rate of both boundaries. This effect decreases with increasing Rayleigh number.

5- Changing the heat barrier location from the hot to the cold boundary decreases the average Nusselt number of the hot boundary while it increases the cold boundary average Nusselt Number.

6- The effect of heat barrier location on dimensionless overall heat transfer rate is greater for enclosures with low Rayleigh number. There is a heat barrier location where dimensionless overall heat transfer rate is minimum. For the enclosure with Ra = 10^3 and K = 100, movement of the heat barrier from $X_h = 0$ to $X_h = 0.5$ results in a decrease of 53% in dimensionless overall heat transfer rate.

7- For the enclosure with a middle-located heat barrier and high conductivity ratio, the overall dimensionless heat transfer rate is influenced by the change of wall thickness. For instance, the dimensionless thickness change of D=0.05 to D=0.2 results in a 25% increase in Q_t^* for Ra = 10^3 and K = 100.

REFERENCES

Acharya, S. and Tsang, C.H. 1987. Influence of wall conduction on natural convection in an inclined square enclosure, *Heat and Mass Transfer* 21: 19-30.

Aksel, M.H. 2003. *Fluid mechanics*. Ankara: METU Press.

Alibaba Global Trade. 2008. http://www.alibaba.com/catalog/11009951/ThermalBreak Aluminium Profiles.html (accessed February 10, 2008).

Basak, T., Roy, S. and Pop, I. Heat flow analysis for natural convection within trapezoidal enclosures based on heatline concept. *International Journal of Heat and Mass Transfer* 52: 2471-2483.

Baytas, A.C., Liaqat, A., Grosan, T. and Pop, I. 2001. Conjugate natural convection in a square porous cavity. *Heat and Mass Transfer* 37: 467-473.

Ben Nakhi, A.E. 2002. Minimizing thermal bridging through window systems in buildings of hot regions. *Applied Thermal Engineering* 22: 989-998.

Ben Nakhi, A.E. 2003. Development of integrated dynamic thermal bridging assessment environment. *Energy and Buildings* 35: 375-382.

Cai, J., Huai, X., Yan, R. and Cheng, Y. 2009. Numerical simulation on enhancement of natural convection heat transfer by acoustic cavitation in a square enclosure. *Applied Thermal Engineering* 29: 1973-1982.

Chapra, S.C. and Candle, R.P. 1988. *Numerical methods for engineerings*. New York: McGraw-Hill Press.

Costa, V.A.F. 2003. Unified streamline, heatline and massline methods for the visualization of two-dimensional heat and mass transfer in anisotropic media. *International Journal of Heat and Mass Transfer* 46: 1309-1320.

Costa, V.A.F. and Bejan, A. 2006. Heatlines and masslines for convection visualization and analysis. *Applied Mechanic Reviews* 59: 126-145.

Dalal, A. and Das**,** M.K. 2008. Heatline method for the visualization of natural convection in a complicated cavity. *International Journal of Heat and Mass Transfer* 51: 263-272.

Dash, S.K. 1996. Heatline visualization in turbulent flow. *International Journal of Numerical Methods for Heat and Fluid Flow* 6: 37-46.

De Vahl Davis, G. 1983. Natural convection of air in a square cavity: a bench mark numerical solution. *International Journal of Numerical Methods in Fluids* 3: 249-264.

Deng, Q.H. and Tang, G.F. 2002. Numerical visualization of mass and heat transport for conjugate natural convection/heat conduction by streamline and heatline. *International Journal of Heat and Mass Transfer* 45: 2387-2396.

Du, Z.G. and Bilgen, E. 1992. Coupling of wall conduction with natural convection in a rectangular enclosure. *International Journal of Heat and Mass Transfer* 35: 1962-1975.

Fabricated Foam Company. 2008. http://www.fabricatedfoam.net/prod5.html (accessed February 10, 2008).

Fukuyo, K. 2003. Heat flow visualization for thermal bridge problems. *International Journal of Refrigeration* 26: 614-617.

Hakyemez, E., Mobedi, M., Oztop, H.F. 2008. Effects of floor located heat barrier on conjugate conduction-natural convection heat transfer and fluid flow in enclosures. *International Symposium on Advances in Computational Heat Transfer*: Morocco.

Hakyemez, E., Mobedi, M. and Oztop, H.F. 2008. Effects of wall-located heat barrier on conjugate conduction and natural convection heat transfer and fluid flow in enclosures. *Numerical Heat Transfer* 54: 197–220.

Hoglund, T. and Burstrand, H. 1998. Slotted steel studs to reduce thermal bridges in insulated walls. *Thin-Walled Structures* 32: 81-109.

Holman, J.P. 1990. *Heat transfer*. New York: McGraw-Hill Press.

Incropera, F.P. and Dewitt, D.P. 2002. *Fundamentals of heat and mass transfer*. New York: John Wiley&Sons Press.

Kaminski, D.A. and Prakash, C. 1986. Conjugate natural convection in a square enclosure: effect of conduction in one of the vertical walls. *International Journal of Heat and Mass Transfer* 12: 1979-1988.

Kim, D.M. and Viskanta, R. 1984. Study of effects of wall conductance on natural convection in differently oriented square cavities. *Journal of Fluid Mechanics* 144: 153-176.

Kim, D.M. and Viskanta, R. 1984. Heat transfer by conduction, natural convection and radiation across rectangular cellular structure. *International Journal of Heat and Fluid Flow* 5: 205-212.

Kimura, S. and Bejan, A. 1983. The heatline visualization of convective heat transfer. *ASME Journal of Heat Transfer* 105: 916-919.

Larbi, B. 2005. Statistical modeling of heat transfer for thermal bridges of buildings. *Energy and Buildings* 37: 945-951.

Liaqat, A. and Baytas, A.C. 2001.Conjugate natural convection in a square cavity enclosure containing volumetric sources. *International Journal of Heat and Mass Transfer* 44: 3273-3280.

Misra, D. and Sarkar, A. 1997. Finite element analysis of conjugate natural convection in a square enclosure with a conducting vertical wall. *Computer Methods in Applied Mechanics and Engineering* 141: 205-219.

Mobedi, M. 1994. A three dimensional numerical study on natural convection heat transfer from rectangular fins on a horizontal surface. *Ph. D. Thesis Study*.

Mobedi, M. and Yuncu, H. 2003. A three dimensional numerical study on natural convection heat transfer from short horizontal rectangular fin array. *Heat and Mass Transfer* 39: 267-275.

Mobedi, M. 2008. Conjugate natural convection in a square cavity with finite thickness horizontal walls. *International Communications in Heat and Mass Transfer* 35: 503-513.

Morega, A.M. and Bejan, A. 1993. Heatline visualization of forced convection laminar boundary layers. *International Journal of Heat and Mass Transfer* 36: 3957-3966.

Roach, P.J. 1976. *Computational fluid dynamics*. Albuquerque, New Mexico: Hermosa Publishers.

Saeid, N.H. 2007. Conjugate natural convection in a porous enclosure: effect of conduction in one of the vertical walls. *International Journal of Thermal Sciences* 46: 531-539.

Saeid, N.H. 2007. Conjugate natural convection in a vertical porous layer sandwiched by finite thickness walls. *International Communications in Heat and Mass Transfer* 34: 210-216.

Sapa Group. 2009. http://www.sapagroup.com/en/Company-sites/Sapa-RC-System---Product-database/profile-systems/windows-and-doors/Avantis-55/ (accessed March 20, 2009).

Thiault, J. 1985. Comparison of nine three dimensional numerical methods for the solution of the heat diffusion equation. *Numerical Heat Transfer* 8: 281-298.

Tosun, M., Mobedi, M. and Ozerdem, B. 2006. Heat transfer through casing of an air handling unit. *37th HVAC&R Congress*: Belgrade.

Varol, Y., Oztop, H.F., Mobedi, M. and Pop, I. 2008. Visualization of natural convection heat transport using heatline method in porous non-isothermally heated triangular cavity. *International Journal of Heat and Mass Transfer* 51: 5040-5051.

Wikipedia. 2009. http://en.wikipedia.org/wiki/LNG (accessed March 19, 2009).

Wong, K.L. and Baker, A.J. 2002. A 3D incompressible Navier-Stokes velocity-vorticity weak form of finite element algorithm. *International Journal for Numerical Methods in Fluids* 38: 99-123.

Yedder, R.B. and Bilgen, E. 1997. Laminar natural convection in inclined enclosures bounded by a solid wall. *Heat and Mass Transfer* 32: 455-462.

Zhao, F.Y., Liu, D. and Tang, G.F. 2007. Application issues of the streamline, heatline and massline for conjugate heat and mass transfer. *International Journal of Heat and Mass Transfer* 50: 320-334.